Universidade de Aveiro Departamento de Electrónica, Telecomunicações e Informática,
2017

Diogo Silva Matos

Sistema para Deteção de Pessoas

Person Detection System

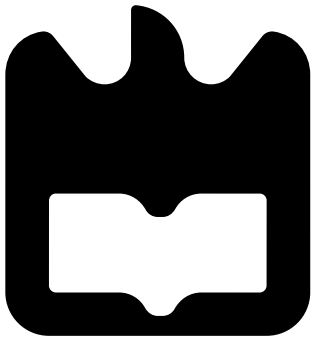

Diogo Silva Matos

Sistema para Deteção de Pessoas

Person Detection System

Dissertação apresentada à Universidade de Aveiro para cumprimento dos requesitos necessários à obtenção do grau de Mestre em Engenharia Eletró nica e Telecomunicações , realizada sob a orientação científica do Professor Doutor João Nuno Pimentel da Silva Matos (orientador), Professor Associado do Departamento de Eletrónica Telecomunicações e Informática da Universidade de Aveiro e do Professor Doutor José Manuel Neto Vieira (co-orientador) , Professor Auxiliar do Departamento de Eletrónica Telecomunicações e Informática da Universidade de Aveiro

o júri / the jury

presidente / president

Nuno Miguel Gonçalves Borges de Carvalho
Professor Catedrático da Universidade de Aveiro

vogais / examiners committee

Sérgio Reis Cunha
Professor Auxiliar na Faculdade de Engenharia da Universidade do Porto (arguente)

José Manuel Neto Vieira
Professor Auxiliar da Universidade de Aveiro (coorientador)

agradecimentos / acknowledgements

Em primeiro lugar agradecer aos meus pais, pelo apoio incondicional ao longo destes 6 anos e por me possibilitarem a concretização desta etapa. Obrigado Pai, obrigado Mãe.

Agradecer também à minha restante família que sempre esteve presente neste percurso.

A todos os meus amigos e à minha namorada, pelo vosso apoio e por me proporcionarem bons percalços ao longo deste percurso e o tornarem na melhor experiência possível, o meu obrigado.

Um agradecimento especial ao meu colega Daniel Malafaia, pela ajuda incansável, disponibilidade e ensinamentos transmitidos ao longo deste último ano.

Obrigado aos meus orientadores, Professor Doutor João Nuno Pimentel da Silva Matos e Professor Doutor José Manuel Neto Vieira pelo apoio, a orientação e a transmissão de conhecimento ao longo deste trabalho.

Agradecer também ao Instituto de Telecomunicações pelas excelentes condições de trabalho proporcionadas, bem como a todos os membros envolvidos neste trabalho, em especial ao Eng. Hugo Mostardinha, pelo seu auxílio.

Palavras-Chave

RADAR, RADAR de múltiplas entradas e múltiplas saídas, Beamforming, Antenas, Rádio Definido por Software, Caraterização de Materiais

Resumo

O RADAR é para fins militares já relativamente antigo que sofreu um grande impulso durante a Segunda Guerra Mundial. Hoje em dia existe um forte desenvolvimento no RADAR em aplicações de navegação ou vigilância/segurança.

Esta dissertação surge no seguimento destas novas aplicações, em que se pretende o desenvolvimento de um RADAR de baixo custo que permita ao utilizador detetar pessoas, bem como, os seus movimentos através de paredes ou objetos opacos.

O desenvolvimento deste RADAR recaiu em tecnologias emergentes como antenas adaptativas e rádio definido por software que permitem uma grande versatilidade e adaptação em termos de aplicações. A utilização de um RADAR com múltiplas entradas e múltiplas saídas fornece uma maior diversidade de informação que garante mais probabilidades de deteção. A aplicação de técnicas digitais de beamforming, possibilita conhecer a posição e o movimento da pessoa.

Com a implementação destas técnicas um prótotipo capaz de detetar pessoas e os seus movimentos através de paredes e tijolos foi desenvolvido com sucesso solucionando o problema inicial.

Na fase de projeto de RADAR houve necessidade de caracterizar a propagação de ondas de rádio em materiais de construção, como tijolos e madeira, medindo-se a sua atenuação. Deste modo foi possível fazer o balanço de potência para vários cenários.

Key words

RADAR, Multiple Input Multiple Output (MIMO) RADAR, Beamforming, Antennas, Software Defined Radio (SDR), Materials Characterization

Abstract

The RADAR is already relatively old for military purposes that underwent a major development during World War II. Nowadays there is a strong development in RADAR in navigation or surveillance/security applications.

This dissertation follows on from these new applications, which aim to develop a low cost RADAR that allows the user to detect people as well as their movements through walls or opaque objects.

The development of this RADAR has relied on emerging technologies such as adaptive antennas and SDR that allow for great versatility and adaptation in terms of applications. The use of a MIMO RADAR provides a greater diversity of information that guarantees more probabilities of detection and the application of digital techniques of beamforming, allows to know the position and the movement of the person.

With the implementation of these techniques a prototype capable of detecting people and their movements through walls and bricks was successfully developed solving the initial problem.

In the RADAR design phase it was necessary to characterize the propagation of radio waves in building materials, such as bricks and wood, by measuring their attenuation. In this way it was possible to perform the power balance for several scenarios.

Contents

Contents i

List of Figures v

List of Tables ix

List of Acronyms xi

1 Introduction 1
- 1.1 Motivation . . . 2
- 1.2 Objectives . . . 2
- 1.3 Thesis Organization Overview . . . 2
- 1.4 Thesis Contributions . . . 3

2 Radar Basic Principles 5
- 2.1 Brief Radar History . . . 5
- 2.2 Radar Parameters . . . 5
  - 2.2.1 Radar Equation . . . 8
  - 2.2.2 Noise Factor . . . 10
  - 2.2.3 Radar Cross Section . . . 11
  - 2.2.4 Radar Resolution . . . 12
  - 2.2.5 Doppler Effect . . . 13
  - 2.2.6 Radar Clutter . . . 14
- 2.3 Types of Radar . . . 14
  - 2.3.1 Pulse Radar . . . 15
  - 2.3.2 Continuous Wave (CW) Radar . . . 15
  - 2.3.3 Frequency Modulated Continuous Wave (FM-CW) Radar . . . 15

3 Through-the-Wall Radar 17
- 3.1 Introduction . . . 17
- 3.2 Software Defined Radio (SDR) . . . 19
  - 3.2.1 Front-End Architectures . . . 21
    - 3.2.1.1 Transmitter Architectures . . . 21
    - 3.2.1.2 Receiver Architectures . . . 22
  - 3.2.2 SDR Advantages . . . 24
  - 3.2.3 Cognitive Radio(CR) . . . 25
- 3.3 MIMO Radar . . . 25

3.3.1 MIMO Virtual Aperture . . . 27
3.3.1.1 MIMO Channel . . . 27
3.4 Antennas . . . 28
3.4.1 Fundamental Parameters . . . 28
3.4.2 Linear Array Antenna . . . 29
3.5 Beamforming Techniques . . . 32
3.5.1 Circuit Beamforming . . . 33
3.5.2 Digital Beamforming (DBF) . . . 34
3.6 Detection Through the Walls Works . . . 36

4 Materials Characterization **41**
4.1 Introduction . . . 41
4.2 Measurement Technique . . . 41
4.3 Materials Characterization System . . . 44
4.3.1 Antennas . . . 44
4.3.1.1 Narrowband Antenna . . . 44
4.3.1.2 Ultra Wide Band (UWB) Antenna . . . 46
4.3.2 Measurement Setups . . . 48
4.3.2.1 Universal Software Radio Peripheral (USRP) Setup . . . 48
4.3.2.2 Vector Network Analyser (VNA) Setup . . . 53
4.3.2.3 Anechoic Chamber Setup . . . 54
4.4 Materials Characterization Results . . . 57
4.4.1 Narrowband Antenna Results . . . 57
4.4.2 UWB Antenna Results . . . 59
4.4.3 Anechoic Chamber Results . . . 62
4.4.3.1 Clay Bricks with Holes . . . 62
4.4.3.2 Solid Clay Bricks . . . 65
4.5 Conclusions . . . 67

5 Radar System Design **69**
5.1 Introduction . . . 69
5.2 Overall System . . . 69
5.3 Field-Programmable Gate Array (FPGA) Xilinx ZC706 . . . 72
5.4 AD-FMCOMMS5-EBZ . . . 74
5.5 Antennas . . . 75
5.5.1 1^{st} Version . . . 76
5.5.2 2^{nd} Version . . . 80
5.6 Conclusion . . . 86

6 Results and Analysis **87**
6.1 Reception Beamforming Algorithm . . . 88
6.2 Results . . . 92
6.3 Conclusions . . . 101

7 Conclusion and Future Work **103**
7.1 Conclusions . . . 103
7.2 Future Work . . . 103

Appendices **105**

A Poster for Students@DETI **106**

Bibliography **109**

List of Figures

2.1 Radar Principle 6
2.2 Basic Radar Block Diagram example 7
2.3 Radar Resolution 13
2.4 Doppler Effect 14

3.1 Formalization of problem 18
3.2 SDR Ideal Model 20
3.3 USRP Examples 20
3.4 Transmitter baseband digitalization architecture 21
3.5 Transmitter Intermediate Frequency (IF) architecture 22
3.6 Transmitter Radio Frequency (RF) architecture 22
3.7 Receiver baseband digitalization architecture 23
3.8 Receiver IF architecture 23
3.9 Receiver RF architecture 24
3.10 Basic MIMO Radar 26
3.11 Linear aggregate with N elements 30
3.12 Linear array factor for different number of elements 32
3.13 Types of beamforming 33
3.14 Butler matrix for a four element array 34
3.15 Digital Beamforming (DBF) for a four element array 35
3.16 Radar developed 36
3.17 Block diagram of the system 37
3.18 Measurement setup 38
3.19 Results for the three different scenarios 39

4.1 Measurement Setup [21] 42
4.2 Attenuation for several materials along the frequency. [24] 43
4.3 Diagram of the developed antenna [25] 44
4.4 Printed antenna 45
4.5 S11 parameter of printed antenna 45
4.6 Vivaldi antenna simulation in Computer Simulation Technology (CST) 46
4.7 Printed Vivaldi antenna 47
4.8 S11 parameters of designed antenna 47
4.9 Generator Test Setups 49
4.10 USRP Rx Test Setup 50
4.11 USRP Tx Test Setup 51

4.12 USRP Tx/Rx Test Setup . . . 52
4.13 Setup used to perform the tests . . . 53
4.14 Anechoic chamber scheme . . . 54
4.15 Wooden structure built . . . 55
4.16 Transmission antenna . . . 55
4.17 S11 parameter of transmission antenna . . . 56
4.18 Receiving antenna . . . 56
4.19 S11 parameter of receiving antenna . . . 57
4.20 Measurements of wood attenuation . . . 58
4.21 Measurements of brick attenuation . . . 58
4.22 Measurements of 2 bricks attenuation . . . 59
4.23 Measurements of wood attenuation . . . 60
4.24 Measurements of brick attenuation . . . 61
4.25 Measurements of 2 bricks attenuation . . . 61
4.26 Measurements with a row of bricks . . . 63
4.27 Measurements with two rows of bricks . . . 64
4.28 Dimension of the brick hole . . . 64
4.29 Measurements with one layer of bricks . . . 65
4.30 Measurements with two layers of bricks . . . 65
4.31 Measurements with three layers of bricks . . . 66
4.32 Setup to measure lens effect . . . 67
4.33 Radiation patterns for various polarizations . . . 67

5.1 General system block diagram . . . 70
5.2 System block diagram . . . 71
5.3 AD-FMCOMMS5 Chip Link . . . 72
5.4 ZC706 Evaluation Kit [32] . . . 73
5.5 Xilinx ZC706 Block Diagram [33] . . . 73
5.6 AD-FMCOMMS5-EBZ Evaluation Board . . . 74
5.7 AD9361 Block Diagram [33] . . . 75
5.8 Antenna layout at CST . . . 77
5.9 1^{st} version printed antenna . . . 77
5.10 Parameter S11 of patch 1 . . . 78
5.11 Parameter S11 of patch 2 . . . 78
5.12 Parameter S11 of patch 3 . . . 79
5.13 Parameter S11 of patch 4 . . . 79
5.14 Radiation pattern of each patch . . . 80
5.15 Antenna radiation pattern with phase feed of all patch . . . 80
5.16 Antenna layout at CST . . . 81
5.17 2^{nd} version printed antenna . . . 82
5.18 Parameter S11 of aggregate 1 . . . 83
5.19 Parameter S11 of aggregate 2 . . . 83
5.20 Parameter S11 of aggregate 3 . . . 84
5.21 Parameter S11 of aggregate 4 . . . 84
5.22 Radiation pattern of each aggregate . . . 85
5.23 Radiation pattern of the full aggregate . . . 86

6.1 Experimental Setup 87
6.2 Phase calibration setup 88
6.3 Angle of incidence calculation 89
6.4 Beam steering algorithm diagram 90
6.5 Algorithm diagram 91
6.6 Detection method explanation 92
6.7 Results for situation where there is no movement 93
6.8 Results for situation where the person is detected at the center without brick 94
6.9 Results with bricks where the person is detected at the center 95
6.10 Results for situation where the person is detected at the right 96
6.11 Results with bricks where the person is detected at the right 97
6.12 Results for situation where the person is detected at the left 98
6.13 Results with bricks where the person is detected at the left 99
6.14 Experimental demonstration of detection behind the wall 100
6.15 Results with person detected behind the wall at center 100

List of Tables

2.1 Frequency Bands [5] 8

3.1 Results of every tests performed 39

4.1 Attenuation for different types of materials [23] 42
4.2 Average Shielding Effectiveness (SE) for different materials [21] 43
4.3 Measurements for both setups 49
4.4 Received power by USRP Rx 50
4.5 Power emitted in relation to Tx gain 51
4.6 Power emitted in relation to Tx gain and increase of power for each jump in gain 52
4.7 Attenuation results for 5.8 GHz 57
4.8 Attenuation results for UWB antenna 60

5.1 Substrate informations 76
5.2 1^{st} version antenna parameters 76
5.3 2^{nd} version antenna parameters 81

6.1 Algorithm parameters 88
6.2 Phases of each patch to perform beam steering 90
6.3 Radar features 101

List of Acronyms

ADC Analog-to-Digital Converter

CNC Computer Numerical Control

CPU Central Processing Unit

CR Cognitive Radio

CST Computer Simulation Technology

CW Continuous Wave

DAC Digital-to-Analog Converter

dB Decibel

dBm Decibel Milliwatt

DBF Digital Beamforming

FDM Frequency Division Multiplexing

FM-CW Frequency Modulated Continuous Wave

FPGA Field-Programmable Gate Array

IEEE Institute of Electrical and Electronic Engineering

IF Intermediate Frequency

LFM Linear Frequency-Modulated

LNA Low Noise Amplifier

LO Local Oscillator

LPF Low-Pass Filter

MIMO Multiple Input Multiple Output

PA Power Amplifier

PC Personal Computer

PLL Phase Lock Loop

RADAR Radio Detection and Ranging

RF Radio Frequency

SDR Software Defined Radio

SE Shielding Effectiveness

SNR Signal-to-Noise Ratio

TDM Time Division Multiplexing

USRP Universal Software Radio Peripheral

UWB Ultra Wide Band

VNA Vector Network Analyser

Chapter 1

Introduction

Over the last few years we have witnessed the emergence and paradigm shift in the design and implementation of radars. RADAR research was initially developed for military applications, due to the restricted nature of the field, the technology was extremely expensive and required a tight controlled access. With the change of paradigm and the emergence of new typologies and applications, as the automotive industry, it leads to the current strong investment in research to make them increasingly robust, efficient and, above all, cheaper.

Despite the areas covered by the new applications, research for military purposes has never been overlooked, and with the exponential growth of technology in recent years, it has also led the military in several countries to develop state-of-the-art technology to prevent possible scenarios of war. It was based on the indispensability of preventing possible scenarios of a civilian guerilla, to take advantage in the vigilance towards the enemy that the opportunity and the necessity arose for the development of this project.

At this moment the state of the art for almost all type of RF applications relapses on reconfigurable technology, which despite being somewhat expensive, when compared to traditional radars is relatively cheap. This type of technology, which encompasses FPGAs and SDR has also undergone a great evolution over the last few years allowing to apply its inherent adaptability and robustness to various scenarios.

The versatility of these technologies, arises the opportunity to develop this concept that will be able to make feasible business on a military level as it will allow security entities to assure the protection, convenience and care of millions of lives.

This dissertation is included in a working group on the SPIDER (Sensor Platform & Network for Indoor Deployment and Exterior-based Radio-frequency Awareness) project, funded by the European Defence Agency (EDA), where a total of four institutions participate. This project aimed to design a proof of concept of an innovative system that allows the introduction of sensors inside and outside of buildings that provides better coverage thus allowing the detection of people and mapping buildings with better performances.

1.1 Motivation

This dissertation follows some recent studies in which new applications for radars are suggested and studied, making them more flexible and adaptable for different situations, as well as reducing their price on a large scale.

Therefore, this dissertation is motivated by the need to develop a low cost RADAR, which is adjustable and flexible, that is able to "see" through walls, that is, to be able to detect moving targets even if they are behind walls or inside buildings. This type of RADAR presents great challenges, since the RF signals are greatly affected when propagated trougth a wall as the signal will suffer a great attenuation and consequently will loose much of the radiated energy. This may lead to failure to detect the desired target and therefore the development of a system capable of emitting sufficient power is required as implement techniques and algorithms capable of improving the probability of detection.

The development of this type of system is of great use for several scenarios, due to its flexibility it can be used at the police or military level in scenarios where the identification of hostages may be an incredibly powerful asset. Beyond to the development of the RADAR system, there are other scientific fields involved. For this work, detection algorithms were developed in addition to all digital signal processing, measurement techniques for material characterization and antenna design.

1.2 Objectives

The objectives of this dissertation are mainly focused on the development of a RADAR that is highly adaptable to several scenarios. One of the key points is to be able to detect the presence of people inside buildings or through walls, but also to allow the detection of movements and to know the origin of these movements. Therefore it is of extreme importance before starting the implementation of the RADAR, to characterize the attenuation caused by the materials that compose the walls and that way adapt the power to emit, as well as, choose the best algorithms to implement that are capable of improving the Signal-to-Noise Ratio (SNR) and increase the detection probability.

1.3 Thesis Organization Overview

This dissertation was organized in seven chapters in order to provide a good analysis and readability of the contents:

- **Chapter 1: Introduction** - In this chapter a framework of the work to be developed is described, as well as the problem to be solved. The more general objectives, motivation and contributions of this work are also presented through this chapter.

- **Chapter 2: Radar Basic Principles** - This chapter presents a brief history about RADAR, its basic operating principles and the most important parameters, but also the most common problems encountered in the study and implementation of radars.

- **Chapter 3: Radar Through Walls** - In this chapter it is presented the major challenges in the development of radars through walls, their state of art and the possible solutions are proposed to try to solve them. Therefore the techniques and architectures to be developed in the RADAR as well as their theoretical backgrounds are presented.
- **Chapter 4: Materials Characterization** - It is in this chapter that a study is made about works and measurement devices that are already existent to characterize the RF propagation of construction materials of materials. It is then based on these same works that are presented the setups developed, as well as, the media system to characterize mainly bricks. The results obtained for all the scenarios are presented with a critical analysis attached.
- **Chapter 5: Radar System Design** - This is the chapter where all the work developed and results obtained throughout the thesis are presented. It is presented the RADAR system implementation, the analysis and explanation of all constituent blocks and the presentation of the developed antennas for the system.
- **Chapter 6: Results and Analysis** - For this chapter it was intended to present and analyse the results obtained for all tests performed, an explanation is given about the algorithms developed as well as the results obtained by the proposed measurement system. For all of them a critical analysis is also made.
- **Chapter 7: Conclusion and Future Work** - The last chapter presents the conclusions of all developed work, the points to retain of the analysis of the results acquired, but also some considerations of a possible improvement in the future of this dissertation.

1.4 Thesis Contributions

As a result of the work developed by the author throughout this dissertation, the following publication was accepted:

[1] **D. Matos**, D. Malafaia, T. Varum, J. Vieira and J. Matos "SDR based RADAR System for Through Wall Detection" in 11.° Congresso do Comité Português da URSI "Novas tecnologias para a mobilidade".

Chapter 2

Radar Basic Principles

In this chapter, it is intended to present the fundamental theoretical concepts to understand the basic principles of RADAR operation.

2.1 Brief Radar History

The history of RADAR dates back to the beginning of the twentieth century when in 1904, the German Christian Hűlsmeyer used, for the first time, radio waves to detect the presence of distant metallic objects, the developed system was called the telemobiloscope.

Until the year 1922 there was not much research, but then some governments realized the potential of this application for military purposes. In that same year Hoyt Taylor and Leo C. Young researchers working for U.S. Navy used a RADAR system to discover a ship for the first time.

It was during World War II that the technology and RADAR systems grew rapidly in an attempt of countries, such USA or Soviet Union, to anticipate their opponents movement and to detect their ships and bomber air crafts.

Since the end of World War II the applications of radars have been increased and beside of the military purposes, now are used for everyday use as for example to help parking a car, to measure the speed of the cars to guarantee the accomplishment of road rules, and others, [1] [2].

2.2 Radar Parameters

The principle of a RADAR system is based on the emission of electromagnetic waves, in a particular type of waveform, a sine wave for example, in a pre-defined direction. That emitted energy will the be reflected by the environment. The RADAR uses those reflected wave, also called echo or scattering, to get information about the target, as well as for example the distance or the direction of the reflecting object, as can be seen in the figure 2.1, [3] [4].

When the backscatter (reflections in the opposite direction to the incident rays) happens, the reflected wave will have a time delay in relation to the emitted wave. With that information is then possible to determine the range to the object or the distance.

So if we measure the time taken by the wave to travel to the target and return, T_R, and assuming that the electromagnetic waves propagates approximately at the speed of light in vacuum, $c = 3 \times 10^8\ m/s$, the range R is given by the following expression

$$R = \frac{c\,T_R}{2} \tag{2.1}$$

In modern RADAR systems it is possible to measure other useful information such as altitude, velocity of an object, its position among others.

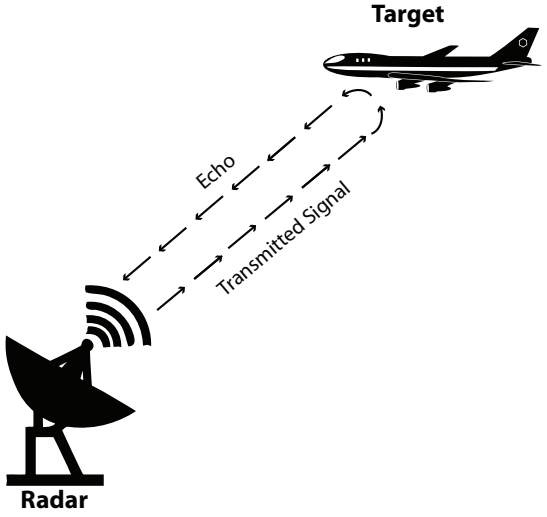

Figure 2.1: Radar Principle

The basic parts of a RADAR can be observed in figure 2.2 where they are illustrated in a block diagram. Usually most radars are composed by the following components:

- Transmitter - the transmitter is responsible for generating and modulating the signals to be sent to the antenna.

- Receiver - its function is to treat the signal received by the the antenna, with several stages of detector filters and later presents the results on a display.

- Antenna - the transmitter power is radiated to the free space using a directive antenna which concentrates the energy into a narrow beam. This process is applied in an identical way on the reception.

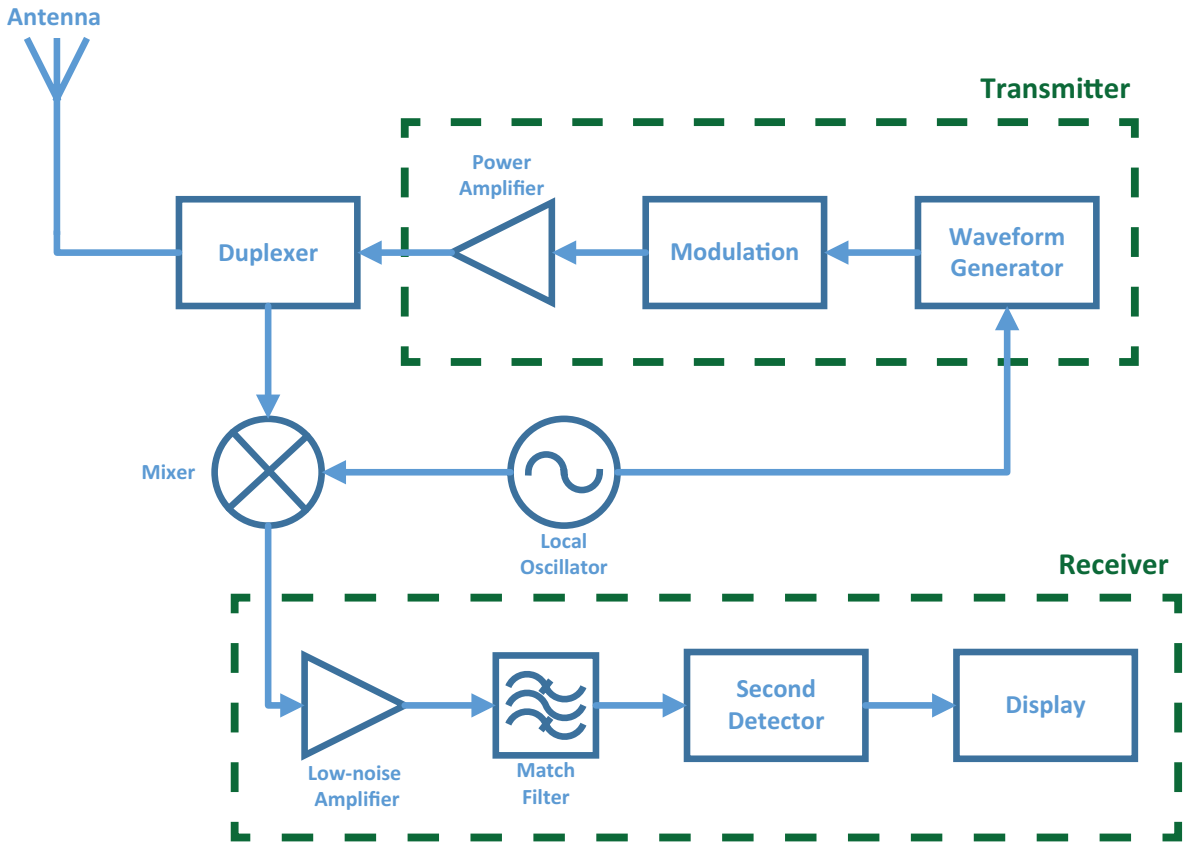

Figure 2.2: Basic Radar Block Diagram example

This principle can be applied to a big range of frequency bands. Table 2.1 shows an overview of the different frequency bands and their nomenclature. This table has been standardised by the Institute of Electrical and Electronic Engineering (IEEE) in IEEE std 521-2002.

Having seen the versatility of the RADAR, it is easily perceived that we can apply this concept to several applications beyond the military. The civil applications have been increased mainly for marine and air navigation. Some of these applications are presented below:

- Air Traffic Control - For this situation radars are deployed for the purpose of controlling air traffic route and in the vicinity of airports. For this kind of applications the traffic is monitored by high-resolution radars.
- Aircraft Navigation - In this case the radars are used to predict and warn the pilot for example about regions of precipitation.
- Ship Safety - In this scenario the radars have the objective to notify the ship's captain of a potential collision with other ships especially in situations of bad visibility.
- Space - The radars allowed for spaceships to find the docking and landing point, for example in space stations or satellites.

Band designation	Frequency Range	Applications
HF	3 - 30 MHz	Over-the-horizon surveillance
VHF	30 - 300 MHz	Long-range air surveillance
UHF	300 - 1000 MHz	Long-range air surveillance, Ground penetrating RADAR
L	1 - 2 GHz	Long-range air surveillance
S	2 - 4 GHz	Medium-range air surveillance
C	4 - 8 GHz	Medium-range air surveillance, Long-range tracking
X	8 - 12 GHz	Short-range tracking, Missile guidance
Ku	12 - 18 GHz	High resolution mapping
K	18 - 27 GHz	Weather
Ka	27 - 40 GHz	Very high resolution mapping
V	40 - 75 GHz	-
W	75 - 110 GHz	Automotive
mm	110 - 300 GHz	-

Table 2.1: Frequency Bands [5]

- Highway safety - The RADAR is used as a speed meter by the police in order of control the velocity and enforcing the speed limits.
- Military - Most of civil applications are also applied in military scenarios for surveillance, navigation and for the control of weapons in battlefield or missions.

2.2.1 Radar Equation

The RADAR equation is probably the most important relation among the factors that influence the characterization of RADARs. This equation relates the range and the characteristics of the transmitter, receiver, antenna, the object for identification and the environment in question. This expression is useful not only to estimate the maximum range but to understand the basic principle of operation of the RADAR, [3], [4].

Considering an isotropic antenna (antenna which radiates equally in all directions) that radiates a power of P_t, the power density of the antenna at a distance R from the RADAR will be equal to the transmitted power divided by the surface area of a sphere, that can be written with the following expression

$$Power\ density\ of\ a\ signal\ radiated\ by\ an\ isotropic\ antenna = \frac{P_t}{4\pi R^2} \tag{2.2}$$

With directive antennas the radiated power P_t, is preferentially transmitted to some particular direction. The gain G is only to increase the radiated power in the direction of the object. So the power density of a signal radiated by a directive antenna with some transmit-

ting gain G is given by

$$Power\ density\ of\ a\ signal\ radiated\ by\ directive\ antenna = \frac{P_t\, G}{4\pi\, R^2} \tag{2.3}$$

When the transmitted radiation intercepts the target a small part of that power is radiated to all directions. The measurement of the quantity of incident power in the target that is radiated back to the RADAR is called the RADAR cross section, σ, the power density of the echo is presented next

$$Power\ density\ of\ echo = \frac{P_t\, G}{4\pi\, R^2} \frac{\sigma}{4\pi\, R^2} \tag{2.4}$$

Considering now the effective area of the receiving antenna, A_e, that captures the energy coming from echo wave, and knowing that P_r is the received power, it is then possible to write the previous expression in the following form:

$$P_r = \frac{P_t\, G\, \sigma A_e}{(4\pi)^2\, R^4} \tag{2.5}$$

Another way to represent this equation is considering that the echo wave power is equal to the minimum detectable signal, or sensitivity of the system, S_{min}. This way it is possible to rewritten the previous expression in order to the maximum range, R_{max}. This R_{max} is the maximum distance that the RADAR can detect. The new expression, the fundamental form of RADAR equation is

$$R_{max} = \left[\frac{P_t\, G\, A_e\, \sigma}{(4\pi)^2\, S_{min}} \right]^{1/4} \tag{2.6}$$

Where S_{min} is represented by:

$$S_{min} = k\, T_0\, B\, F_n \frac{S}{N}_{min} \tag{2.7}$$

- k = Boltzmann's constant;
- T_0 = reference temperature (290 K);
- B = receiver bandwidth;
- F_n = noise factor;
- $\frac{S}{N}_{min}$ = minimum signal-to-noise ratio;

The relation between transmitting gain and the receiving effective area is given by antenna theory,

$$G = \frac{4\,\pi\,A_e}{\lambda^2} \tag{2.8}$$

- λ = wavelength;

The equation 2.6 can be represented in two different manners

$$R_{max} = \left[\frac{P_t\,G^2\,\lambda^2\,\sigma}{(4\pi)^3\,S_{min}}\right]^{1/4} \tag{2.9}$$

and

$$R_{max} = \left[\frac{P_t\,A_e^2\,\sigma}{4\pi\,\lambda^2\,S_{min}}\right]^{1/4} \tag{2.10}$$

None of these expressions consider factors that condition the practical performance of the RADAR. In a practical situation the values obtained with these expressions shall be subject to caused by the real-world environment.

2.2.2 Noise Factor

The main factor that limits the sensitivity (equation 2.7) of a receiver or performance of a system is noise. Due to this it is convenient to obtain some way to understand and describe the effect of the noise in systems overall, [3], [4].

Noise is basically undesired electromagnetic energy which interferes with the behaviour of the receiver on detect the desired signal. The noise can have multiple origins, such as, the receiving antenna, the environment or the noise created by thermal motion in the ohmic blocks of the receiver. This last mentioned is called thermal noise or Johnson noise. This noise is directly proportional to the temperature of the blocks/circuits that compose the receiver.

The thermal noise generated by a receiver is equal to:

$$Thermal\ noise = k\,T\,B_n \tag{2.11}$$

- k = Boltzmann's constant;
- T = reference temperature (290 K);
- B_n = receiver bandwidth (Hz);

The noise power in non ideal receivers is often greater than what can be accounted for by thermal noise alone.

Due to this in practical receivers some noise is added by other components, such amplifiers, filters, mixers due to mechanisms other than thermal motion. Therefore the total noise at

the receivers' output is equal to the thermal noise of an ideal receiver and one factor called noise figure. This noise figure, denoted by F_n is defined by the following equation:

$$F_n = \frac{N_0}{k\, T_0\, B_n\, G_n} \tag{2.12}$$

- N_0 = output noise from the receiver;
- k = Boltzmann's constant;
- T_0 = reference temperature (290 K);
- B_n = receiver bandwidth (Hz);
- G_n = available gain;

If we consider N_0 as the output noise, the available gain is the ratio between the output signal S_0 and the input signal S_i and the thermal noise (equation 2.11) as the input noise, the equation 2.12 can then be rewritten and take the following form:

$$F_n = \frac{S_i/N_i}{S_0/N_0} \tag{2.13}$$

With this expression the noise figure can be interpreted as a degradation of the SNR of the signal that cross the receiver, and it is possible to rewrite the equation of the sensibility and for last put this losses in the RADAR equation.

$$S_i = \frac{k\, T_0\, B_n\, F_n\, S_0}{N_0} \tag{2.14}$$

Considering S_{min} as S_i, corresponding to the minimum ratio of the output SNR necessary, then the equation 2.7 take the form:

$$S_{min} = k\, T_0\, B_n\, F_n \left(\frac{S_0}{N_0}\right)_{min} \tag{2.15}$$

Finally, by combining the equation 2.15 with the equation 2.6 the RADAR equation can then be described by:

$$R^4_{max} = \frac{P_t\, G\, A_e\, \sigma}{(4\pi)^2\, k\, T_0\, B_n\, F_n\, (S_0/N_0)_{min}} \tag{2.16}$$

2.2.3 Radar Cross Section

A RADAR can detect or identify a target only because the received echo signal. Therefore it is necessary in the RADAR system design to know how to quantify this echo and be able do describe the target in terms of size or shape, [3], [4].

For this purpose an effective area of the target is assign an effective area called *RADAR cross section*. The RADAR cross section is a "fictional" area that is exposed to electromagnetic energy, intercepts an amount of power and then disperse that energy in all directions equally. To this phenomenon is called *scattering*.

The energy scattered back to the RADAR (*backscattering*) creates the echo of the target at the RADAR. The definition of RADAR cross section is presented in the next equation:

$$\sigma = \lim_{R \to \infty} 4\pi R^2 \left| \frac{E_r}{E_i} \right|^2 \tag{2.17}$$

- R = distance between RADAR and target;
- E_r = reflected field strength at RADAR;
- E_i = reflected of incident strength at RADAR;

The characteristics of the echo will depend of the nature, size or shape of the target's section exposed to the electromagnetic waves. For example, the amplitude of the echo is small if the target is smaller than the wavelength as the wavelength is too long to give all the details of the target.

2.2.4 Radar Resolution

The RADAR resolution is the ability to detect different targets (two or more) that are very close from each other, distinguish them as distinct objects and not as a single block. This resolution depends of many factors, but the most important are the width of the pulse, the nature of the target and the efficiency of the system, [3], [4].

The RADAR resolution, represented by ΔR, can be described for the next equation:

$$\Delta R = \frac{c}{2B} \tag{2.18}$$

- c = speed of light;
- B = bandwidth;

By analyzing the previous equation it follows that it is possible to achieve a higher resolution by increasing the bandwidth. The price to be paid for the increase in the resolution will be reflected in a lower maximum range of the RADAR. The next image has the comparison between one RADAR which has a high resolution and other RADAR with a small resolution and the respective response obtained.

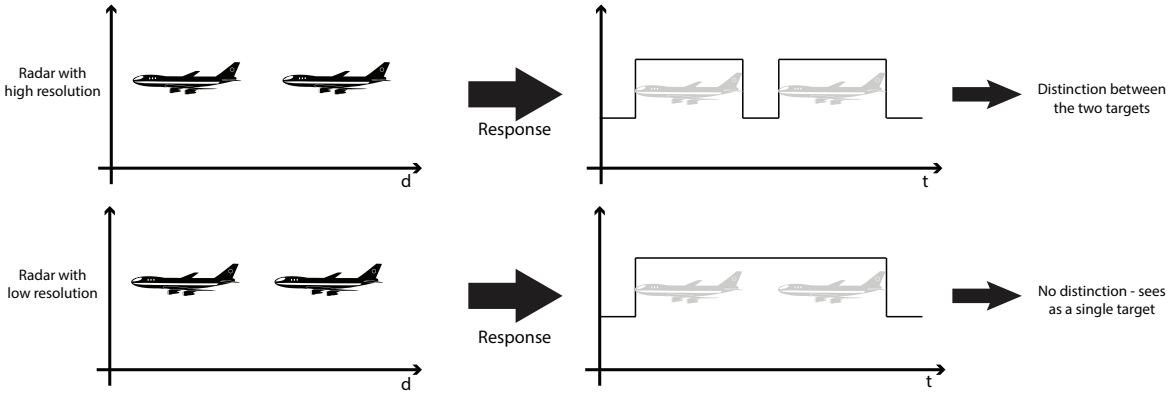

Figure 2.3: Radar Resolution

2.2.5 Doppler Effect

The Doppler Effect is based of the CW RADAR. The Doppler effect consists in a variation in the frequency or wavelength for an observer that is moving in relation to the signal source. This effect was proposed by Christian Doppler an Austrian physicist in 1842, [3], [4].

The most common example to explain the Doppler effect is the frequency heard from a siren or horn from a moving object. It is precipitable that the sound is different when the vehicle approaches, passing or when it distanced itself from the observer.

The frequency when compared with emitted frequency is higher when the vehicle is approaching the observer, it is equal during the instant of passing by and is lower when the vehicle goes away from the observer. The figure 2.4 has the illustration of the given example.

The difference between the emitted frequency and the echo received is called Doppler frequency shift, denoted by f_d, and it is given by the following expression

$$f_d = \frac{2\, f_0\, v_R}{c} \tag{2.19}$$

- f_0 - emitted frequency;
- v_R - relative velocity of target to the RADAR;
- c - speed of light.

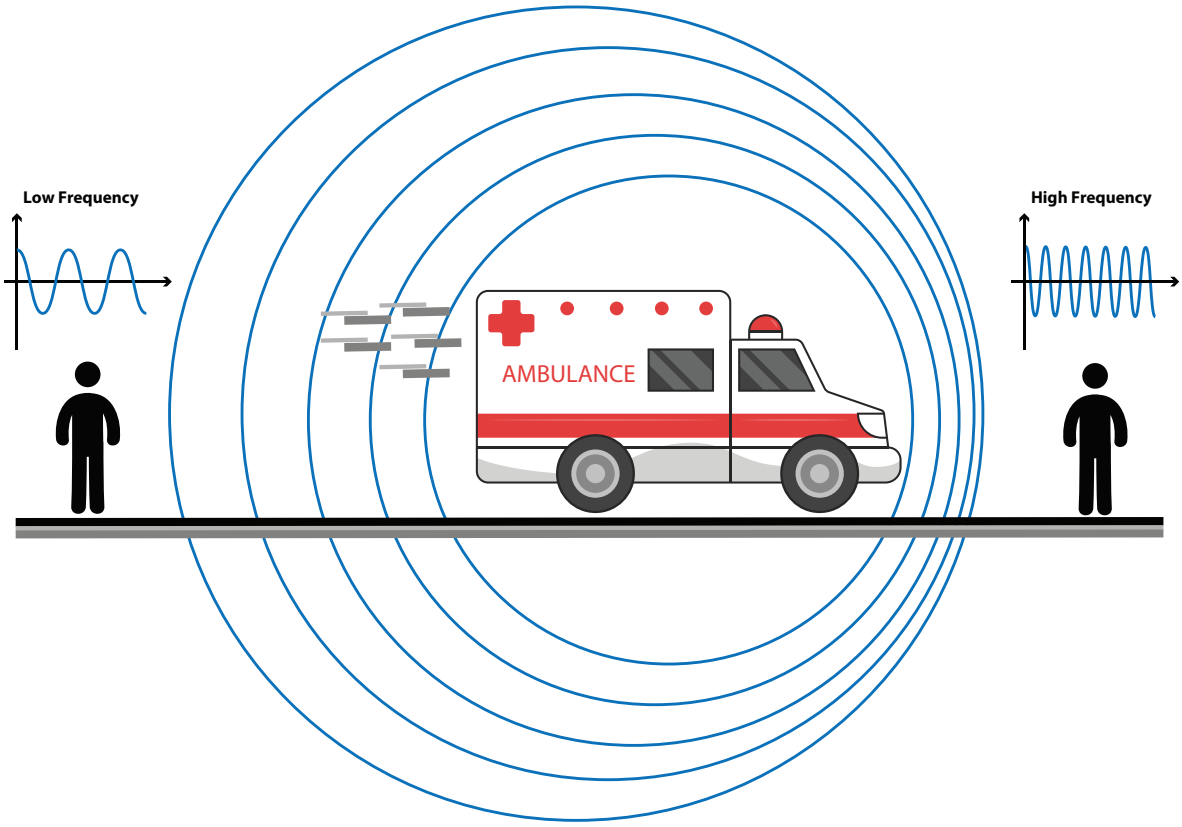

Figure 2.4: Doppler Effect

2.2.6 Radar Clutter

When the RADAR must detect a small target located on either the surface of the sea or land, the interfering unwanted clutter echoes can severely limit the detectability of the target. When clutter power dominates receiver noise power, the range equation is simply reduced to an expression for the signal-to-clutter ratio. This ratio is equal to the ratio of the target cross section to the clutter cross section. If clutter is distributed more or less uniformly, the clutter echo will depend on the area illuminated by the RADAR resolution cell. Surface (ground or sea) clutter is described by the ratio of the clutter echo to the area illuminated by the RADAR, [3], [4].

2.3 Types of Radar

As previously explained, since the construction of the first RADAR, various types of RADAR system have been developed. There is available, nowadays, a wide range of radars where can choose a variety of configurations for transmitter, the receiver, the antenna, the wavelength, the waveform, the periodicity of emission beyond others. In this section some of them will be addressed, [3] [6]

2.3.1 Pulse Radar

A pulse RADAR is a system that uses pulse-timing techniques to determine the distance to a target. The RADAR emits short and powerful pulses and then in the silent period (period of time it does not transmit), receives the echoes. Usually the modulation of transmission pulses is very short, typically the duration of the pulse is between 0.1 and $1\mu s$.

Most of the pulse radars are designed for big distances and due to that the main applications for this type of RADAR is in military field. In nowdays are also used in air traffic control, weather or measure the respiratory rate. [7], [4].

2.3.2 CW Radar

As the name itself indicates the CW RADAR is a system that transmit continuously electromagnetic energy in a known frequency. The advantages of using this type of RADAR are simplicity of use and implementation, there is almost no limit in range and for that reason is possible to use them in big or small distances. For these reasons the applications of this RADAR goes from monitoring sensors, such heart rate or respiratory activity, to traffic control RADAR which measure the car's speed in order to detect infractions [7], [4].

2.3.3 FM-CW Radar

The FM-CW RADAR is one type of a CW RADAR whereas unlike the previous is used frequency modulation. His principle of operation is based on CW RADAR, but in this case the frequency of the wave is increased along the time. These days the main applications for this type of RADARs are focused on automotive safety, such as, advanced driver assistance systems. FM-CW RADARs fulfils the requirements of automotive active safety systems because of their accurate short-range measurements and low sensitivity to clutter, [7], [4].

Chapter 3

Through-the-Wall Radar

As mentioned in the previous chapters, the aim of this work is to develop a RADAR capable of detecting people through opaque obstacles. This chapter presents the state of the art of the existing techniques taken into account for the implementation of the system and some published works considered relevant.

3.1 Introduction

The interest and the investigation in the detection of people through walls has undergone a great growth in the last years due to the range of applications in which it can be used. The application that motivates the most advances is the military industry, since it can be applied in situations of hostage rescue, but also for rescue in natural catastrophes scenarios [8].

Detection of people using radars can be challenging. Since this detection can require some movement performed by trapped target, as the heart beat or even is breathing pattern, it is then possible to perform this detection as these movements will cause changes in the frequency, phase or amplitude of the transmitted signal. When considering the scenario of detection through walls the challenge becomes more complex since the changes caused in the signal that were referred are in much less scale especially if the scenario contains bricks, concrete or other obstacles.

As will be described in more detail in section 4, the attenuation caused by these materials will be one of the major challenges to overcome due to the degradation caused in the signal sent. As a demonstrative example, if it is intended detect a person through a wall having 65 Decibel (dB) attenuation would require about 4 kW of power. This can be a great obstacle, as it requires the use of large power supplies and adequate transmitters, which can be quite expensive.

Considering a system presented in figure 3.1,[1], we can also identify another adversity. The clutter, which was already presented in section 2.2.6 are unwanted signals/echoes. These echoes can cause interference and make it difficult to detect objects or targets in question, since they have high energy and can saturate the receiver and thus it will be more difficult to

[1]Figure taken from: `http://www.extremetech.com/extreme/133936-using-wifi-to-see-through-walls` Accessed on: 25-08-2017

detect signals with information about a possible detection but have less energy. A concrete example can be reflections on the ground plane, in the sea or even in birds. These reflections may have sufficient power to affect the performance of the RADAR system,[4].

Figure 3.1: Formalization of problem

In view of the main problems faced in this type of applications, it is now necessary to outline a solution to achieve the objectives that have been proposed. Since so-called traditional radars are quite expensive, it is necessary according to the available budget to implement a low-cost version and at the same time be highly reconfigurable.

Due to the problems faced we decided to separate this work into two different phases/parts. The first part of the work consists of the study and characterization of materials, that is, the measurement of the attenuation caused by different materials as well as their reflection. All related information is presented in section 4.

For the RADAR system it was decided to use a SDR architecture, because besides being relatively low cost, it has the advantages of being incredibly flexible and can be easily adapted to the most varied scenarios. It was also understood that the implementation of a MIMO system would be a good way to get around some adversities, since it would allow a greater

diversity of both transmitted and received signals. Finally, the development of beamforming algorithms was considered important because it allows a significant improvement of the SNR because it permits focusing the beam of the antenna in a certain direction that grant the reception of the maximum possible energy.

These proposals are presented in more detail in the following sub-chapters, as well as their theoretical background. Note that these are the most relevant techniques for the work and in this way it is equally given more emphasis throughout this chapter. Other techniques used in a timely manner will be explained in the same way when they are used.

3.2 Software Defined Radio (SDR)

The wireless communications systems have, in the last decades, undergone great growth and consequently a constant evolution. With the emergence of new protocols, the existing systems until then were not adequate to the needs, because the main problem was about the redesign/adjustment of the system. It was for this reason that led to the investigation of these new radios. Since the redesign of the system is the most expensive and time-consuming process, it was important to develop a radio with the up-to-date software and hardware, that is, reconfigurable radios, which ensure that the needs are aware of existing technologies. SDR were created, which are now viable solutions for the construction/implementation of low cost radars. [9]

It was then in 1995 that the term arose, suggested by Joseph Mitola, to designate reconfigurable radios. In this paper the following definition was proposed:

> *"A software radio is a radio whose channel modulation waveforms are defined in software. That is, waveforms are generated as sampled digital signals, converted from digital to analog via a wideband Digital-to-Analog Converter (DAC) and then possibly upconverted from IF to RF. The receiver, similarly, employs a wideband Analog-to-Digital Converter (ADC) that captures all of the channels of the software radio node. The receiver then extracts, downconverts and demodulates the channel waveform using software on a general purpose processor."* [10]

A SDR, in its ideal model, is defined by a radio that implements its entire interface using software, making them highly reconfigurable. The ideal model of the transceiver proposed by Joseph Mitola is present in the figure 3.2. Looking at the figure it can be verified that the front-end of the radio consists of an ADC and a DAC that perform conversions of the analog signal to digital signal and vice versa. [9] [11]

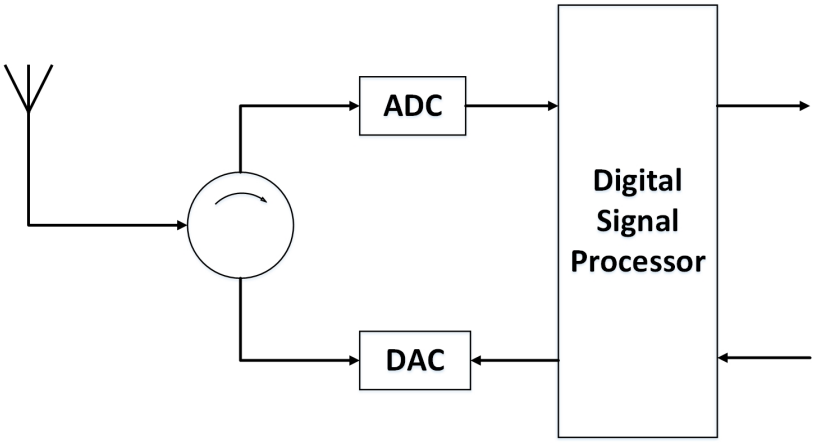

Figure 3.2: SDR Ideal Model

Some more well known examples of SDRs and commonly used for research and introduction to the concept, USRPs are presented below.

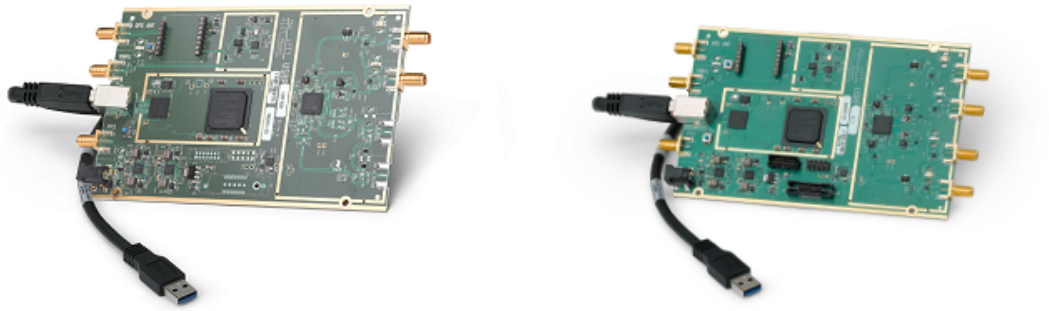

(a) USRP B200 (b) USRP B210

Figure 3.3: USRP Examples

The difference between these USRP/SDR passes for example the possibility of building a full duplex radio, MIMO 2x2 with the USRP of the figure 3.3(b) [2], whereas with the USRP of the figure 3.3(a) [3] is only possible the implementation of a single input single output full duplex radio.

[2]Figure taken from: `https://www.ettus.com/product/details/UB210-KIT`. Accessed on: 18-04-2017
[3]Figure taken from: `https://www.ettus.com/product/details/UB200-KIT`. Accessed on: 18-04-2017

3.2.1 Front-End Architectures

Since the ideal SDR model presented is not possible to implement, it was necessary to consider other types of architectures. These architectures differ in the location where the digitalization occurs, and are presented in the following sections for both transmission and reception architectures.

3.2.1.1 Transmitter Architectures

Baseband Digitalization In this type of architecture the signal is digitized in the baseband stage, that is, the DAC is placed at this stage, as is visible in the figure 3.4 and the baseband signal undergoes two up-conversion to pass the RF signal. Although the architecture is more usual, easier to implement and have a low power consumption, it also has some limitations. These limitations focus primarily on the bandwidth of components, especially the DAC, making the system less versatile.

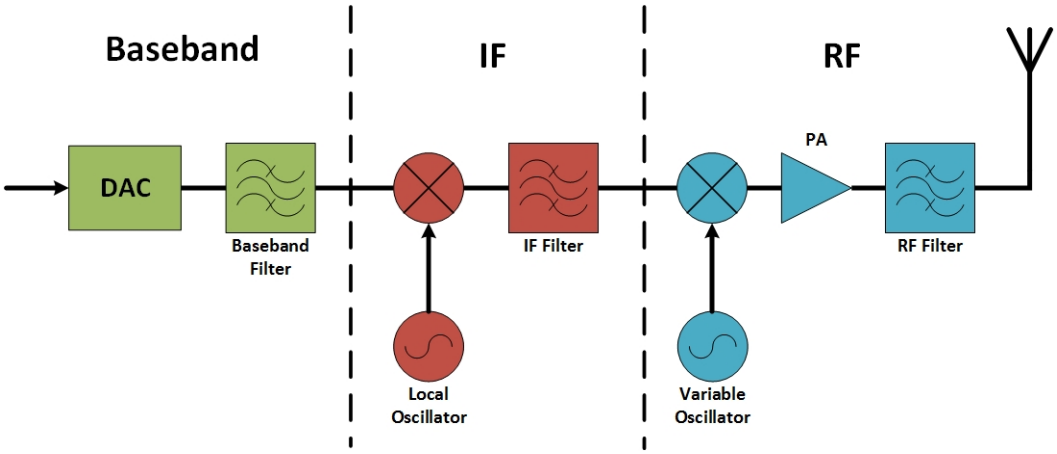

Figure 3.4: Transmitter baseband digitalization architecture

IF Digitalization In this step, the DAC is placed in the IF stage rather than the baseband step, as shown in figure 3.5, whereby the digitalization of the signal is now effected in an architecture in which all the baseband processing is performed by software and the signal only suffers an up-conversion to pass the RF signal.

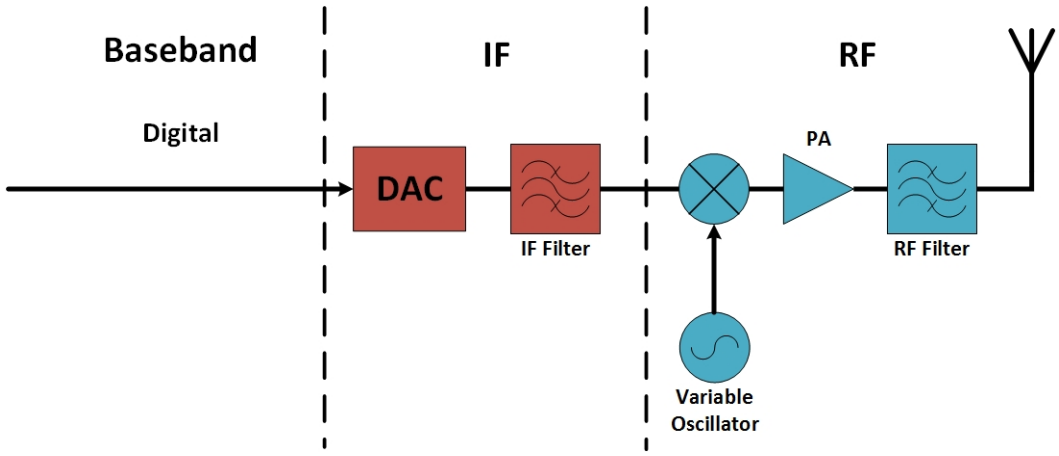

Figure 3.5: Transmitter IF architecture

RF Digitalization For the latter case, RF digitalization architecture is the one that most resembles the ideal SDR model, as it is depicted in the figure 3.6. This architecture, despite being the one closer to the ideal model and provide a greater number of solutions it is also the one that presents more difficulties and obstacles. One of the biggest challenges is to achieve a DAC with a high bandwidth and sampling rate and a Power Amplifier (PA) that introduces low noise into the system.

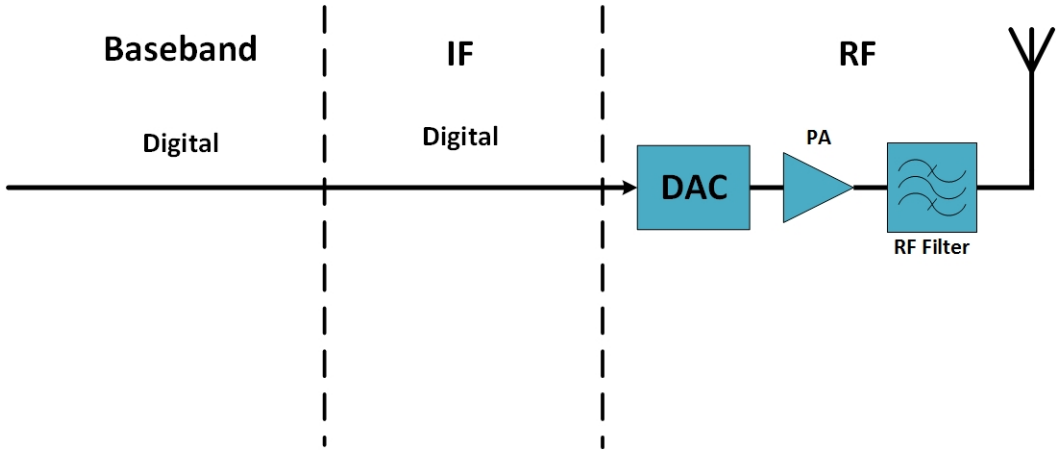

Figure 3.6: Transmitter RF architecture

3.2.1.2 Receiver Architectures

Baseband Digitalization In this type of architecture, the signal digitization is performed in the baseband stage, as can be seen in the figure 3.7. This is the most common type of receiving architecture in which the RF signal is passed to baseband after undergoing two down-conversions and the ADC is also placed in this step. Although it is the most used architecture, it is not the most appropriate for SDR, since narrowband components are used that in spite of the low energy consumption will place restrictions on the behaviour of the SDR, making it limited to a single function, [9] [11].

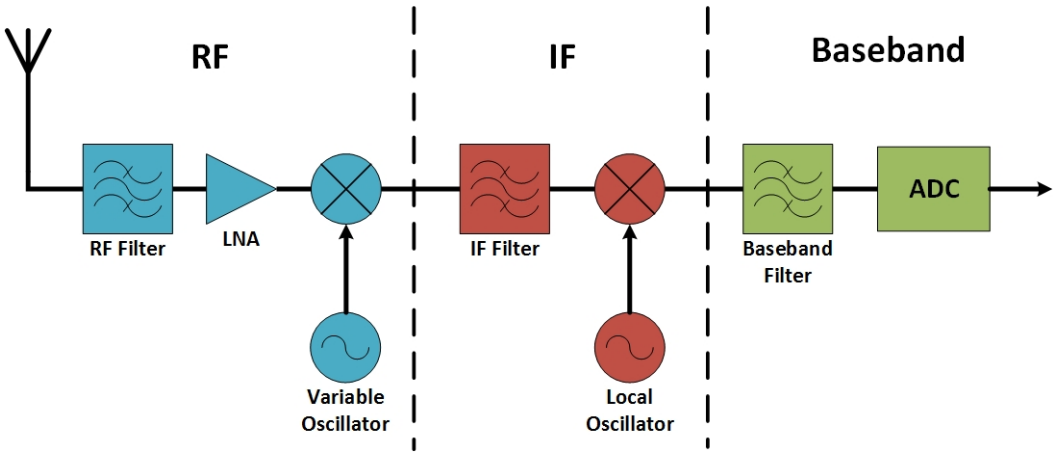

Figure 3.7: Receiver baseband digitalization architecture

IF Digitalization In the second architecture the ADC is placed in the IF step as shown in the figure 3.8. This type of configuration allows for greater bandwidth compared to the one presented previously and allows a greater number of standards implemented since the reception bandwidth is larger because all the baseband part is implemented by software thus eliminating some components. In this case the RF signal only undergoes a down-conversion to IF, [9] [11].

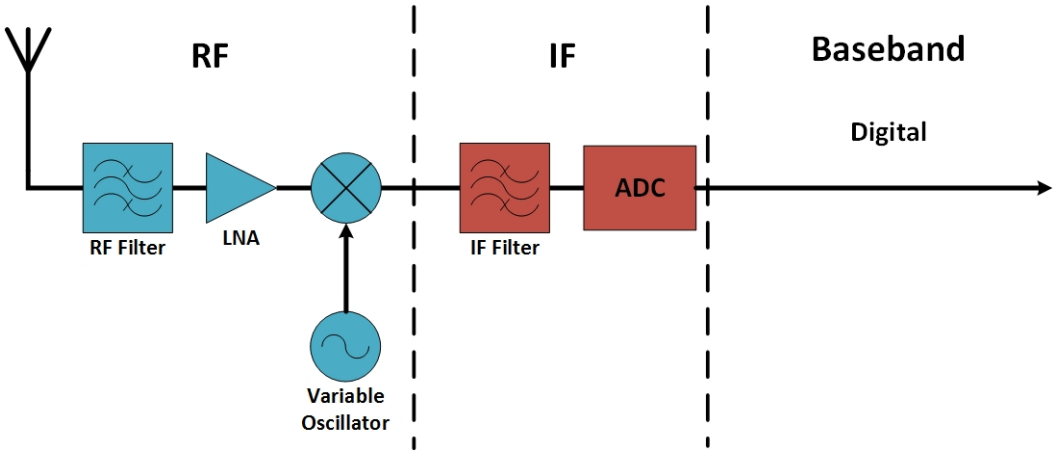

Figure 3.8: Receiver IF architecture

RF Digitalization Placing the ADC in the RF step as pictured in the figure 3.9 is the most equivalent architecture of the ideal SDR proposed by Joseph Mitola. Despite the advantages that this architecture presents, it also poses great challenges. The ADC must be able to meet various specifications, including having a large dynamic range and high sampling rates. The Low Noise Amplifier (LNA) should introduce low noise into the system and cover the whole spectrum. In terms of digital signal processing, large processing capacity is required in order to process the high number of samples from the ADC. Besides these restrictions, it is also the most expensive architecture, but it manages to have a good behaviour to all situations, supporting several protocols and modulation techniques, [9] [11].

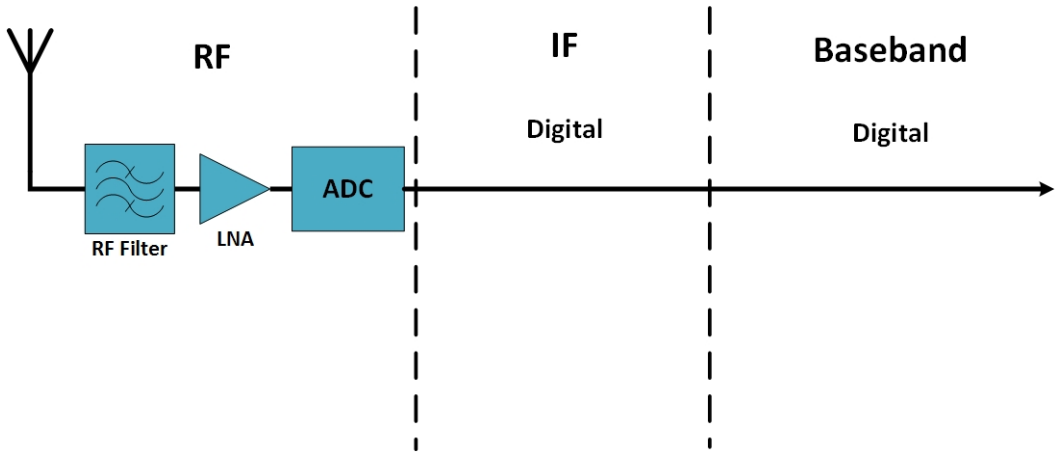

Figure 3.9: Receiver RF architecture

3.2.2 SDR Advantages

As already mentioned the implementation of the ideal SDR model is not totally possible. In spite of this it has a flexible architecture and adaptable to the different situations to which it is exposed. So these characteristics put this type of radios in advantages over conventional radios. Among others these are the factors that stand out in the SDR, [9].

- **Multifunctionality** - The implementation of an SDR allows to to support additional protocols just by download a software update. In the case of conventional radios the distribution of complementary services is limited since they are reduced to the protocol initially implemented.

- **Global Mobility** - Unlike conventional radios, SDRs are able to adjust and reconfigure to various standards and protocols. In this way, this capability provides the advantage of adhering to the scenarios to which they are subject, being able to interact with several protocols in several geographic points.

- **Compressing capacity and energy efficiency** - Instead of large-scale architectures that serve conventional radios, SDRs are able to have a more compact implementation that can provide greater energy efficiency because of its architecture.

- **Ease of construction** - Generally RF components have oscillating performances which hinders their standardization. As SDRs can perform a scan of the signal, the amount of these components will be greatly reduced, as will the parasitic elements introduced by them. In this way the construction of SDR is quite simpler than the conventional ones.

- **Constant update** - With wireless communications constantly evolving, radios will need regular updates. Now these updates should not interfere with the performance of the radio and must be performed in real time. In this way, the SDR update boils down to a simple software download, whereas in conventional radios it would involve hardware changes.

3.2.3 Cognitive Radio(CR)

With the concept of SDR defined, Joseph Mitola comes up with a new concept, a new layer applied to the SDR platform called Cognitive Radio (CR). This new radio can be seen as a smart radio that knows the environment and conditions to which it is subject, thus allowing to use its location an knowledge of the RF spectrum usage. The CR can make its own decisions based on the knowledge that is acquired by itself, in order to provide the best service to the users. In making these decisions, the CR also needs to obey the basic rules of spectrum sharing, it must be able to operate in a large frequency band, it must be able to withstand various standards and be reprogrammable, just as it was the SDR. The main advantage of the CR in relation to SDR is essentially that it is able to make its own decisions.

3.3 MIMO Radar

A MIMO RADAR is a system with multiple transmission and reception points (such as antennas), as shown in figure 3.10. The MIMO concept emerged for enhanced wireless communications performance, and uses multiplexing techniques to improve the range and resolution of the system, [12].

Let us consider a narrowband signal system which has M_t antennas for transmission and M_r for receiving. This MIMO system has a baseband signal that is transmitted by the mth transmitting antenna and is denoted as $x_m(n)$. Assuming that θ is an angle and considering that the propagation is almost perfect the signal that indicates de location of a target is given by the expression:

$$\sum_{m=1}^{M_t} e^{-j2\pi f_0 \tau_m(\theta)} x_m(n) = \mathbf{a}^*(\theta)\mathbf{x}(n), \quad n = 0, 1, ..., N-1 \tag{3.1}$$

where f_0 is the central frequency of the carrier, and $\tau_m(\theta)$ is time that the signal travels from the mth transmit antenna until the target in question. N represents the number of samples acquired of the transmitted signal and

$$\mathbf{x}(n) = [x_1(n) \;\; x_2(n) \;\; ... \;\; x_{M_t}(n)]^T \tag{3.2}$$

and

$$\mathbf{a}(\theta) = \left[e^{j2\pi f_0 \tau_1(\theta)} \;\; e^{j2\pi f_0 \tau_2(\theta)} \;\; ... \;\; e^{j2\pi f_0 \tau_{M_t}(\theta)}\right]^T \tag{3.3}$$

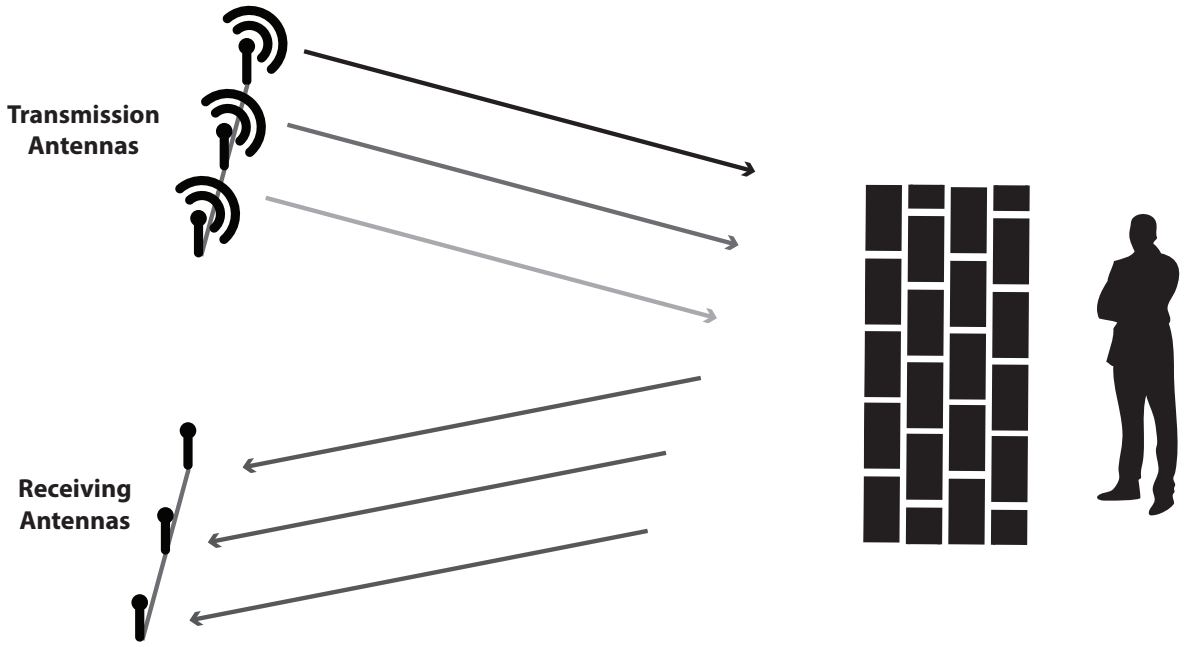

Figure 3.10: Basic MIMO Radar

In the MIMO RADAR there is a wide range of techniques to process the transmitted and received signals. For example, is usual to consider that the waves emitted by the transmitter are orthogonal that although it is not a requirement for MIMO RADAR will make easier the processing. The reason why is considered this is because the transmitted signal can be or not correlated to each other, and then the receiving antennas have to separate that signals, what can make the processing a bit harder.

To achieve the orthogonality there are usually two methods, or Time Division Multiplexing (TDM) or Frequency Division Multiplexing (FDM). This two methods however can have a bad performance if the coherence is lost, and since the scatter response of the obstacle is time-varying or frequency-selective limits the capacity of to combine the signals coherently. To solve this problem usually is introduced a correlation between the signals in order to improve the system.

Although there are several types of MIMO RADAR, there are usually two that are considered the basic operating regimes of such a RADAR. The first is called *statistical* MIMO RADAR, where both the transmitting antennas and receivers are far apart from each other which allows the signals to be collected independently. The second case, *coherent* MIMO RADAR, that is completely the opposite of the one presented previously. In this case, both the transmitting and receiving antennas are positioned close to one another, which means that the response will be the same for all antennas, only affected with a slight delay.

Despite of all advantages that MIMO can bring, depending on the case, the most usual improvements in the systems are:

- Target detection performance;

- Accuracy in angle estimation;
- Minimum detectable velocity decreases;

By giving a few concrete examples, if it is considered the first type addressed, *statistical* MIMO RADAR, which has the individual and widely separated transmitting and receiving antennas, allows the various received signals as well as the angles of those same signals to improve the performance of the detection. Likewise, it reduces the likelihood of a false detection occurring in case the target is failed, all due to the diversity of the signals that are received.

Regarding the second type presented, *coherent* MIMO RADAR, which has relatively close transmitting and receiving antennas, the performance of the angle estimation is improved. In a certain way the performance of MIMO systems can be improved and characterized by a virtual array that is "created" by the convolution of the positions of the transmitting and receiving antennas. Thus, at the outset this virtual array will be larger than the real array constituted by the antennas and therefore a MIMO system will have a better resolution when compared to the common radars.

3.3.1 MIMO Virtual Aperture

In this section we will introduce the MIMO channel and all the adjacent theoretical background. Next is a table with the notation used through this section.

x_m	location of the mth transmit antenna
y_n	location of the nth receive antenna
n_R	number of receiving antennas
n_T	number of transmitting antennas
n_s	number os samples in block
k	wave number (2π/wavelength)
$\mathbf{u}$	pointing vector from transmitter (or receiver) to scatterer
$Z \in \mathbb{C}^{n_R \times n_S}$	receive data matrix
$H_\delta \in \mathbb{C}^{n_R \times n_T}$	channel matrix for delay δ
$S_\delta \in \mathbb{C}^{n_R \times n_S}$	transmitted signal matrix delayed by time δ

3.3.1.1 MIMO Channel

The channel can be defined as the medium between the transmitter and the receiver. The purpose of the RADAR processing is to evaluate and interpret this channel, and henceforward a baseband signal is considered. The received data is saved in the matrix Z, that is given by:

$$Z = \sum_{\delta} H_\delta S_\delta + N \tag{3.4}$$

where N is considered as external noise or other interference exterior to the system. The expression 3.4 has a delay δ because that corresponds to different cells with different ranges. If the illuminated area of the obstacle has a single scatterer, as shown in 3.10, in a far field the delay δ should be zero except H_δ that is given by:

$$(H_\delta)_{n,m} \propto e^{ik\mathbf{u}.(y_n + x_m)} \tag{3.5}$$

where $k\mathbf{u}$ is the wavevector. This one together will x_m and y_n, are three vectors that represent the location of the transmitters and receivers centers phase. The exponential argument represents the difference between the lengths to the transmitter and the receiver phase centers, and $\mathbf{u}$ as the direction of the obstacle in far-field.

Next is presented an example, which the transmitter and the receiver have both three antennas, separated by d. So if the antennas are located in the line -d,0,d, in direction $\mathbf{d}$ the channel matrix has the following form:

$$H_\delta \propto \begin{pmatrix} e^{i\eta 2d} & e^{i\eta d} & e^{i\eta 0} \\ e^{i\eta d} & e^{i\eta 0} & e^{-i\eta d} \\ e^{i\eta 0} & e^{-i\eta d} & e^{-i\eta 2d} \end{pmatrix} \tag{3.6}$$

wherein

$$\eta = k\mathbf{u} \cdot \frac{\boldsymbol{d}}{\|\mathbf{d}\|} \tag{3.7}$$

Observing the equation 3.6 is possible to withdraw two important points. The first consists in the phase offsets interval, from $e^{i\eta 2d}$ up to $e^{-i\eta 2d}$, these are larger than the real arrays created by the antennas. This fact is one of the biggest motivation for the MIMO virtual array, because in this particular case we can define five virtual arrays, when there are only three antennas. The second point shows that some entries are replicated. In this example it is shown that some values in the matrix presented in 3.6 appear duplicated ($e^{i\eta d}$ for example).

3.4 Antennas

The antenna is one of the most important elements in a wireless communications system because it is responsible for transmitting and receiving electromagnetic waves. Their use is so comprehensive that they are an integral part of television systems, satellites and radars, [13].

It is due to its importance in a RADAR system, that in this section will be presented the most important parameters to characterize an antenna, but also a presentation of the theory of antenna arrays microstrip. All the contents presented in this section are based on [13] and [14].

3.4.1 Fundamental Parameters

Radiation Pattern The radiation pattern of an antenna allows the precept of how it radiates and receives the electromagnetic waves but also how it distributes the power received in space. Normally when observing a radiation pattern one or several main lobes can be observed (except in antennas that have an omnidirectional radiation diagram), that is, they correspond to the direction where the radiation of energy is maximum.

Directivity Directivity is the parameter that describes how an antenna radiates the energy that comes to it, that is, the amount of energy that is radiated in a certain direction. An antenna that has a large directivity will concentrate radiated energy into a smaller area. This parameter is the comparison ratio between the intensity of radiation produced in a certain direction and an isotropic antenna.

Gain The gain of an antenna is given by the comparison between the intensity of radiation of the antenna that we are analyzing with the intensity of radiation that an isotropic antenna produces, when fed with the same power.

Bandwidth The bandwidth of an antenna is given by the band or frequency range in which its performance, according to certain properties, is acceptable. Bandwidth is affected by the various parameters that characterize an antenna.

3.4.2 Linear Array Antenna

Normally the radiation pattern of a single antenna element is quite broad, and has low gain values relative to the isotropic antenna. Situations where high gain is required also implies an increase in antenna size. One way to increase the gain of the antenna in a given direction, without increasing its size can be to add several elements in a certain configuration, geometrically and electrically. This aggregation of elements creates a new antenna, usually referred to as arrays. The total field of these arrays is given by the addition of the fields radiated by the various elements.

An aggregate is defined linear if it is composed by identical elements that are distributed with equal spacing, power, and equal phase differences, on a single axis. In the figure 3.11 we can see an aggregate of N elements, where each element is isotropic, distributed along the zz axis, which are also separated by a distance d and with an alpha phase difference α.

If we consider an isotropic source, fed by a current $\mathbf{I}$, the E-field radiated by it, is given by:

$$E = \mathbf{I}\frac{e^{-j\beta r}}{4\pi r}, \ \ where \ \ \mathbf{I} = Ie^{j\phi} \tag{3.8}$$

As mentioned before for an aggregate to be linear it was necessary that the feeding of all elements was the same, therefore we have:

$$\mathbf{I}_1 = Ie^{j\phi_1}; \ \ \mathbf{I}_2 = Ie^{j\phi_2}; \ \ ... \ \mathbf{I}_N = Ie^{j\phi_N}; \tag{3.9}$$

Where α is given by the phase difference between consecutive elements, i.e., for example $(\alpha_2 - \alpha_1) = \alpha$ and so on. Knowing then that the current supplied to each element, it is possible to calculate which is the E-field radiated by each element, which is presented in the following equation:

$$E_1 = \mathbf{I}e^{j\phi_1}\frac{e^{-j\beta r_1}}{4\pi r_1}; \ \ E_2 = \mathbf{I}e^{j\phi_2}\frac{e^{-j\beta r_2}}{4\pi r_2}; \ \ ... \ E_N = \mathbf{I}e^{j\phi_N}\frac{e^{-j\beta r_N}}{4\pi r_N} \tag{3.10}$$

The E-field in a zone far from radiation, where $r \gg d$, where if we consider that all the rays are parallel between them, we can draw the following conclusions:

- $\theta \simeq \theta_1 \simeq \ ... \ \simeq \theta_n$;
- $r_2 = r_1 - d\cos\theta, \ ... \ , r_N = r_{N-1} - d\cos\theta = r_1 - (N-1)d\cos\theta$;
- $r_1 \simeq r_2 \simeq \ ... \ \simeq r_N$;

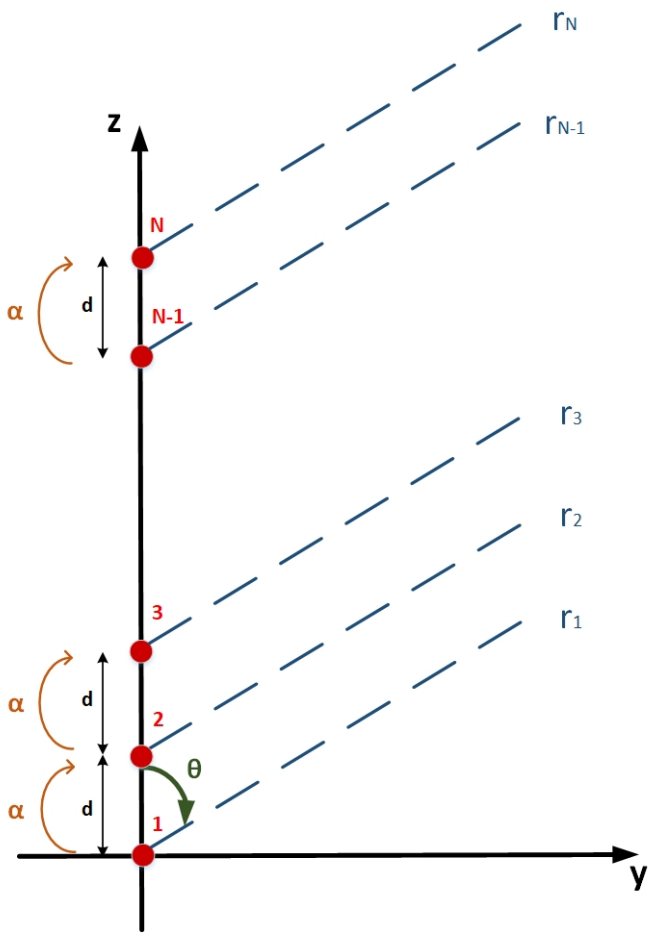

Figure 3.11: Linear aggregate with N elements

Given this, knowing that the overlap of the fields generated by each element gives rise to the field produced by the aggregate, we have that the total field of an aggregate of N elements is given by:

$$E_T = \sum_{n=1}^{N} E_n \tag{3.11}$$

The expression may also take the following form:

$$E_T = Ie^{j\phi_1}\frac{e^{-j\beta r_1}}{4\pi r_1}[1 + e^{j(\beta d\cos\theta+\alpha)} + ... + e^{j(n-1)(\beta d\cos\theta+\alpha)} + ... + e^{j(N-1)(\beta d\cos\theta+\alpha)}] \tag{3.12}$$

Where $Ie^{j\phi_1}\frac{e^{-j\beta r_1}}{4\pi r_1}$ corresponds to the element factor and the second element of the expression to the aggregate factor. By observing the equation 3.12 we can observe that the aggregate factor depends directly on the number of elements, the distance and the phase difference between them, while the element factor corresponds to the radiation of an isotropic source, as can be seen in equation 3.10.

In a simpler way, the aggregate factor can also be described by:

$$FA = \sum_{n=1}^{N} e^{j(n-1)\Psi}, \qquad \Psi = \beta d \cos\theta + \alpha \tag{3.13}$$

Since we can consider the expression a geometric progression, in this case of N elements, the aggregate factor can then be normalized and take the following form:

$$|FA|_n = \frac{\sin(N\frac{\Psi}{2})}{N\sin(\frac{\Psi}{2})} \tag{3.14}$$

Maximum The aggregate factor takes its maximum value when:

$$\frac{\Psi}{2} = \pm m\pi \Rightarrow \Psi = \pm 2m\pi, \qquad m = 0, 1, 2, ... \tag{3.15}$$

Substituting into the expression, we have to:

$$\beta d \cos\theta_{max} + \alpha = \pm 2m\pi \Rightarrow \theta_{max} = \pm\cos^{-1}\left[\frac{\lambda}{2\pi d}(\pm 2m\pi - \alpha)\right] \tag{3.16}$$

Nulls The aggregate factor is null when its numerator is zero and therefore:

$$\sin N\frac{\Psi}{2} = 0 \Rightarrow N\frac{\Psi}{2} = \pm n\pi \Rightarrow \Psi = \pm\frac{2n\pi}{N}, \;\; n = 0, 1, 2, ... \; and \; n \neq N, 2N, 3N, ... \tag{3.17}$$

Substituting in the expression, the nulls of the aggregate factor are given by:

$$\beta d \cos\theta_n + \alpha = \pm\frac{2n\pi}{N} \Rightarrow \theta_n = \pm\cos^{-1}\left[\frac{\lambda}{2\pi d}\left(\pm\frac{2n\pi}{N} - \alpha\right)\right] \tag{3.18}$$

$$n = 0, 1, 2, ... and \; n \neq N, 2N, 3N, ...$$

The figure 3.12 presents an example of the behaviour of a linear antenna array with different number of elements. In every example the elements are separated of $\lambda/2$.

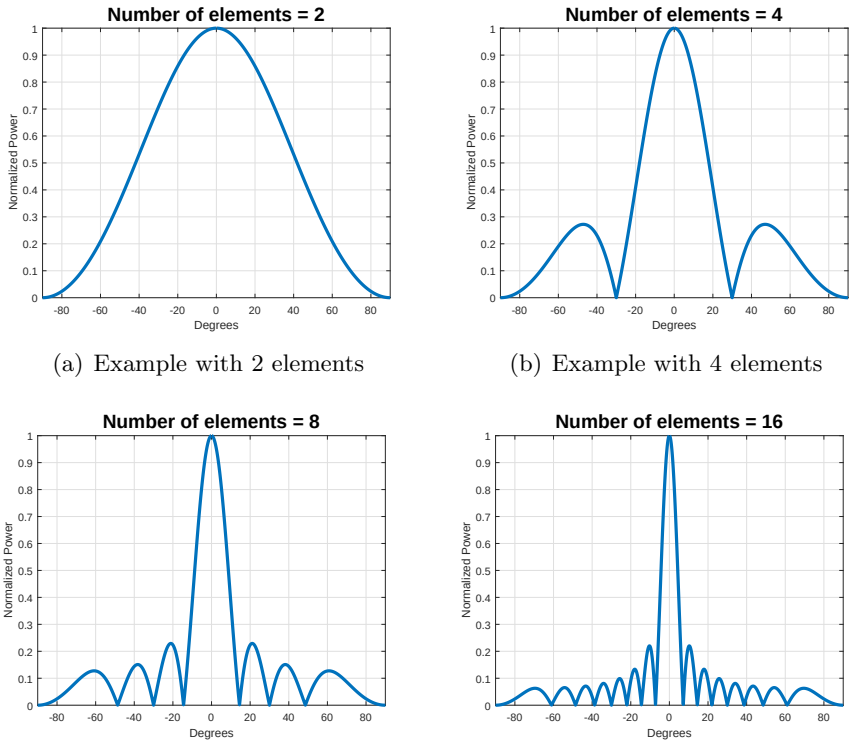

(a) Example with 2 elements

(b) Example with 4 elements

(c) Example with 8 elements

(d) Example with 16 elements

Figure 3.12: Linear array factor for different number of elements

Observing at the previous figures it is possible to draw the following conclusions:

- With increasing number of elements, the main lobe narrows, making the array more directive.
- The number of secondary lobes increases as the quantity of elements growths.

3.5 Beamforming Techniques

This section aims to approach some existing beamforming techniques. The whole theoretical background will be presented.

Beamforming can be defined as combining RF signals to produce a directional beam. Since it has already been seen a radiant element in an antenna have low gain and directivity and with the use of techniques of beamforming it is possible to produce a beam with greater directivity but also to control the direction of the main lobe by varying the amplitude and phase of the feeding of each element, [16].

These techniques have several advantages because this reduces the interference between elements but also improves the performance of communication systems since it is possible to control the direction of the main lobe without having to physically move the antenna.

The beamforming techniques can be divided into two strands, digital beamforming and analog beamforming, as can be seen in figure 3.13. In relation to digital beamforming, all processing is allocated to RF front ends using DACs and ADCs, digital attenuators and mixers to control the phase and amplitude of the signal for each element. Analog beamforming can be done in several ways, including using lenses to focus the main lobe in a certain direction, or using circuits, such as phase shifters that allow you to change the phase of each element.

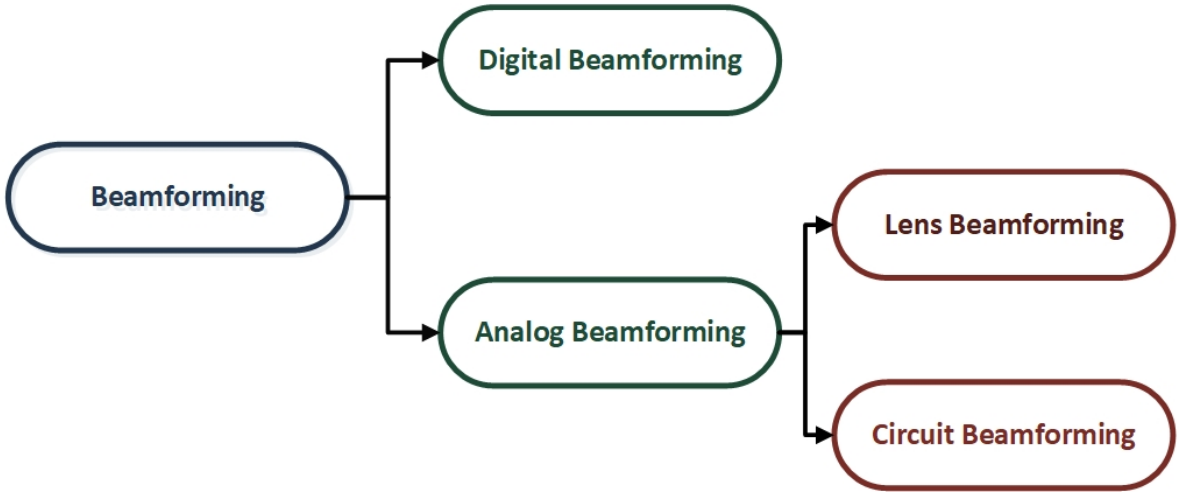

Figure 3.13: Types of beamforming

3.5.1 Circuit Beamforming

One of the most common circuit-based beam forms is the Butler Matrix, because due to the use of microstrip transmission lines, it makes its implementation much less complex compared to other existing configurations, for example the Blass Matrix. [15], [16].

The Butler matrix is a type of a circuit beamforming network that depends on which of N inputs is accessed, making the antenna beam is then steered in a specific direction. Usually the Butler Matrix is a 2^n x 2^n network. As can seen in the figure 3.14, is also composed by hybrid couplers and phase shifters that are responsible for the beamsteering. The example presented is a 4x4 Butler Matrix, but typically a Butler matrix as N number of input and N number of output that will create N number of orthogonal beams. If we consider another example that consists on N inputs and M outputs, the Butler matrix will produce N orthogonal beams, because the number of inputs, N, determine the number of beams produced while the number of outputs M, will determine the number of radiating elements, which will to influence the beamwidth of the main lobe.

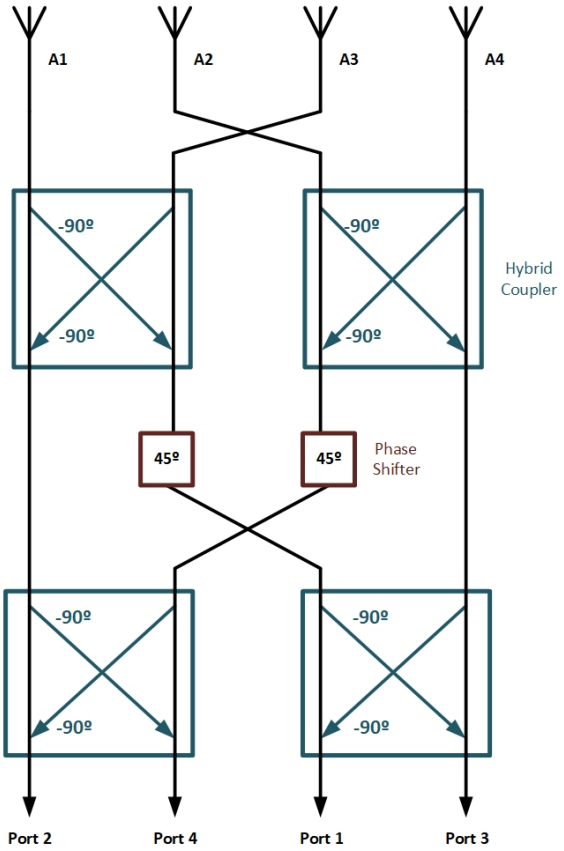

Figure 3.14: Butler matrix for a four element array

3.5.2 Digital Beamforming (DBF)

As the name indicates, in DBF the change of direction of the radiation diagram is performed without recourse to analog components as is the case presented previously. The DBF can be applied in both the transmission and the reception, and considering the reception case it has the following advantages over analog beamforming, [17]:

- Multibeam operation, which allows you to examine a large angle using few narrow beams simultaneously
- High resolution techniques, for situations where the sources have closer angular spacing than one beamwidth.
- Correction of the element radiation pattern, due to mutual coupling effects between the elements.

Usually, digital beamforming techniques require the use of digital components, such as FPGAs and SDRs. This is due to the fact that this type of devices have programmable and reconfigurable elements through software that allow real-time control of all its constituent elements, [18].

In most cases, systems capable of performing DBF are constituted by a FPGA and RF front-ends with SDR architecture, as can be proved in figure 3.15. With this type of system it is possible through software, in the case of the transmission to generate the desired waveform, control its modulation and through digital components, such as oscillators, mixers, amplifiers, attenuators, control the amplitude and phase of each channel independently, thus allowing the steer of the antenna beam.

In the case of reception, the process is similar, in which reception and reconstruction of the received data is done, and by means of digital signal processing techniques it is possible, again using the components available in the RF front-end, to control the phase and amplitude of each channel independently and then perform the beamsteering. This case also allows us to approach certain techniques of signal processing, called direction of arrival, which intends and allows estimating the signal of a given direction. Already known algorithms such as MUSIC or ESPRIT, allow for exemaple, to find the direction relative to the array where the sound source is located.

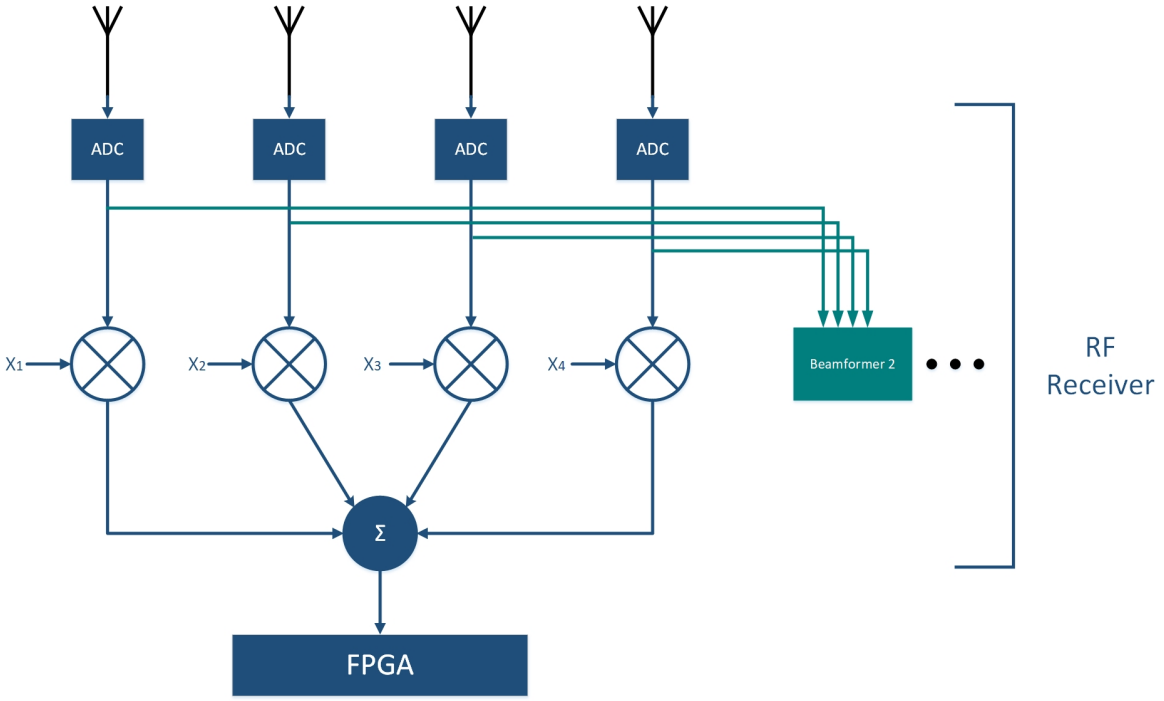

Figure 3.15: DBF for a four element array

Observing again the figure 3.15, it is possible to verify the existence of more than one unit of beamforming, this because these units are exclusively dependent on the number of channels that the system has, and therefore this is the only limitation for the number of units of beamforming that we can have. The figure represents a possible system for 4 channels.

3.6 Detection Through the Walls Works

With this section it is intended to present works in detection through the walls radars, which represent the state of the art in this field. Some articles are presented through the section, as well, the used techniques and hardware developed.

The ability to locate targets within buildings with devices located at a distance from them can greatly improve the performance of defence forces in an urban guerilla setting. It was in this way that John Peabody and his team developed a RADAR capable of locating moving targets through walls. All the information presented hereafter are based in [19], [20].

This team has developed a RADAR that operates in the S band and uses an FM-CW architecture, with a central frequency of 3 GHz with a 2 GHz UWB chirp in order to improve the chances of penetrating the wall. MIMO array and TDM architectures were also implemented in order to produce the least complex solution and low cost possible.

Their idea is to mount the RADAR in a vehicle that is directed to a distance near the building and thus to try to obtain information about the building. Their objective is to be able to display the data they receive in a 10.8Hz video frame rate, which they have developed for a data pipeline and an image algorithm.

The system was designed to be able to detect a human being at about 20 m with a solid concrete wall 20 cm thick and for this they have developed an FM-CW system that transmits Linear Frequency-Modulated (LFM) chirps from 2 to 4 GHz every 1 ms with 1W peak power at 50% duty cycle.

The following figures show the system developed:

(a) Antenna Array Developed

(b) Transmitter, receiver, power supplies, diagnostic oscilloscope, and computer used on the system

Figure 3.16: Radar developed

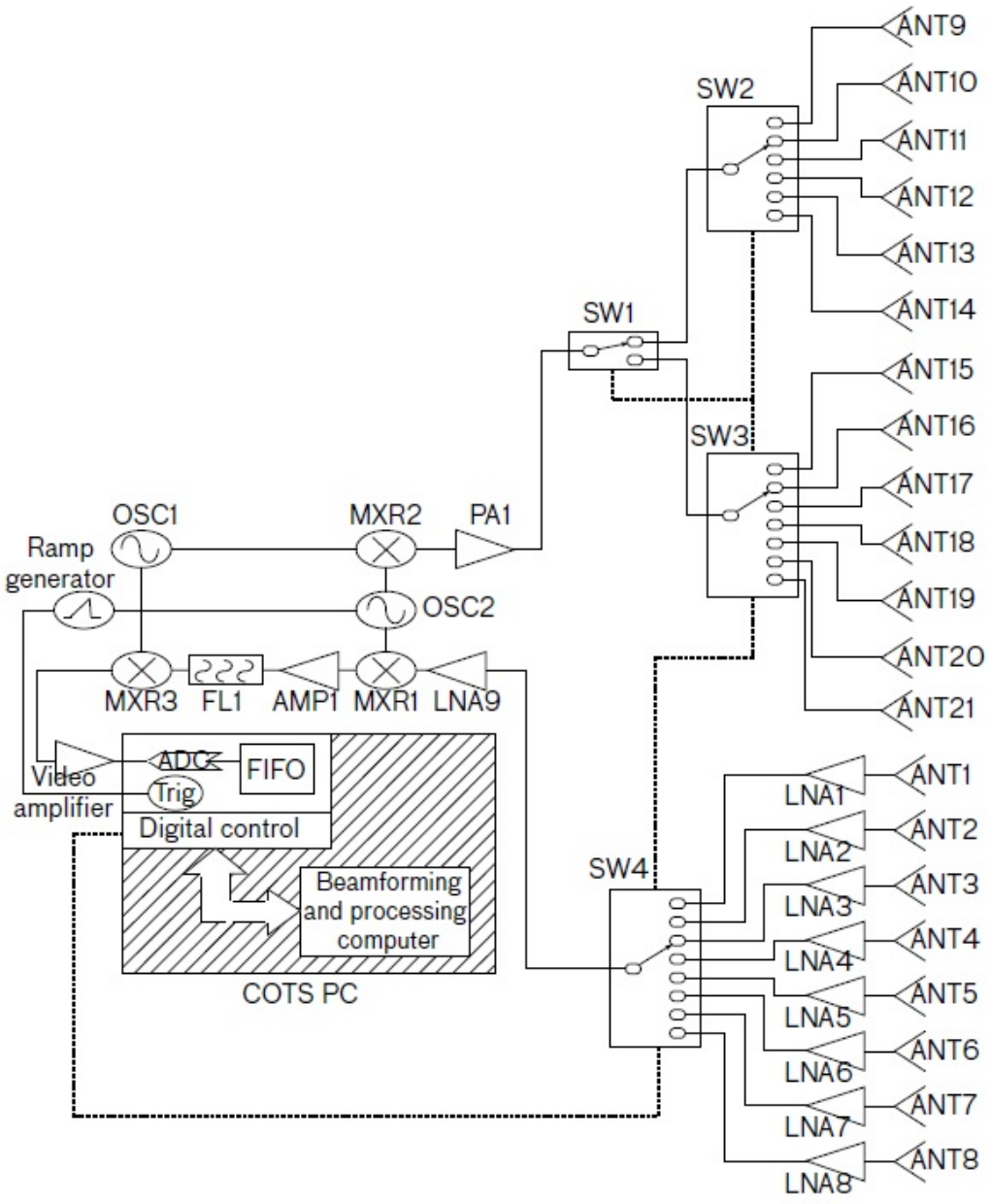

Figure 3.17: Block diagram of the system

Regarding the results obtained, these were separated into three different scenarios. The first one is performed in free space, as a reference, and then tests were performed with a wall of 10 cm and 20 cm thickness. The RADAR is placed about 6 m from the wall while people position themselves about 10 m from the RADAR behind the wall as you can see in the figure diagram 3.18.

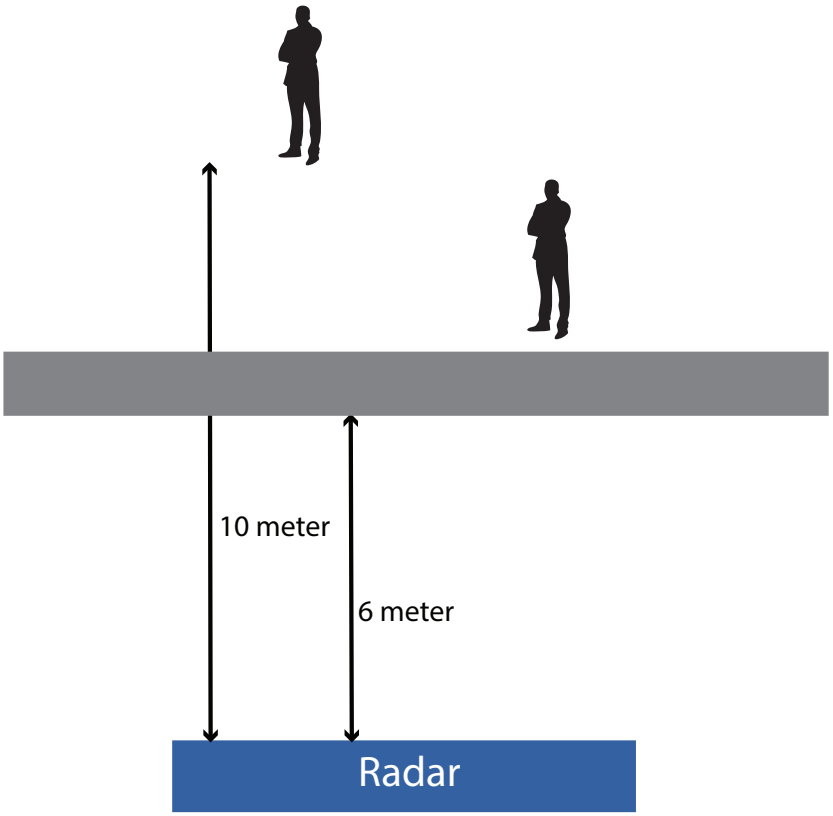

Figure 3.18: Measurement setup

According to the results obtained it was possible to draw the following conclusions:

- The results for those behind the wall of 10 cm in thickness differ slightly from the results obtained for free space experience, where they are clearly detected.

- For the 20cm thick wall the received energy is significantly lower, where the clutter is much higher and the noise received is visible. In spite of all this the detection of people's location continues to be noticeable.

The following figures show the results presented regarding the situations presented previously.

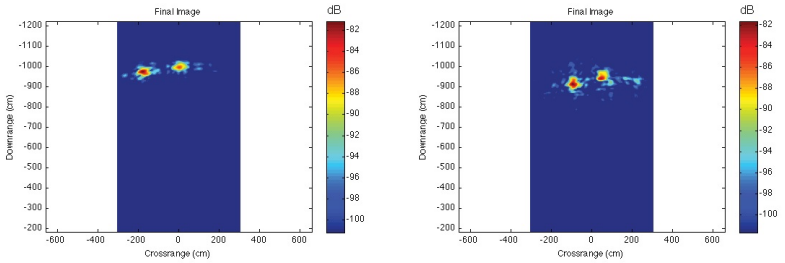

(a) Free Space Measurement (b) 10 cm thick wall measurement

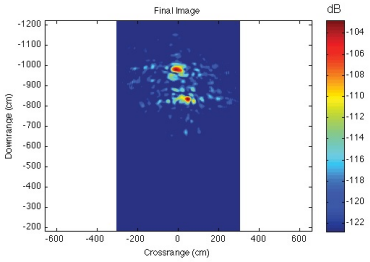

(c) 20 cm thick wall measurement

Figure 3.19: Results for the three different scenarios

Beyond these tests, others were performed for different situations that are not presented in this dissertation, since the objective was the demonstration of the success of this work. At the end of the paper John Peabody also presents a table where is shown the results for all tested scenarios, that is presented below:

Wall type	**One walking**	**Two walking**	**Standing stil**	**Siting stil**	**Standing stil holding breath**	**Siting stil holding breath**
20 cm concrete	✓	✓	±	×	×	×
Cinder block	✓	±	✓	±	✓	×
10 cm concrete	✓	✓	✓	✓	✓	×
Free space	✓	✓	✓	✓	✓	✓

Where,
✓ Good results with clearly detection
± Results with notorious interferences
× Detection not achieved

Table 3.1: Results of every tests performed

Chapter 4

Materials Characterization

4.1 Introduction

This section follows on from what has been presented previously, in which it is intended to implement a RADAR capable of detecting people through walls. Seen this we considered preponderant to study and to analyse materials attenuation that are part of these same walls.

Although there are already several studies and investigations regarding the characterization of materials, their attenuation, permittivity and other merit factors, we believe that our own study may well be carried out, not only to verify and confirm the veracity of the works analysed, but also with the intention to deepen our knowledge in the subject and be precise in measures.

In the next sections are presented, the measurement technique used, which antennas are used and developed to perform the measurements, as well as the setups defined for each experiment. Likewise all the results obtained are presented with the respective analysis.

4.2 Measurement Technique

Since the objective of this work is to be able to detect people through objects, it is crucial to know some characteristics commonly used as building materials. One of the most important factors to study is the attenuation that these objects will cause in the signal that will be received.

In recent years, some researchers have done some studies to characterize the attenuation of materials that constitute walls of the most varied types of buildings, usually to study the implementation of radio access network services. As this work will be based on the same frequency bands, it is important to know at the outset which phenomena can occur and to have values for later comparison.

To make a good characterization of the materials to be studied, it is necessary to know the losses in the free space first, in order to make a comparison with the different types of materials. In the figure 4.1 , it is presented one possible configuration to measure the values, using a VNA, [21].

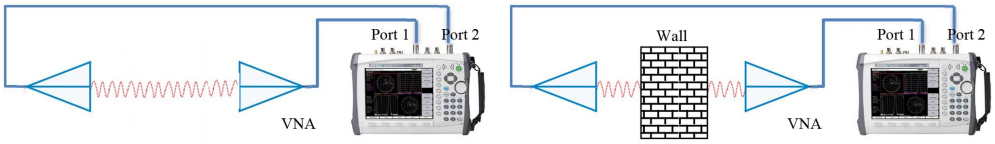

(a) Measure in free space (b) Measure with obstacle

Figure 4.1: Measurement Setup [21]

This measurement is called SE. The SE of walls is measured for normal incidence by comparing the module of scattering parameters of transmission (dB) in free space to that obtained when the wall is placed between the antennas [22].

$$\text{SE (dB)} = S_{21(FreeSpace)} - S_{21(Wall)} \text{ [22]} \tag{4.1}$$

This measurement technique, although easy to implement, presents some limitations and problems. Some of them go through the difficulty of keeping constant the distance between the antennas, as well as their alignment. Besides this problems can also arise hardware problems, propagation problems, such as multipath, and errors of time domain measurement techniques.

Usually these measures are performed in building walls, whether internal or external. Thus allowing to characterize the type of environment where the radio access network will be deployed. In this work, it is important to know these attenuations in order to be able to "map" the scenario in question.

Following are some figures and tables of results obtained in some studies. These values will be taken as reference for future work results.

Material	**Thickness**	**Attenuation (dB) @ 6 GHz**
Plywood Wet	2 cm	4
Lumber Dry	15 cm	22
Brick	27 cm	40
Concrete	20 cm	50
Reinforced Concrete with 2% of iron	20 cm	65
Brick-Faced Concrete	20 cm	72

Table 4.1: Attenuation for different types of materials [23]

Material	Internal of External Wall	Thickness	Attenuation (dB) @ 5 GHz
Concrete	Internal	70 cm	45
	External	20 cm	11
Brick	Internal	40 cm	14,5
Concrete & Marble	External	50 cm	20
	External	80 cm	36
	Internal	50 cm	5
	Internal	70 cm	9

Table 4.2: Average SE for different materials [21]

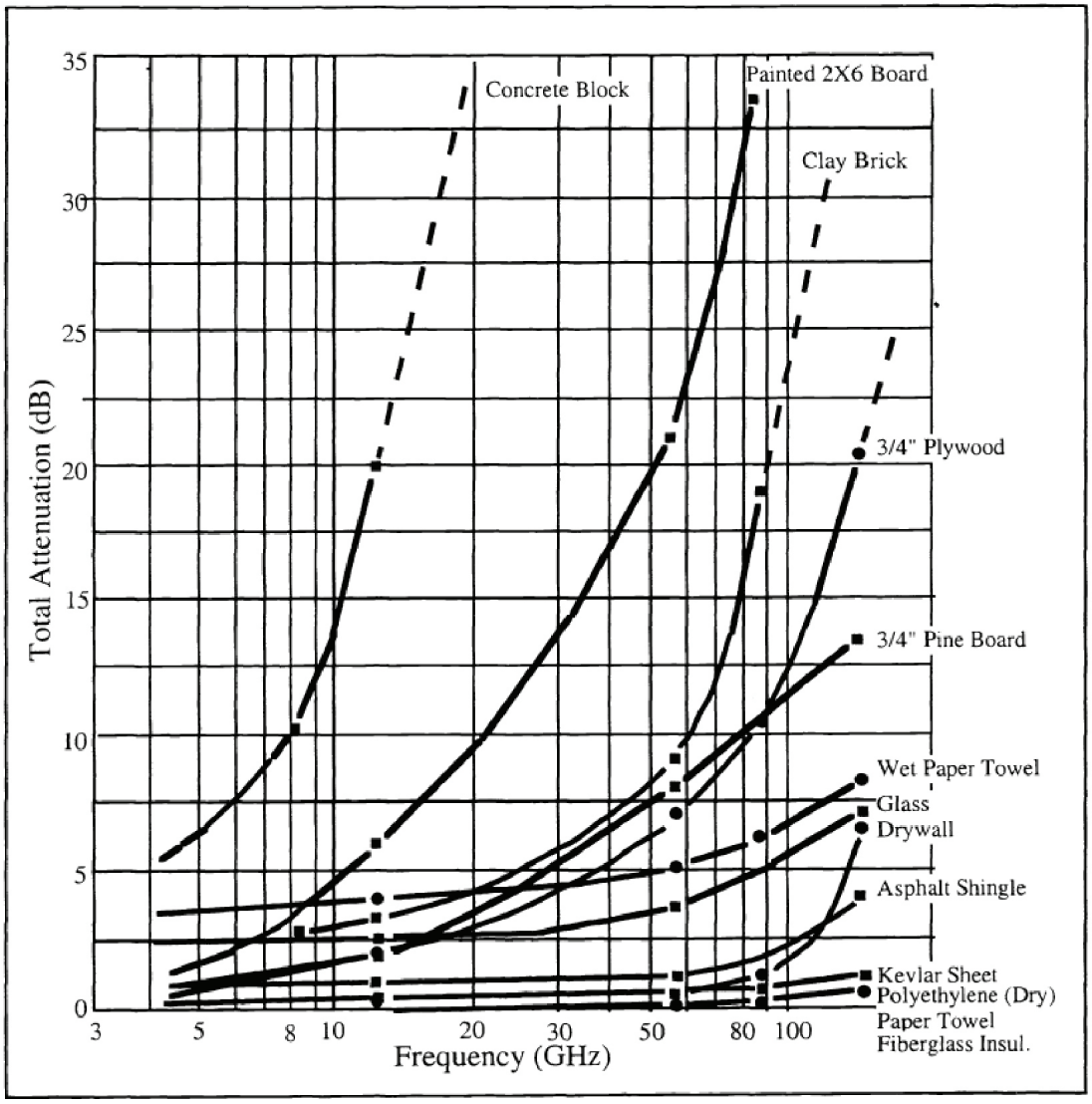

Figure 4.2: Attenuation for several materials along the frequency. [24]

4.3 Materials Characterization System

Throughout this section is presented a study performed by the author with the purpose of characterize the RF attenuation of different materials. In this way the entire measurement process, the setups, the antennas developed for this series of measurements, as well as the remaining material involved in the process are described.

4.3.1 Antennas

This subsection is dedicated to present the antennas used during the tests performed.

4.3.1.1 Narrowband Antenna

It was initially defined that the frequency of the system would be around 5.8 GHz due to the fact that it is in a free band, there is a great amount of work both in radars and in antennas and also the design of these antennas is relatively accessible without being necessary the use of elements of great dimensions. In this way, the antennas were chosen that had some necessary requirements, such as gain and high directivity.

In order to save resources, we have used antennas that were designed during another Master's thesis and that have the necessary requirements for the experience. These antennas were designed by colleague Tiago Varum, Post PhD Researcher at Instituto de Telecomunicações in Universidade de Aveiro, [14].

Below are images related to the antenna's electrical scheme, the printed antenna along with a graph showing the behaviour of the S11 parameter along the frequency.

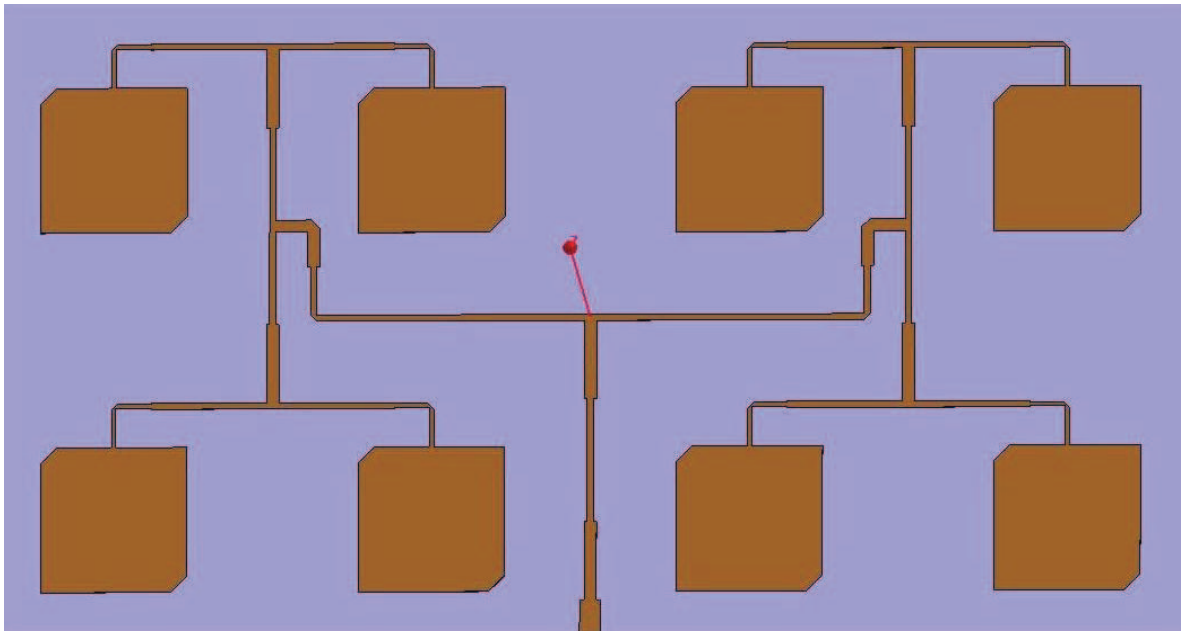

Figure 4.3: Diagram of the developed antenna [25]

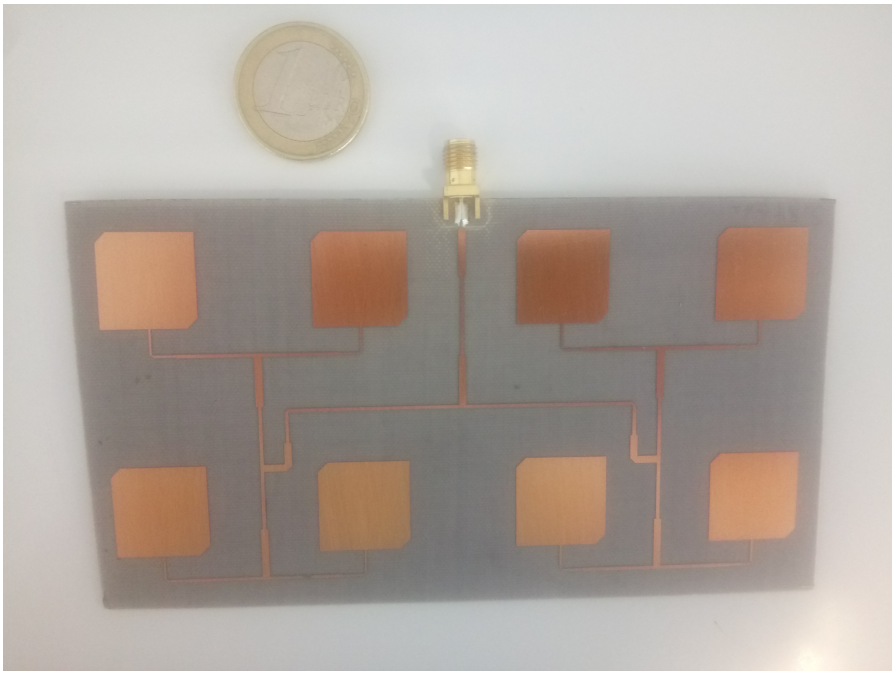

Figure 4.4: Printed antenna

Although the antenna is not centred at 5.8 GHz, it can be seen from the figure 4.5 that the value of parameter S11 at 5.8GHz is about -15 dB which makes the antenna well adapted for this frequency.

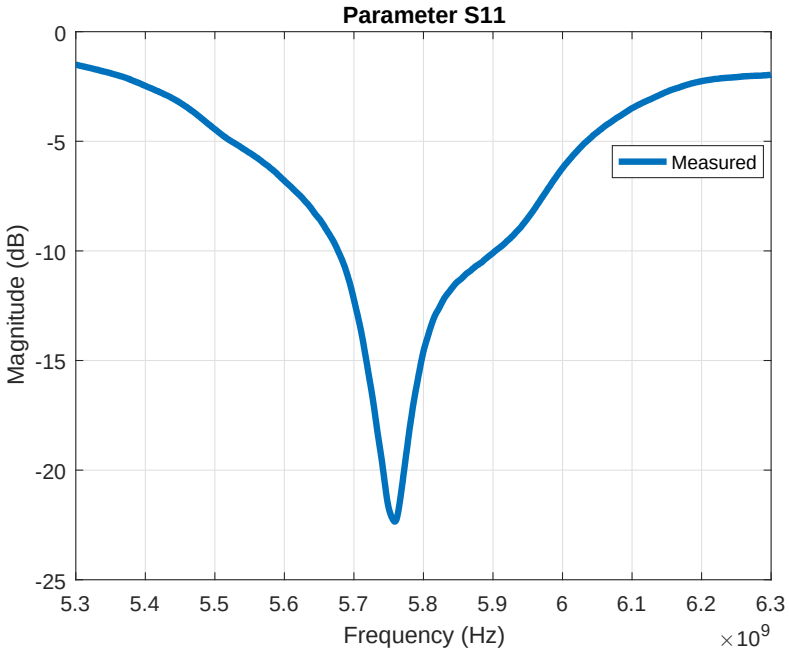

Figure 4.5: S11 parameter of printed antenna

Due to the large bandwidth of the antenna, around 200 MHz, it has been possible to perform a frequency scan from 5.7 GHz up to 5.9 GHz, as can be seen in section 4.4.1.

4.3.1.2 UWB Antenna

In order to perform this study as comprehensively and accurately as possible we concluded that the best solution would be to use UWB antennas and in this way to understand the behaviour of each material for a wide range of frequencies. Therefore, it was used the CST to design and simulate an antenna that fulfilled the necessary requirements. It was selected a Vivaldi antenna design, since it presents a great bandwidth and at the same time a relatively high gain.

The antenna dimensions as well as the simulation result can be visualized in the figure 4.6. Figure 4.7 represents the antenna produced. These antennas were designed by colleague Daniel Malafaia, PhD student at Instituto de Telecomunicações in Universidade de Aveiro.

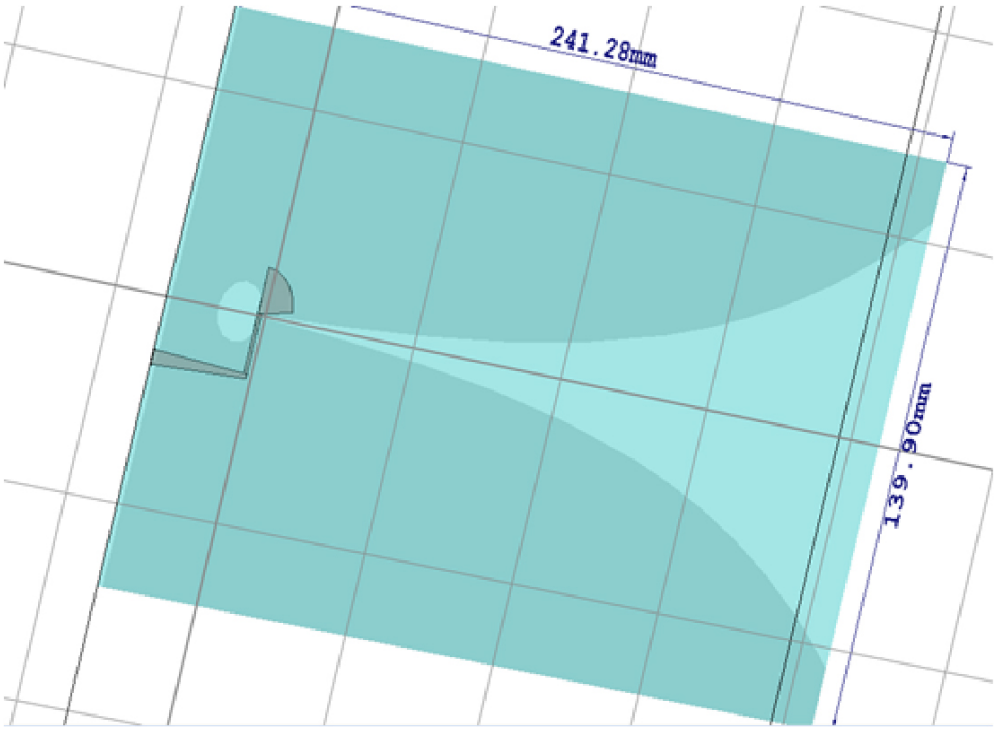

Figure 4.6: Vivaldi antenna simulation in CST

This antenna has a bandwidth from $1.5\,GHz$ up to $7\,GHz$, and was design and simulated on CST. The RF substrate used for the design was ISOLA IS680 which has a thickness of $h = 1.52mm$, with a copper coating of $t = 35\mu m$ and $\epsilon_r = 3.38$.

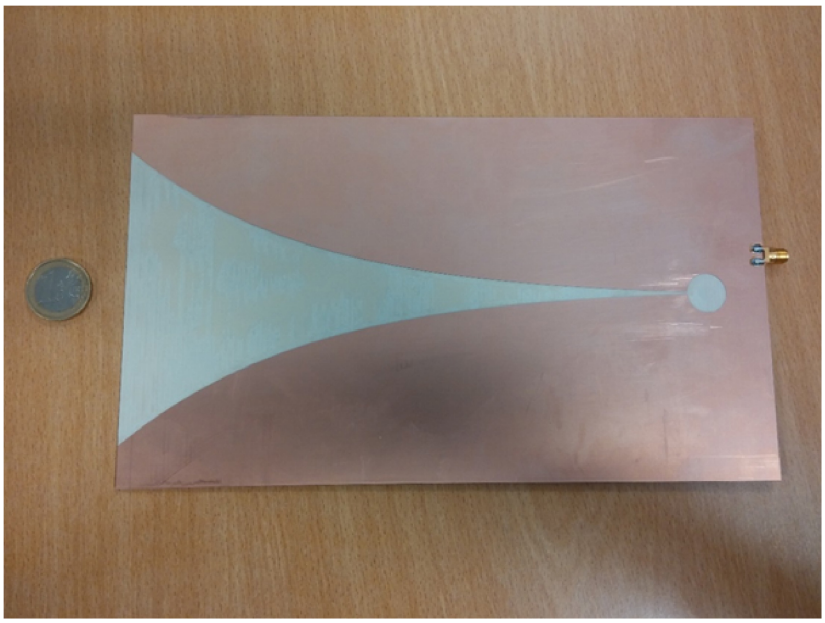

Figure 4.7: Printed Vivaldi antenna

Once it was printed using a Computer Numerical Control (CNC) machine, the S_{11} parameter were measured on VNA in order to confirm the results that were obtained in the simulation. Both results are shown in figure 4.8.

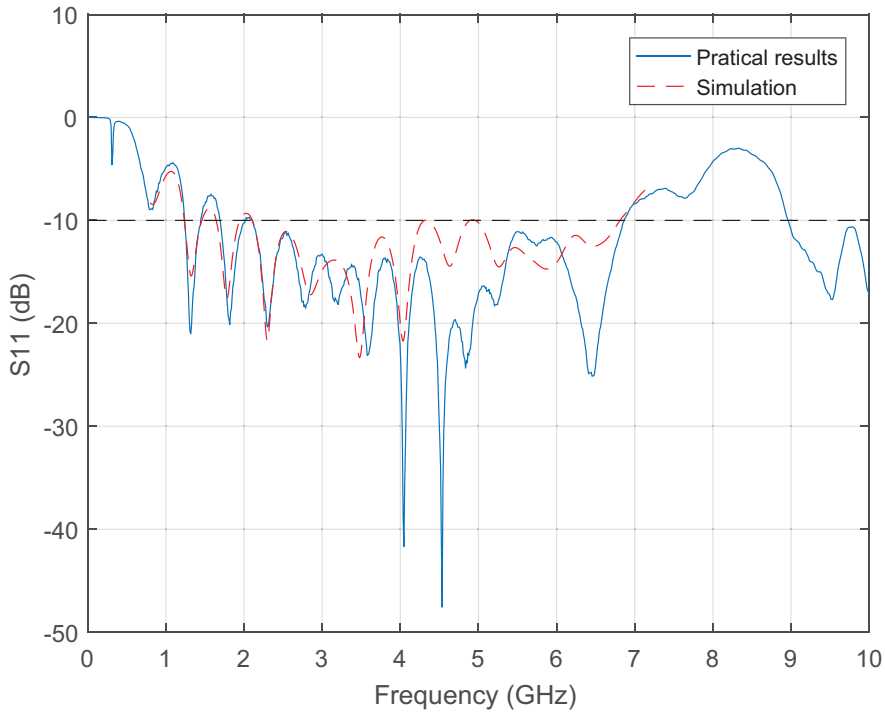

Figure 4.8: S11 parameters of designed antenna

From the figure, it can be concluded that the practical results are generally in agreement with those that resulted from the simulation, therefore fulfilling the requirements that were established.

4.3.2 Measurement Setups

4.3.2.1 USRP Setup

In section 4, most of the measurements performed for this purpose are performed using a VNA. It was in this way that was tried to perform the same experience but with a USRP. A calibration setup was developed for the USRP, so that all the results it presented were reliable.

Since the USRP presents results regarding the samples taken from the signal sent, it is necessary to guarantee its good operation before starting for other measurements. In this way, a series of tests were performed, guaranteeing the veracity and reliability of the results to be presented. In all these tests a calibrated measuring instruments were used.

Below is presented a short list of measuring instruments used to perform the tests, is presented.

- Signal Vector Generator SMU S200A;
- Microwave Analyser Keysight N9917A;
- Power Meter Agilent N1913A;
- Cable Mini Circuits 1651-141.1MSM+;
- Ettus Research USRP B210;
- Power Splitter MiniCircuits ZN2PD2-63-S+;

In the next points are presented in more detail the tests performed.

Generator Test

The first step is to verify the calibration of the generator (Signal Vector Generator SMU S200A [26]). For this, the generator is connected directly to the Microwave Analyser Keysight N9917A [27], and afterwards is connected to the Power Meter Agilent N1913A[28].This connection is made using the Cable Mini Circuits 1651-141.1MSM+ (which has 1.02dB of losses), according to figure 4.9.

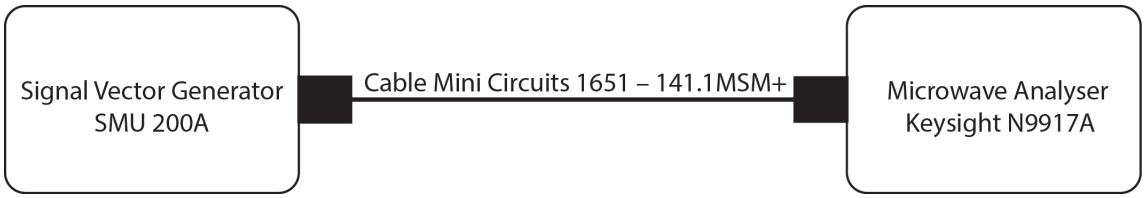

(a) Setup with a Microwave Analyser

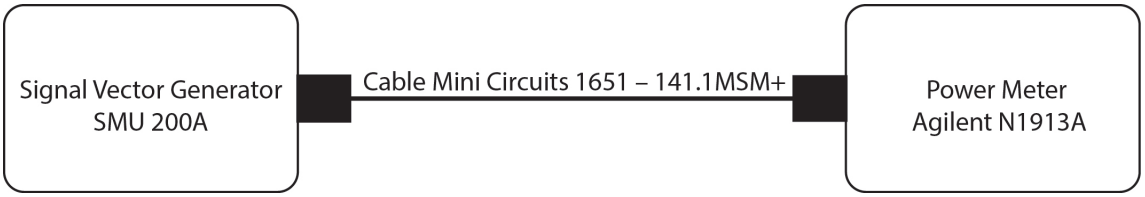

(b) Setup with a Power Meter

Figure 4.9: Generator Test Setups

Since the maximum power that the generator can emit without causing signal distortion is about -10 Decibel Milliwatt (dBm), a power sweep was performed from -60 dBm to -10 dBm with a 5 dBm jump between each measurement. The frequency of the signal generated is 5,8 GHz. The results obtained for the situations considered can be observed in the table 4.3.

Emitted Power (dBm)	**MA Keysight N9917A**		**PM Agilent N1913A**	
	Received Power (dBm)	**Δ (dB)**	**Received Power (dBm)**	**Δ (dB)**
-60	-61,36	-1,36	-66.45	-6,45
-55	-54,46	-1,46	-58,09	-3,09
-50	-51,5	-1,5	-52,62	-2,62
-45	-46,49	-1,49	-47,45	-2,45
-40	-40,93	-0,93	-41,94	-1,94
-35	-35.88	-0,88	-36,92	-1,92
-30	-30,91	-0,91	-31,94	-1,94
-25	-25,87	-0,87	-26,88	-1,88
-20	-20,93	-0,93	-21,87	-1,87
-15	-15,86	-0,86	-16,89	-1,89
-10	-10,92	-0,92	-11,95	-1,95

Table 4.3: Measurements for both setups

Observing table 4.3 it can be concluded that the results obtained are in agreement with the expected values, in which for the first setup the losses, due to the cable used, are verified. On the other hand it can be observed that the losses for the second situation are larger, between about 1-2 dB, which can be justified by probe that is attached to the instrument.

USRP Receiver Test

With the validation of the operation of the generator it was then possible to move on to the next test. It consists in the connection of the generator to the receiver of the USRP B210[29], which in turn is connected to the computer. The objective of the test is in line with the previous one, in which it is intended to evaluate the USRP receiver and verify that it works correctly. The image 4.10 represents the setup used in the test

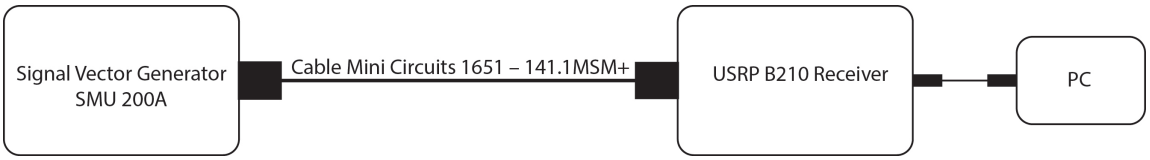

Figure 4.10: USRP Rx Test Setup

As in the previous test the central frequency is 5,8 GHz and a power sweep is performed from -60 dBm to -10 dBm, but this time with 5 dBm jumps at each measurement. The results obtained from the test can be visualized in the table 4.4.

Emitted Power (dBm)	**Received Power (dBm)**	**Δ (dB)**
-60	-60,48	0,48
-55	-57,60	2,60
-50	-53,98	3,98
-45	-49,47	4,47
-40	-44,39	4,39
-35	-39,40	4,40
-30	-34,47	4,47
-25	-29,46	4,46
-20	-24,46	4,46
-15	-19,52	4,52
-10	-14,60	4,60

Table 4.4: Received power by USRP Rx

As can be seen from table 4.4, the results meet what was expected, since growth is approximately linear. The small differences between the values can be justified by the cable losses.

USRP Transmitter Test

Validated the operation of the receiver, it was considered that it would be important to know the range of powers that the USRP is capable of emitting. For this, a third test was carried out in which the power emitted by the transmitter of the USRP was measured according to its gain. The gain was varied between 0 dB and 89.75 dB with 5 dB jumps for each test. These measures were observed by the Microwave Analyser Keysight N9917A as shown in figure 4.11.

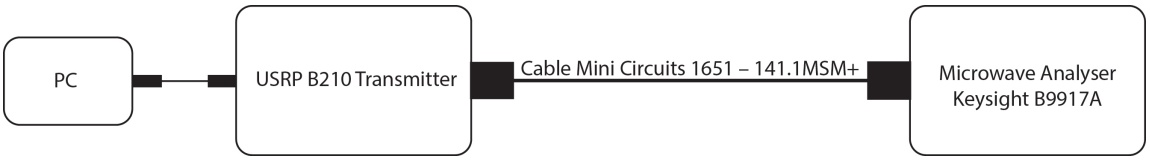

Figure 4.11: USRP Tx Test Setup

The table 4.5 is shown below. In the table it is possible to check which power values can be transmitted considering the gain of the USRP transmitter. The working frequency is once again 5,8 GHz.

Tx Gain (dB)	**Received Power (dBm)**	**Increase (dB)**
5	-70,36	-
10	-66,25	4,11
15	-62,95	3,3
20	-57,04	5,91
25	-51,98	5,06
30	-46,71	5,27
35	-41,52	5,19
40	-36,66	4,86
45	-31,67	4,99
50	-26,75	4,92
55	-21,77	4,98
60	-16,79	4,98
65	-11,78	5,01
70	-6,79	4,99
75	-1,67	5,12
80	3,30	4,67
85	7,70	4,4
89,75	11,41	3,71

Table 4.5: Power emitted in relation to Tx gain

USRP Transmitter/Receiver Test

In this last test it was intended to validate the system as a whole and ensure the proper functioning of both the transmitter and receiver of USRP B210. To perform this study, the transmitter of USRP was connected to the Power Splitter Mini-Circuits ZN2PD2-63+[30] (with about 3 dB losses) which in turn connected the Microwave Analyser Keysight N9917A and the receiver of USRP according to the figure 4.12.

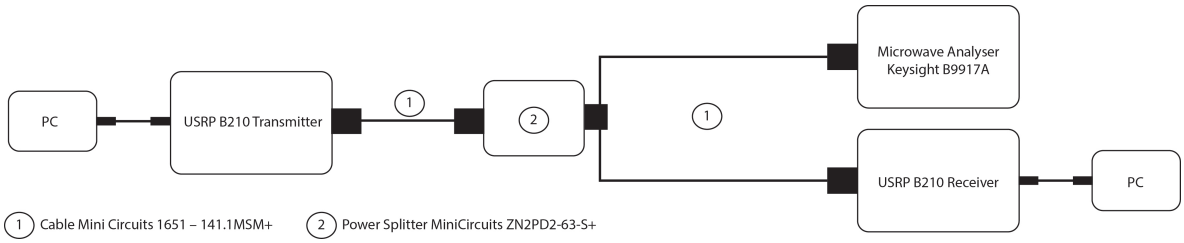

Figure 4.12: USRP Tx/Rx Test Setup

Similarly to the previous test, the central frequency is 5,8 GHz and the transmitter gain was varied between 0 dB and 89.75 dB with jumps of 5 dB for each measurement. In this way, it was verified the power received by the receiver but also if the 5 dB jumps that were effected in the transmission were verified also in the reception. The test results are present in the table 4.6.

Tx Gain (dB)	**Received Power in Rx (dB)**	**Increase (dB)**
5	-76,59	-
10	-76,54	0,05
15	-76,29	0,24
20	-75,69	0,61
25	-74,15	1,53
30	-71,10	3,05
35	-67,03	4,08
40	-62,42	4,61
45	-57,51	4,91
50	-52,63	4,88
55	-47,67	4,97
60	-42,68	4,98
65	-37,72	4,97
70	-32,74	4,97
75	-27,71	5,04
80	-22,80	4,91
85	-18,48	4,32
89,75	-14,92	3,56

Table 4.6: Power emitted in relation to Tx gain and increase of power for each jump in gain

Analysing table 4.6 it can be concluded that the jumps performed on the transmission part are only approximately linear up from the 35 dB gain. This shows that in future tests an equal or greater gain should be considered. Another important fact is that the power values in the receiver are relatively lower when compared to the previous test results. This decrease is due to the introduction of a Power Splitter (about 4 dB of losses), but also by the algorithm used to calculate the power reaching the USRP receiver.

Three other tests were also performed, in which different values were defined for the gain of the receiver. The performance of these tests was due to the need to know from which values the receiver would reach the saturation point and thus choose the appropriate value for the

following tests.

Conclusion

These tests allowed to obtain a greater knowledge about the operation and behaviour of the USRP, since this one was subject to different scenarios throughout the process. These results are not only useful to get to know the equipment better, but several factors have been obtained that will be extremely important for future experiences.

The most important factors to take away from these tests are:

- System sensitivity (section 4.3.2.1);
- Maximum power that the equipment can transmit (section 4.3.2.1);
- Variation of received power in relation to transmitter gain (section 4.3.2.1)

4.3.2.2 VNA Setup

The setup below displayed is the one that will be used to perform the measurements. Based on other studies, it was defined that the setup should approximate that which is used in specialized articles in the characterization of materials.

It was then defined that the measuring instrument to be used would be the VNA R&S ZVB20, for the reliability and guarantees that its results represent. The antennas were placed 1 meter from each other, the objects under test are either to the transmitter or receiver, This allows us to check the behaviour of the materials for different scenarios.

When the test setup was set up, it was decided to place the objects at 20 cm both Tx and Rx. The emission power of the VNA was set at 10 dBm for all scenarios in a frequency range defined between 5.7 GHz and 5.9 GHz for the test with the narrowband antennas and between 1 GHz and 7 GHz for the tests with the UWB antennas. All setups were mounted within an anechoic chamber in order to eliminate possible parasitic reflections and thus not affect the results. The setup scheme can be seen in figure 4.13.

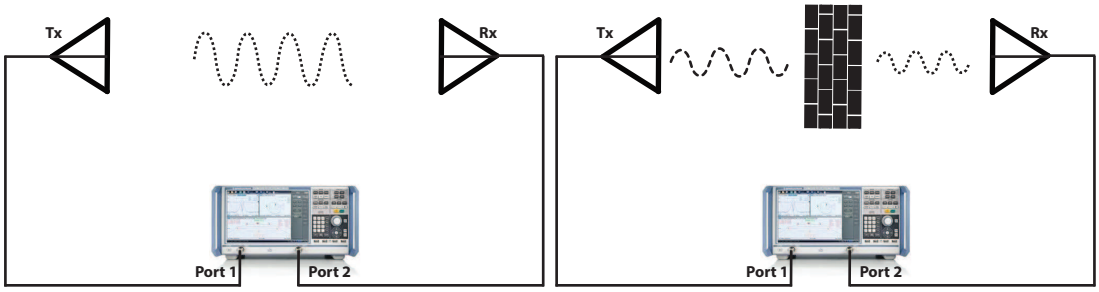

(a) Measure in free space (b) Measure with materials

Figure 4.13: Setup used to perform the tests

The objective of these two setups is to present the normalized measurements with respect to the "air", that is, first the free space attenuation is measured and then normalize the measurements of the different materials with respect to these losses in free space and in this way the result will be only the attenuation caused by the material. This technique is presented in the section 4 and on the equation 4.1.

4.3.2.3 Anechoic Chamber Setup

This setup follows on from those previously presented, not only due to some less successful results but also to achieve a setup that was immune to factors external to the experience.

This setup consists of the use of the anechoic chamber available in the Department of Electronics and Telecommunications of the University of Aveiro, where it is intended to use calibrated antennas, also available in the same department, which are usually used to characterize the antennas that are printed.

In figure 4.14, it can be observed the scheme of the available anechoic chamber in which it is possible to see the presence of later supports to place the antennas. In the setup developed the receiver antenna is placed inside the anechoic chamber, that is in the support on the left side of the image, and transmitting antenna in the support that is outside the camera, that is in the holder on the right side of the image.

For the placement of the materials to be studied, a wooden structure was constructed, which can be visualized in figure 4.15, which is placed against the window, which is present on the right side of the figure 4.14, on the outside.

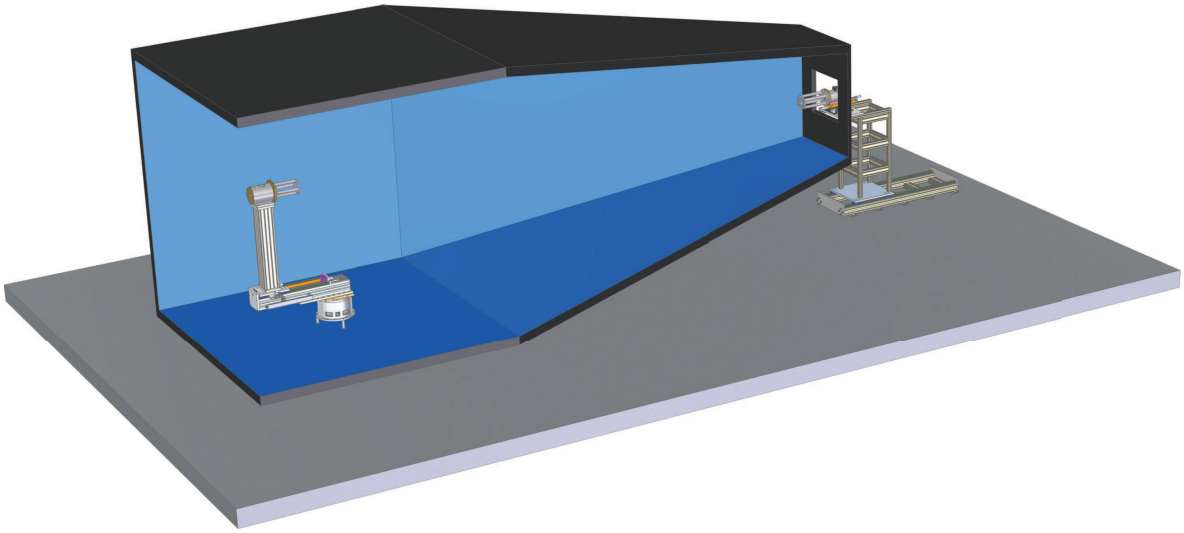

Figure 4.14: Anechoic chamber scheme

Figure 4.15: Wooden structure built

Due to the limited number of antennas available, it was decided that the study to be carried out would be between 2.5 and 6 GHz as it fits into the working frequency of the developed RADAR and due to the availability of an antenna with a range of 0.5 to 6 GHz and another 2.5 to 6 GHz.

In figure 4.16, the transmitting antenna is shown, which, as already mentioned, covers the 2.5 to 6 GHz band. The S11 parameter along the frequency are shown in the following figure.

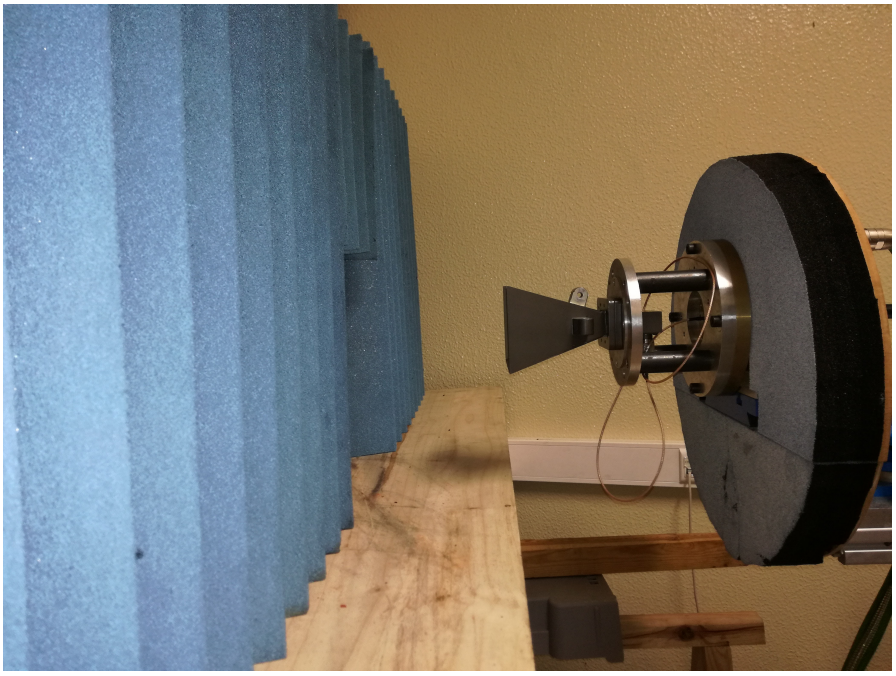

Figure 4.16: Transmission antenna

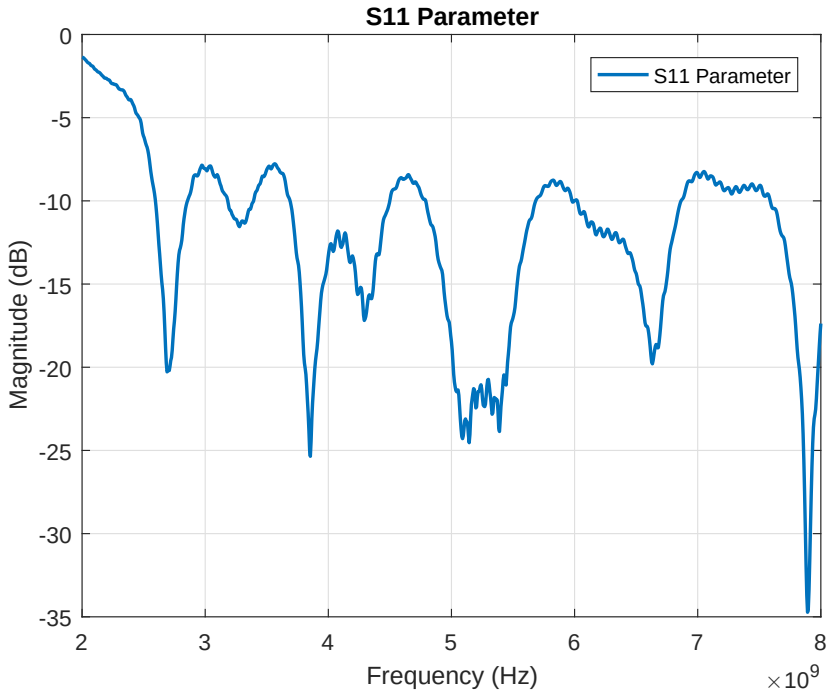

Figure 4.17: S11 parameter of transmission antenna

In figure 4.18, the receiver antenna, which covers the band from 0.5 to 6 GHz, is presented. As before, the S11 parameter along the frequency are shown in the figure that follow.

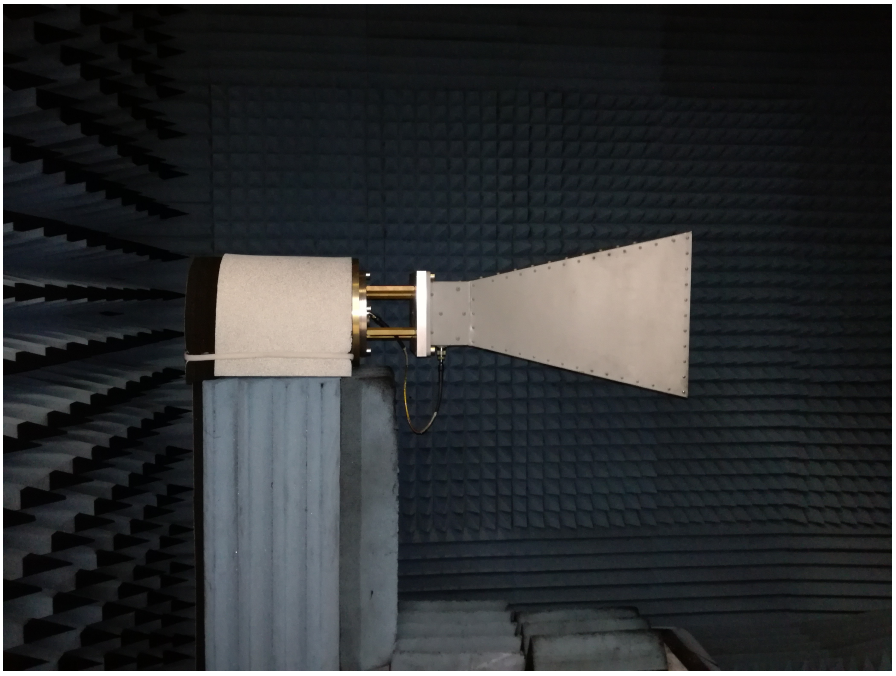

Figure 4.18: Receiving antenna

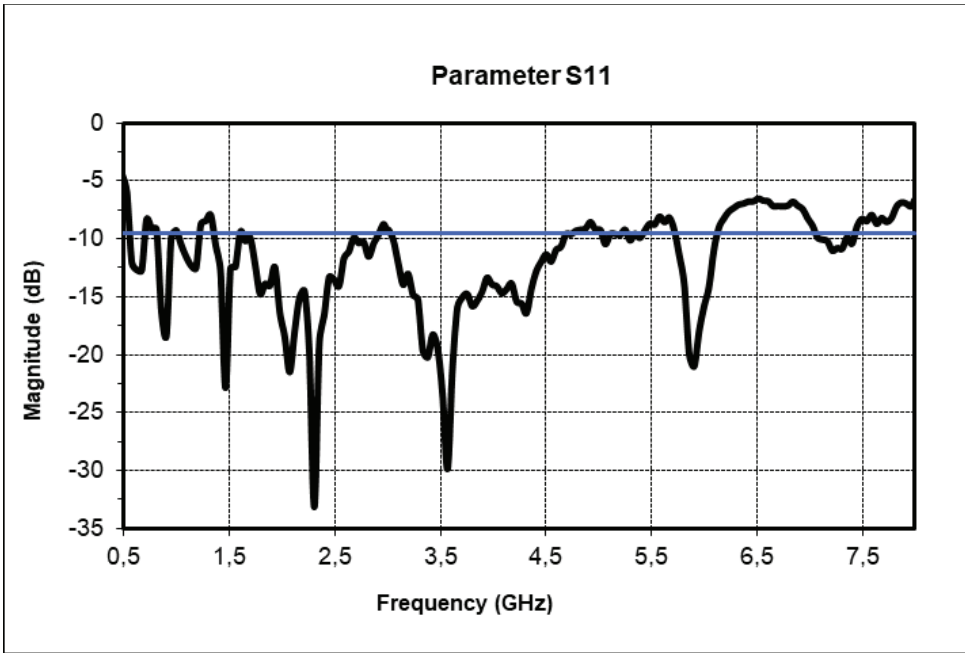

Figure 4.19: S11 parameter of receiving antenna

4.4 Materials Characterization Results

This section is also splitted in three subsections where is intended to present the results achieved for the characterization of the materials taking in account the setups and the antennas described in the section 4.3.

4.4.1 Narrowband Antenna Results

In this section is presented the measurements obtained for the tests performed according to the description made in the sections 4.3.1.1 and 4.3.2.2. The experimental setups executed are also presented in order to provide more information about how the measures were made.

The table 4.7 shows some preliminary results obtained from the measurements performed at 5.8 GHz. Although the experience provides more results, these are the most relevant for the work since the working frequency of the RADAR is 5.8 GHz. However the full results are also presented and can be observed in the figures 4.20, 4.21 and 4.22.

Material	**Thickness**	**Attenuation (dB) @ 5.8 GHz**
Wood	1 cm	$\approx 0,9$
1 brick	8 cm	≈ 7.5
2 brick	16 cm	≈ 9

Table 4.7: Attenuation results for 5.8 GHz

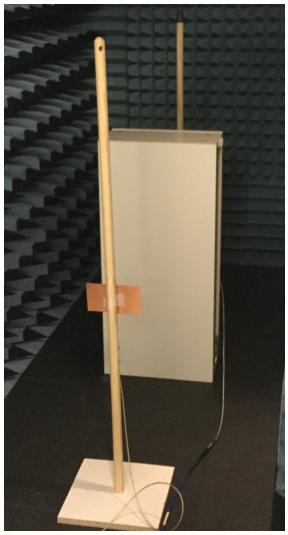

(a) Experimental setup

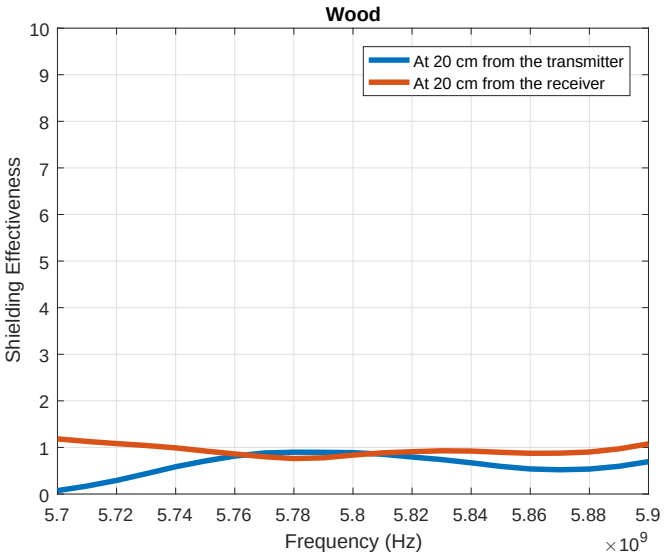

(b) Wood attenuation

Figure 4.20: Measurements of wood attenuation

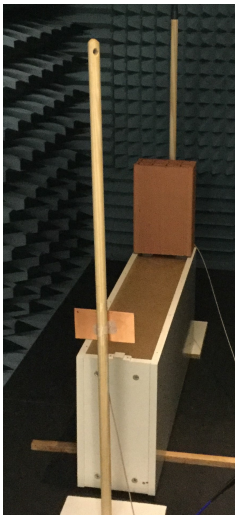

(a) Experimental setup

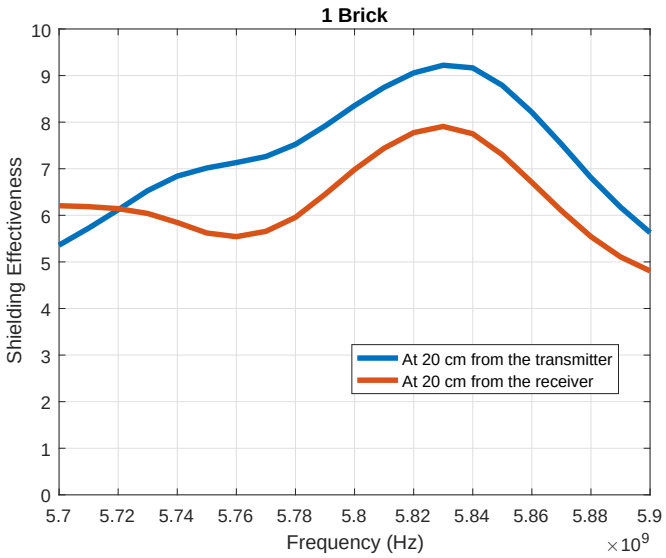

(b) 1 brick attenuation

Figure 4.21: Measurements of brick attenuation

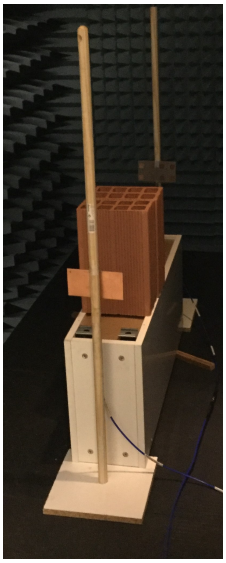

(a) Experimental setup

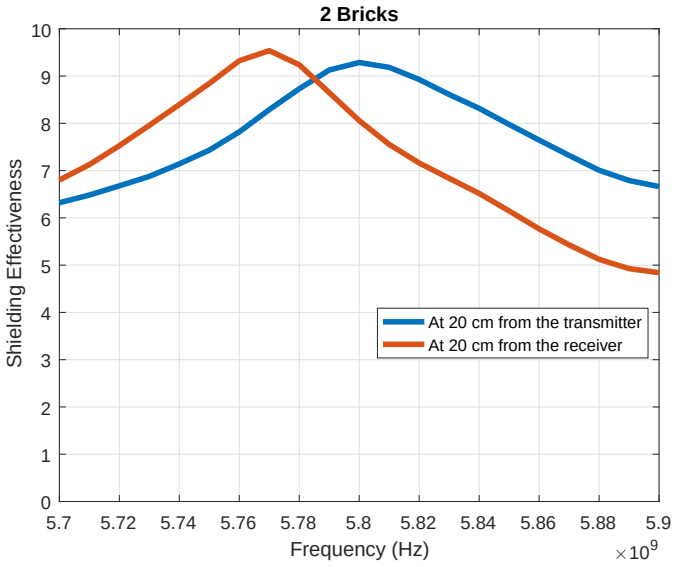

(b) 2 brick attenuation

Figure 4.22: Measurements of 2 bricks attenuation

From the analysis of the results of table 4.7 it can be concluded that when compared with the data presented in the beginning of the chapter, that the measurements acquired are very similar, although some very slightly differences. In this case these differences are due to the occurrence of a strange phenomenon, which can be observed in the figures 4.21 and 4.22. Considering figure 4.21 it can be seen that up to about 5.83 GHz the attenuation of the material grows, being in agreement with what was expected. However from this frequency a decrease of the attenuation value is observed. However, this phenomenon, although difficult to analyse, can be justified by the existence of signal and multipath diffraction, which are more strong signals than that which crosses the material , leading to denigration of results. The same type of phenomena occurs in the same way in the figure 4.22, except that in this case it is observed from 5.76 and 5.8 GHz. Despite all of this, in general the results are very satisfactory and are in agreement what was expected.

4.4.2 UWB Antenna Results

The tests and measurements performed in this section were obtained according to the description made in the sections 4.3.1.2 and 4.3.2.2. The experimental setups executed picture are also presented in order to provide more visual information about how the measures were performed.

The table 4.8 shows some preliminary results obtained from the measurements performed for some certain frequencies. However the full results are also presented and can be consulted in the figures 4.23, 4.24 and 4.25.

Material	Thickness	Attenuation (dB)				
		2 GHz	3 GHz	4 GHz	5 GHz	6 GHz
Wood	1 cm	≈ 1	≈ 3	≈ 4	$\approx 2,5$	$\approx 3,5$
1 brick	8 cm	≈ 0	≈ 0	≈ 4	≈ 4	≈ 6
2 brick	16 cm	≈ 0	≈ 0	≈ 5	≈ 7	$\approx 12,5$

Table 4.8: Attenuation results for UWB antenna

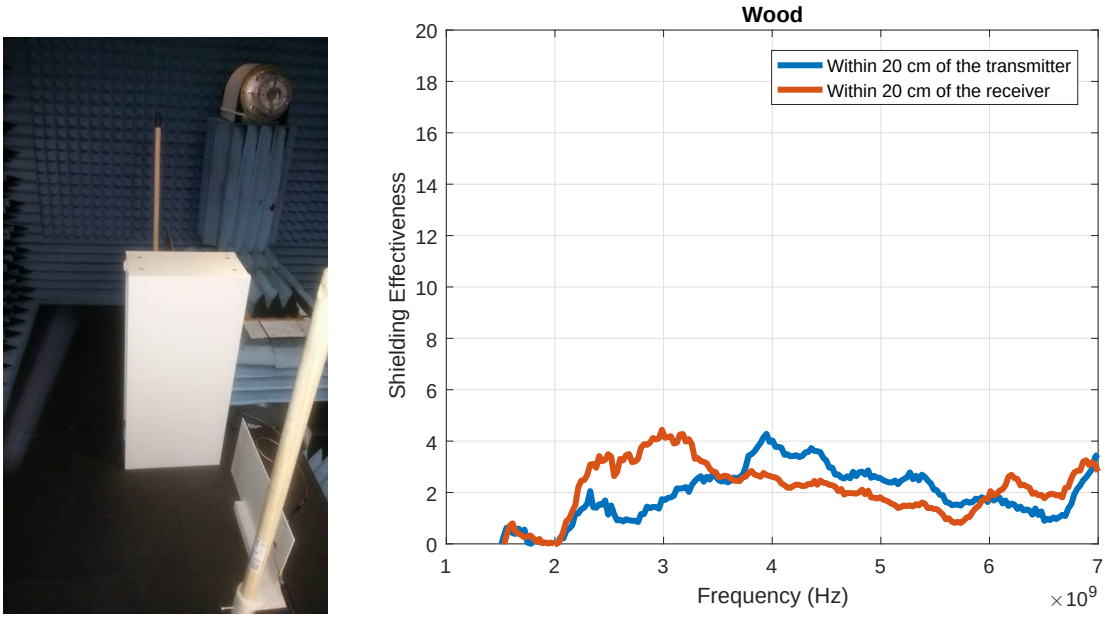

(a) Experimental setup

(b) Wood attenuation

Figure 4.23: Measurements of wood attenuation

By analysing the figures 4.24 and 4.25 it can be seen that the phenomenon observed in section 4.4.1 in figures 4.21 and 4.22 occurs again in these measurements. Starting with figure 4.24, it is possible to observe an almost linear growth of attenuation, except at 4.5 and 6 GHz, where there is a peak of attenuation that can be justified by the same facts presented previously. In the figure 4.25 the frequency response is practically the same as the peaks occurring approximately at the same frequencies. The most noticeable difference is that, in general, the attenuation values are relatively higher when compared to those in figure 4.24.

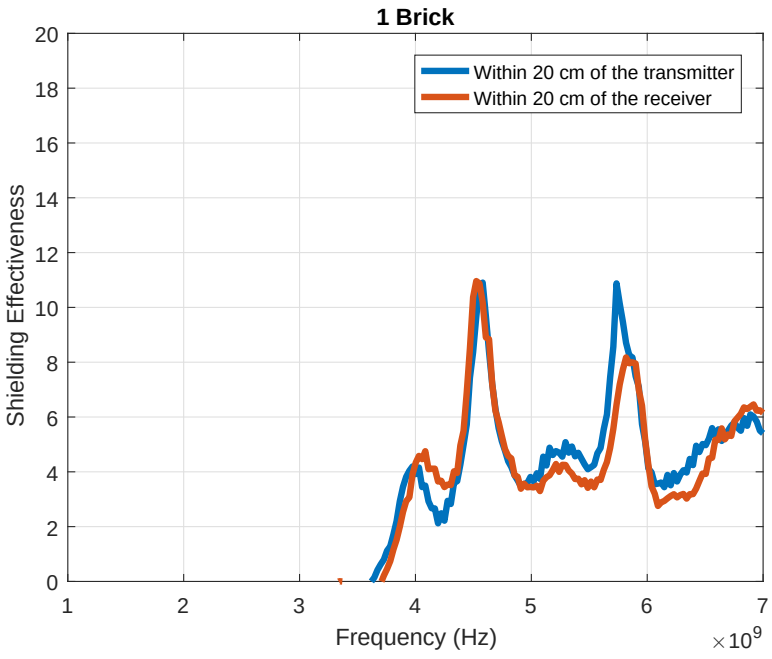

Figure 4.24: Measurements of brick attenuation

(a) Experimental setup

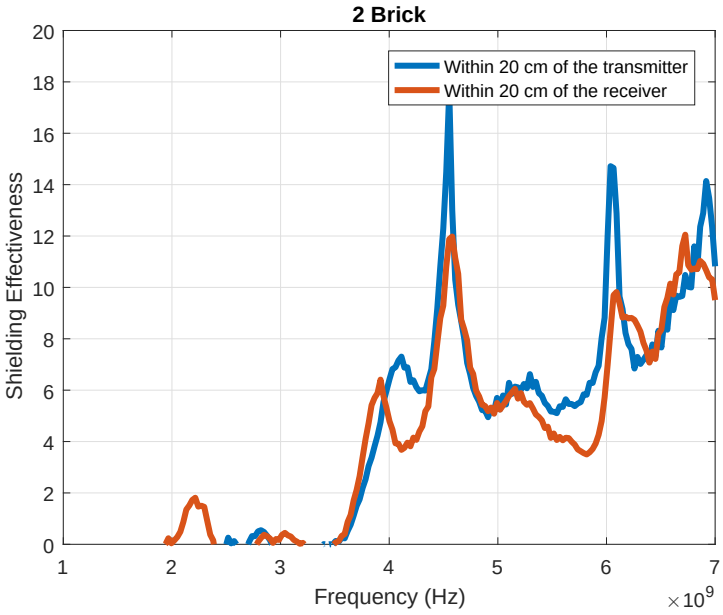

(b) Wood attenuation

Figure 4.25: Measurements of 2 bricks attenuation

4.4.3 Anechoic Chamber Results

The tests and measurements performed in this section were obtained according to the proceeding detailed in section 4.3.2.3. The experimental setups executed picture are also presented in order to provide additional information about how the measures were performed.

In this experiment only bricks were analysed in which they were placed in a kind of wall. Tests were performed with two types of bricks, clay bricks with holes and solid clay bricks. Throughout the tests the thickness of the wall was varied, increasing the number of layers of bricks, thus perceiving the attenuations for more or less thin walls. These results are presented in the following subsections.

4.4.3.1 Clay Bricks with Holes

The measurements performed in this section focused on measuring the attenuation of clay bricks with holes. This was to confirm the results obtained in the section 4.4.2. The results as well as their analysis are presented below.

Analysing the figures 4.26 and 4.27 it can be seen that the attenuation increases as the frequency increases. In spite of this, it is possible to observe some attenuation peaks, which appear, for example, between 3.5 and 4.5 GHz. Considering the dimensions shown in figure 4.28, it can be seen that the brick hole is about 4 cm long side and the diagonal is about 5 cm.

Knowing that the wavelength (λ) is calculated by the following expression, where c is the speed of light in the air and f corresponds to the frequency in question::

$$\lambda = \frac{c}{f} \tag{4.2}$$

When we consider, for example, the frequency 3.7 GHz (approximately the frequency at which the first peak appears) and calculate the wavelength, the result is approximately 8.1 cm. Now this value is approximately the double of the length of the brick hole. So it can be concluded that for certain frequencies where their wavelengths are a multiples of the length of the hole, this will behave like a cavity and thereby increases the attenuation value. This may also explain the peaks that appear in the graphs relating to the measurement of the attenuation of the bricks on section 4.4.2.

(a) Experimental setup

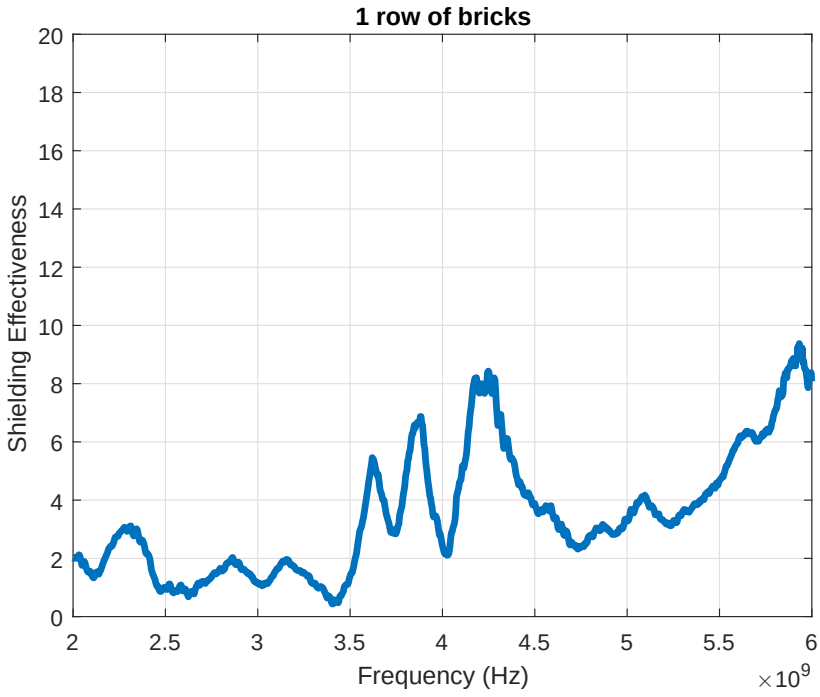

(b) Measurement result

Figure 4.26: Measurements with a row of bricks

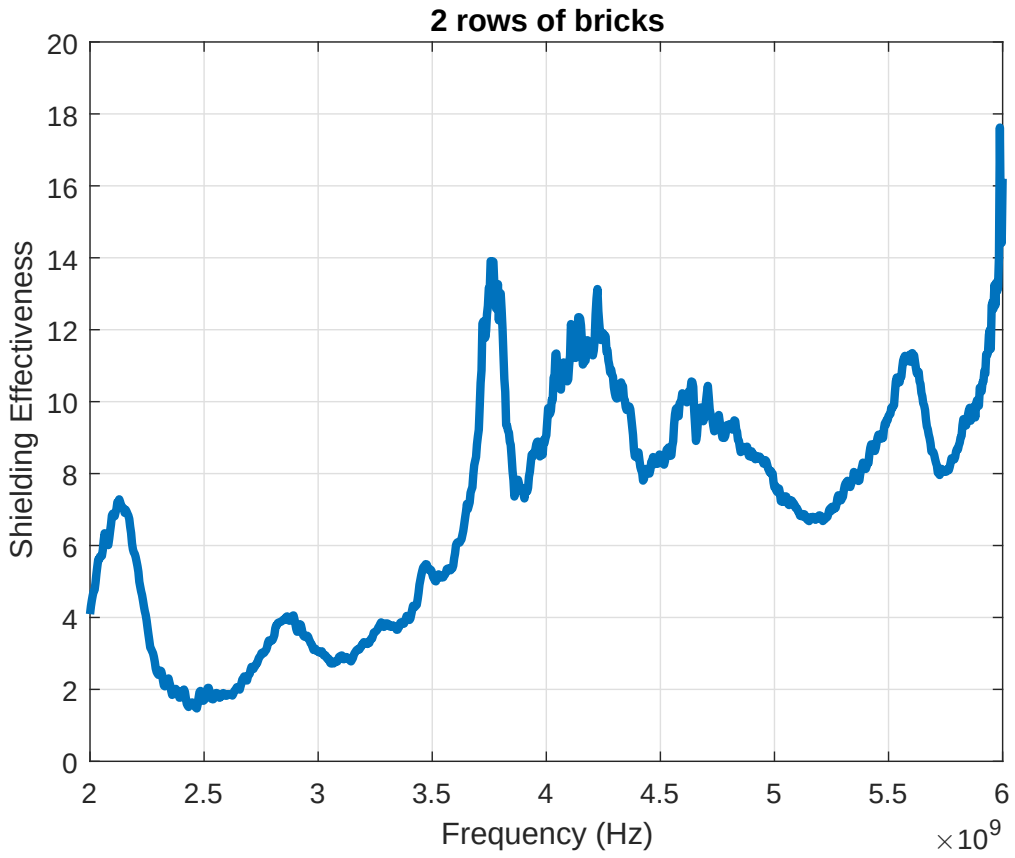

Figure 4.27: Measurements with two rows of bricks

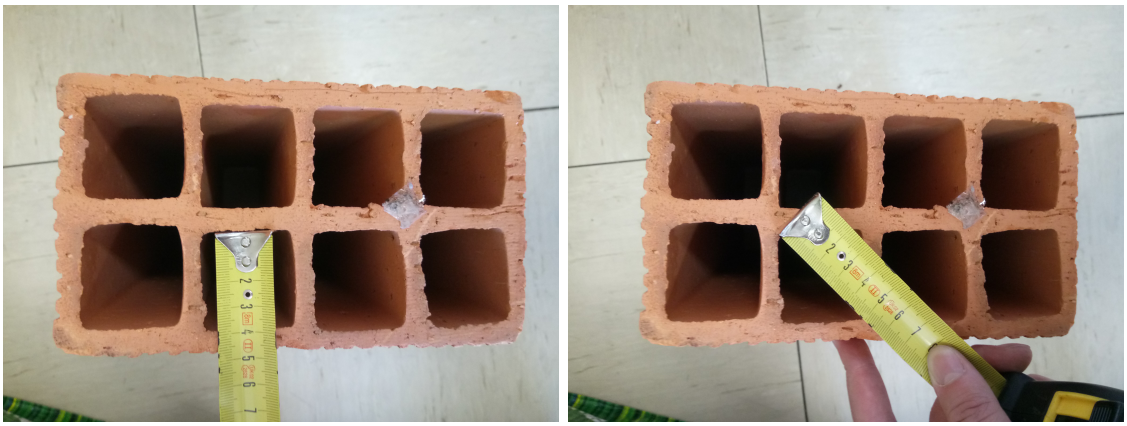

(a) Hole length (b) Measurement result

Figure 4.28: Dimension of the brick hole

4.4.3.2 Solid Clay Bricks

In this section we intend to study the attenuation of other types of bricks, in this case of solid clay bricks, in order to expand the study, but also because the building of the Instituto de Telecomunicações is coated with this type of material.

In this experiment only bricks were analysed in which they were placed in a kind of wall. In order to know the relationship between thinner or coarse objects, three experiments were performed in which walls were analysed with a layer of bricks up to three layers. These results are presented in the following figures.

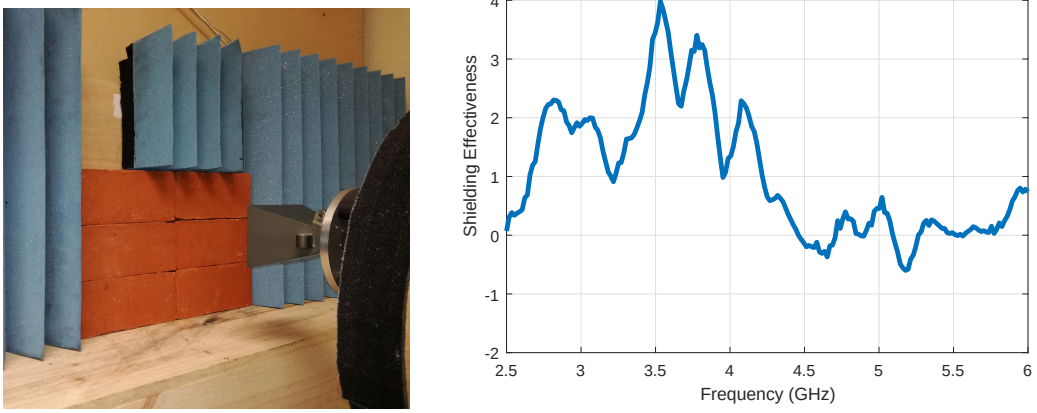

(a) Experimental setup (b) Measurement result

Figure 4.29: Measurements with one layer of bricks

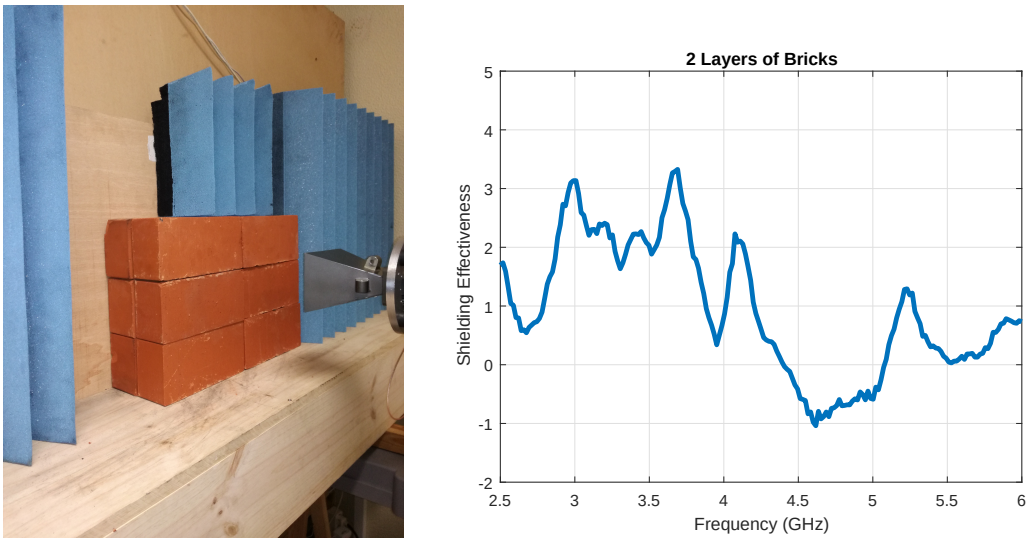

(a) Experimental setup (b) Measurement result

Figure 4.30: Measurements with two layers of bricks

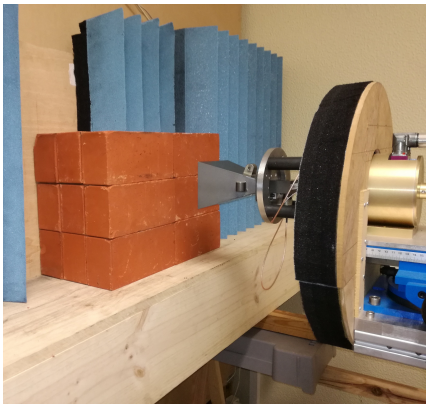

(a) Experimental setup

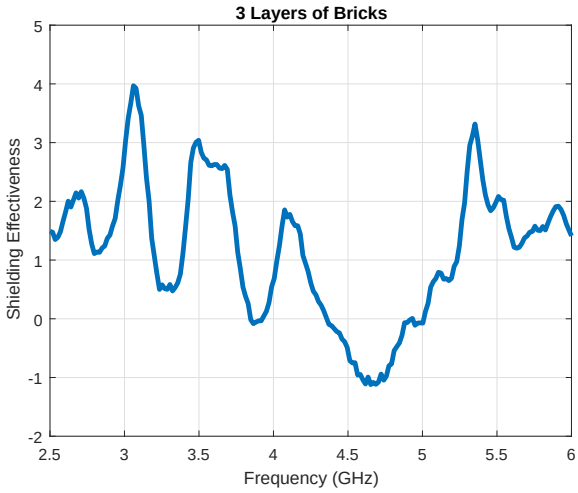

(b) Measurement result

Figure 4.31: Measurements with three layers of bricks

Analysing the figures presented previously it can be affirmed that the results are not at all what was expected and intended. It can be observed in the graphs presented that the values obtained do not tend to increase along the frequency as predicted, but also presents great oscillations in their values, even in some cases "gain".

Given these results, we sought an explanation for these results. Given the values obtained, and as mentioned, in some cases the existence of gain was hypothesized to be before a lens effect caused by the wall constructed. After that, a setup was mounted to prove the presence of this phenomenon.

This test was performed under the same conditions as the previous experiment, that is, it was performed in the anechoic chamber and the same antennas were used. In this case the position of the antennas has been changed, that is, the transmitter has passed the receiver and vice versa.

The experience to prove the existence of the lens effect consists of measuring the radiation pattern of the antenna with and without obstacle in front of it. In this way two measurements were made, one in which the radiation diagram was measured in open space, as shown in figure 4.4.3.2 (a) and another where a brick was attached to the antenna, figure 4.4.3.2 (b), and its radiation pattern was measured again. The measurement was made for 3.5 GHz.

To affirm that we are in the presence it is necessary that at least two conditions are verified. The first is the narrowing of the beam width that will cause the energy to be focused on a smaller area. The second concerns the energy received, in which the energy will be greater with the lens effect.

(a) Experiment in free space

(b) Experiment with brick

Figure 4.32: Setup to measure lens effect

By observing the graphs of figure 4.33, we can affirm that the presence of a lens effect is proved when trying to measure the attenuation of this type of brick. For both horizontal polarization and vertical polarization we see that the beam width is relatively smaller when the brick is placed in front of the antenna but also receives a little more energy.

With these results, the results obtained for the attenuation measurement can therefore be justified. In this case we have studied only the effect of a brick, but it can be expected that the presence of more bricks and more layers will affect the results on a larger scale.

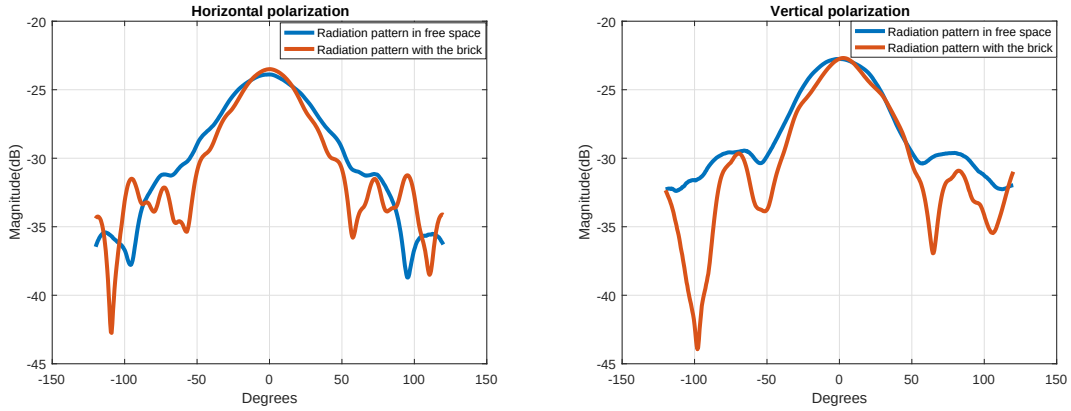

(a) Horizontal Polarization

(b) Vertical Polarization

Figure 4.33: Radiation patterns for various polarizations

4.5 Conclusions

With the analysis of the results presented in section 4.4.1, it can be concluded that in general the results are in agreement with those that were presented at the beginning of the

chapter, despite the occurrence of the phenomena. To a certain extent, a portion of the results are in agreement with what was expected.

In section 4.4.2, it was again observed the presence of external phenomena to the measure, which ended up leading to less positive results in certain parts, since these results generally denigrate the results. However, despite the oscillations observed, most of the results are in agreement with those that were used as reference, not invalidating all the results obtained.

Observing and analysing the results in the section 4.4.3, it can be concluded that we have good and not so good results. In section 4.4.3.1 the results were quite positive, despite the presence of some peaks. In any case, an explanation was presented to justify its existence, in which case, the justification presented is that for certain frequencies the brick hole behaves like a cavity, increasing the attenuation value. The section 4.4.3.2 presents results not so encouraging, however, despite the poor results we tried to find a justification and we were able to prove the existence of a phenomenon that would have affected in a large scale the results obtained, in this case, the lens effect.

Despite several attempts and efforts in these experiments, it was not possible to calculate the channel model in order to be able to justify the observed phenomena due to the lack of temporal availability, but a critical analysis of the work was done and an attempt was made to provide an explanation for the phenomenon that occurred. In section 7.2 is provided suggestions that may improve the results.

Chapter 5

Radar System Design

This chapter aims to present all systems and setups developed throughout this work, as well as a description/function all the blocks that are part of the system.

5.1 Introduction

In this chapter the developed RADAR system is presented, using a block diagram of the same. Then, there is a presentation of the elements that are part of this RADAR, where a small explanation of its operation and the main characteristics are given. The antennas developed for this project are also presented. Finally, the algorithm developed for the detection of persons and the presentation and analysis of the results obtained are presented.

5.2 Overall System

In this section we will present the complete system developed in order to achieve the objectives proposed for this dissertation. Therefore, in the several sections is presented each part of the full system, the reason why these were chosen and his function in it.

The proposed and implemented RADAR system consists of three main blocks, the FPGA Xilinx ZC706 (section 5.3), the RF front-end with SDR architecture AD-FMCOMMS5 (section 5.4), and the developed antennas (section 5.5), as can be seen in the figure 5.1.The system also has a connection to a Personal Computer (PC) via Ethernet to the FPGA, to control and set all the parameters in the system by MATLAB. In the following paragraphs a detailed description of the functions of each block in the system is presented.

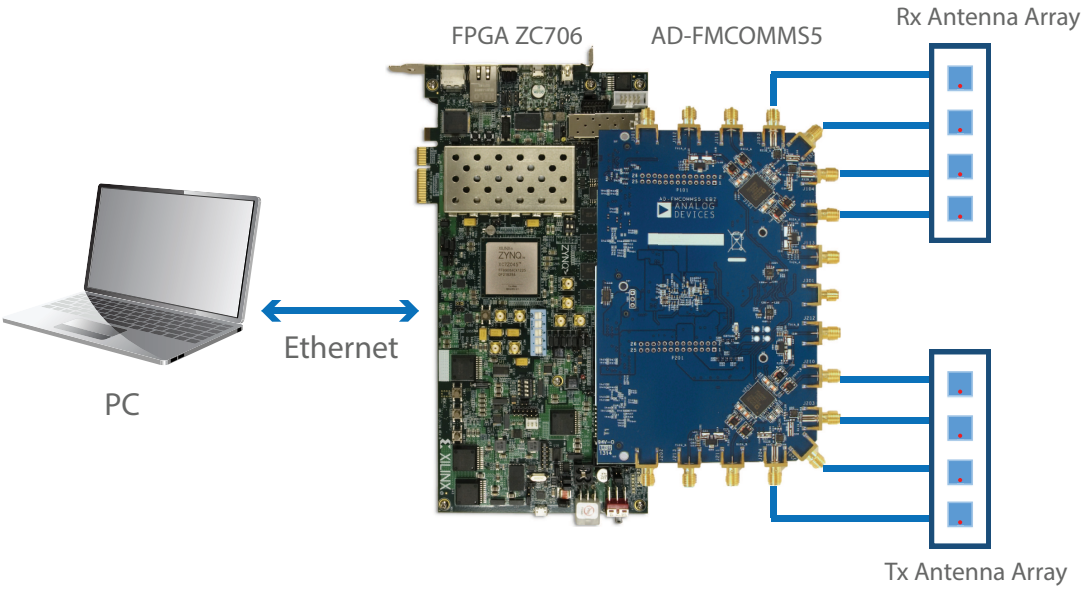

Figure 5.1: General system block diagram

The PC is an integral part of the system as it controlls and monitors the proposed system. Through an Ethernet connection between the PC and the FPGA it is possible to define all the parameters, which are defined by software, of the system. It is also at this stage that all software is developed, such as algorithms that are later loaded into the FPGA and all the signal processing.

The FPGA besides providing the connection to the AD-FMCOMMS5 board and the PC is also responsible for the analysis and processing of the signals. In this processing, the entire received signal passes through a low pass filtering stage in order to eliminate some existing noise and subsequently sends that data to the PC where all signal processing is performed.

Considering now to the RF front end AD-FMCOMMS5, it uses the AD9361 Radio Frequency Integrated Circuits (RFICs), allowing to generate, modulate and demodulate RF signals. The signals are generated in baseband, then are modulated for the desired RF frequency and before they are sent to the antennas, the signals are amplified by a PA, that end the transmission stage. In the other way, the reception stage has exactly the same steps but to demodulate the signals from RF frequency to baseband. Note that in the section 5.4 it is mentioned the existence of two chips AD9361 inside the board AD-FMCOMMS5 and observing the figure 5.2 is easily perceivable the presence of the blocks of one of the chips. This is due to the fact that the other chip has exactly the same architecture and therefore would not be relevant to present it. It is also important to note that the two chips share the same reference oscillator, each with two transmitters and two receivers, that allows the implementation of a MIMO 4x4 radio as well as supports the realization of beamforming.

Finally, the antennas are responsible for radiating the signals generated and modulated

by the RF front-end to the air and likewise receiving echoes from the reflections in the most diverse objects and forwarding them back to the RF front-end and proceed to the processing of the data received.

The figure 5.2 shows the complete system block diagram of the system.

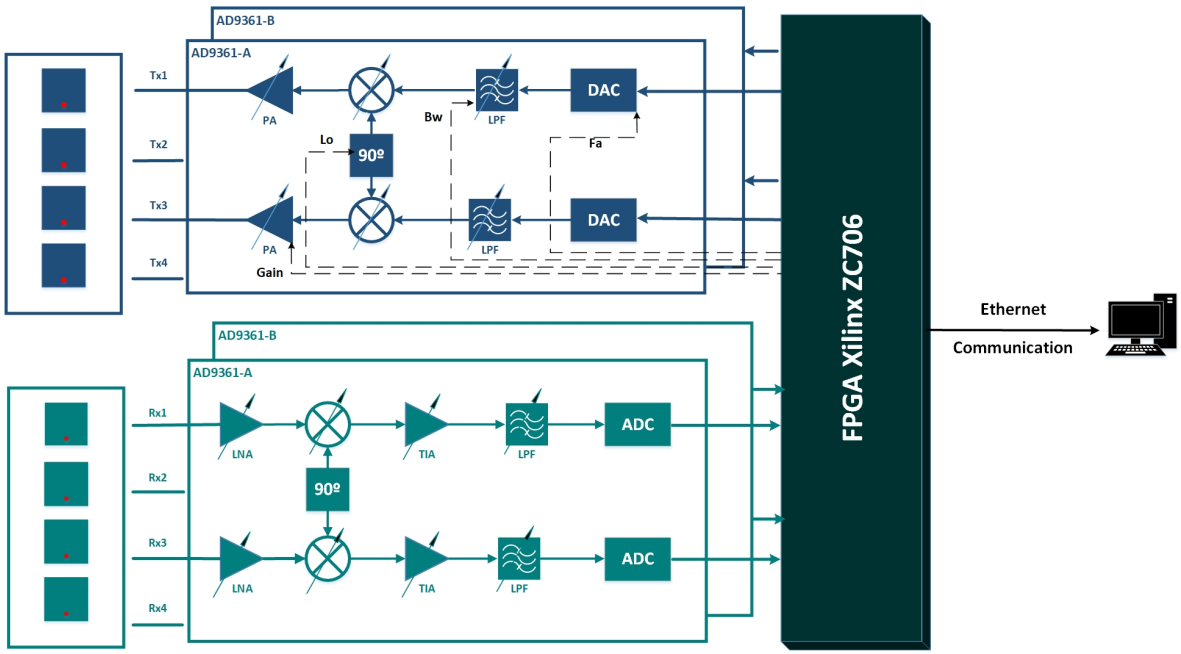

Figure 5.2: System block diagram

As mentioned before, the two AD9361 chips share the same reference oscillator, as can be seen in the figure 5.3, that ensures that the Local Oscillator (LO) frequency of chip A (f_{LO_A}) is equals the LO frequency of chip B (f_{LO_B}). However this configuration does not guarantee that the chip A phase (θ_A) is equal to the phase of the chip B (θ_B) since the Phase Lock Loop (PLL) of the LO of each chip does not lock at the same time and in this way there will be a phase difference between the two chips that needs to be compensated in order to have a coherent and synchronous system.

$$f_{LO_A} = f_{LO_B} \overset{Does\ not\ guarantee}{\Longrightarrow} \theta_A = \theta_B \tag{5.1}$$

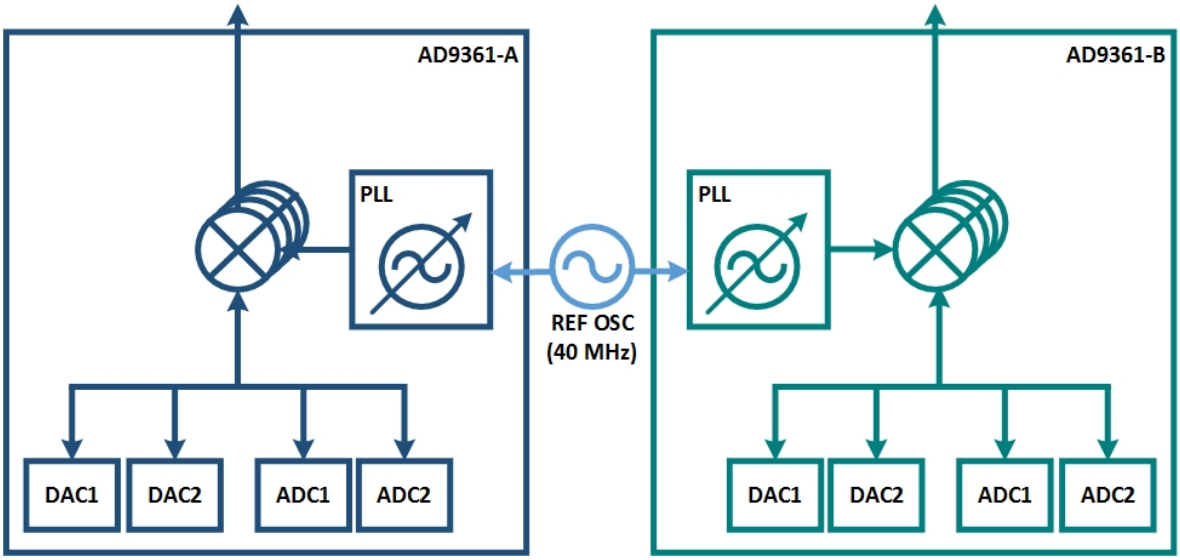

Figure 5.3: AD-FMCOMMS5 Chip Link

In order to have the system completely synchronous, a calibration algorithm was developed by Daniel Malafaia, PhD Student at Instituto de Telecomunicações, which is based on the connection of the chips to switches where a comparison is made between the phase of the DAC of a chip with the DAC phase of the other chip. Knowing this phase difference it is possible to make the necessary compensation in the other elements to make the system synchronous.

5.3 FPGA Xilinx ZC706

Advanced SDR systems are essential for performing tasks such as data processing, communications, real-time task constraints, and the user interface that may have different bandwidth requirements. According to the previously described it can be concluded that for applications like radars is also necessary a radio with great capacity of processing and in this way the hardware chosen for the implementation of the same one must be the most robust possible, that allows possible updates and improvements . It was then considering all aspects that the Xilinx Zynq-7000 All Programmable SoC ZC706 was chosen, because it provides a great performance in signal processing as it also contains configurable logic. The figure 5.4 is the image of the board with the signalling of the most important pins and ports, [31].

Among others the most relevant specifications of this board are: [31]

- Dual ARM Cortex-A9 core processors - Central Processing Unit (CPU) frequency: Up to 1 GHz;
- 1 GB DDR3 Component Memory;
- 1 GB DDR3 SODIM Memory;

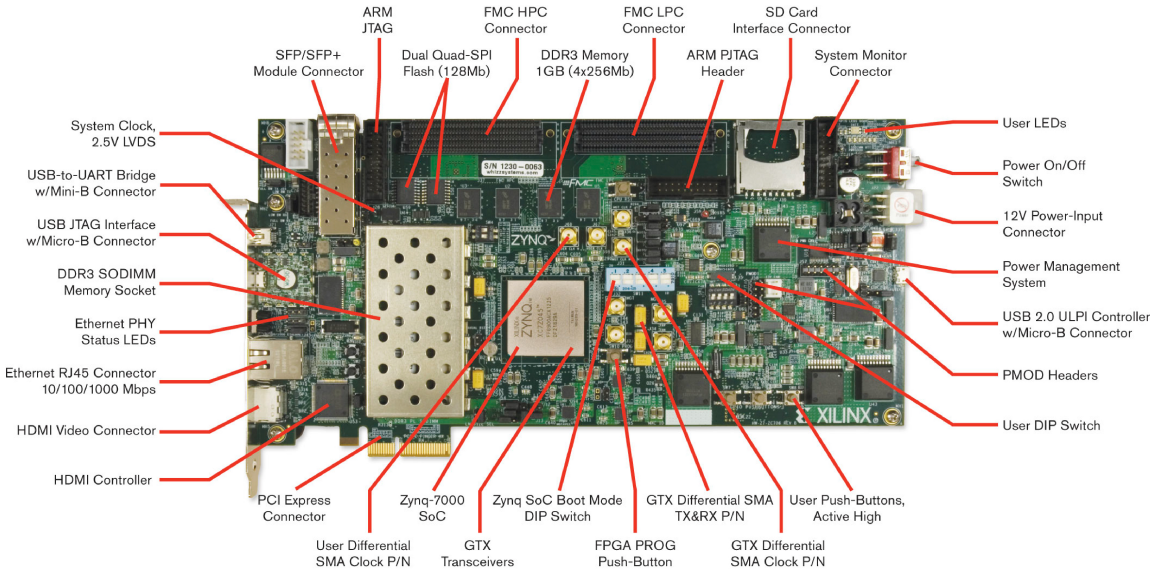

Figure 5.4: ZC706 Evaluation Kit [32]

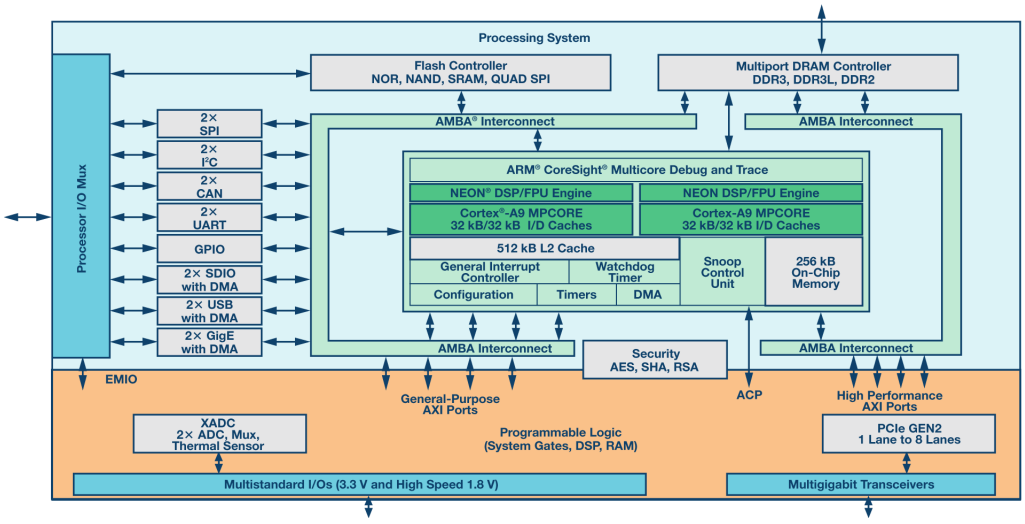

Figure 5.5: Xilinx ZC706 Block Diagram [33]

The figure 5.5 [1] shows the internal block diagram of the plate where it is possible to visualize the various sub-blocks that constitute it. The processor supports operating systems, in this case Linux that allows using of the board without having to configure the programmable logic, since the company has developed this software.

Analysing the characteristics of the FPGA it can be verified that all the requirements are covered by this, and in this way it has become easy to choose this equipment to perform all the data processing necessary for the implementation of the RADAR.

[1] Figure taken from: `http://www.xilinx.com/products/boards-and-kits/ek-z7-zc706-g.html#overview`. Accessed on: 18-04-2017

5.4 AD-FMCOMMS5-EBZ

In recent years the SDR market has undergone major revolutions in the development of SDRs capable of fulfilling the requirements of today's systems. Analog Devices has been a pioneer in this field and the AD-FMCOMMS5-EBZ board is a prime example of this. This board has two AD9361 chips (its block diagram is shown in figure 5.7[2]) which are currently one of the most commercialized for applications such as wireless communications, electronic defence systems due to its high performance and highly integrated RF transceiver. With these devices it is possible to combine the RF front end with mixed-signal baseband section and frequency synthesizer as well as the configuration of an interface with an FPGA [3].

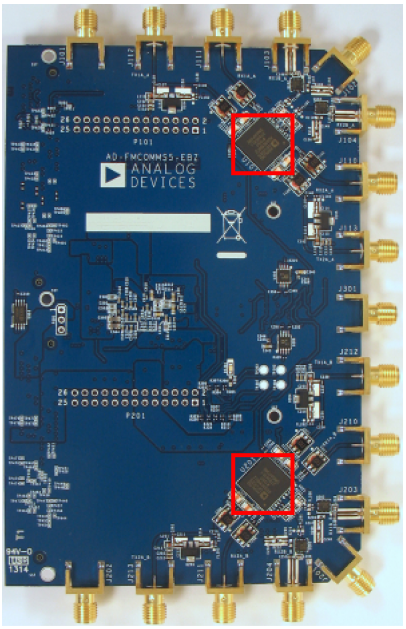

Figure 5.6: AD-FMCOMMS5-EBZ Evaluation Board

The figure 5.6 shows an image of the AD-FMCOMMS5-EBZ board, where it is possible to verify the presence of the two AD9361 chips (in red squares) as well as all its ports. Among others the most relevant specifications of this board are [33]:

- RF 2x2 transceiver with 12-bit DACs and ADCs;
- Tx band from 47 MHz to 6 GHz;
- Rx band from 47 MHz to 6 GHz;
- Channel bandwidth from 200 kHz to 56 MHz;
- Phase and frequency synchronization, enabling the implementation of a MIMO 4x4 platform;

[2]Taken from: `http://www.analog.com/en/analog-dialogue/articles/using-model-based-design-sdr-1.html`. Accessed on 19-04-2017

[3]Taken from: `http://www.analog.com/en/analog-dialogue/articles/using-model-based-design-sdr-1.html`. Accessed on 19-04-2017

- Equipped with dual FMC connectors, allowing for connectivity with the Xilinx ZC706 board.

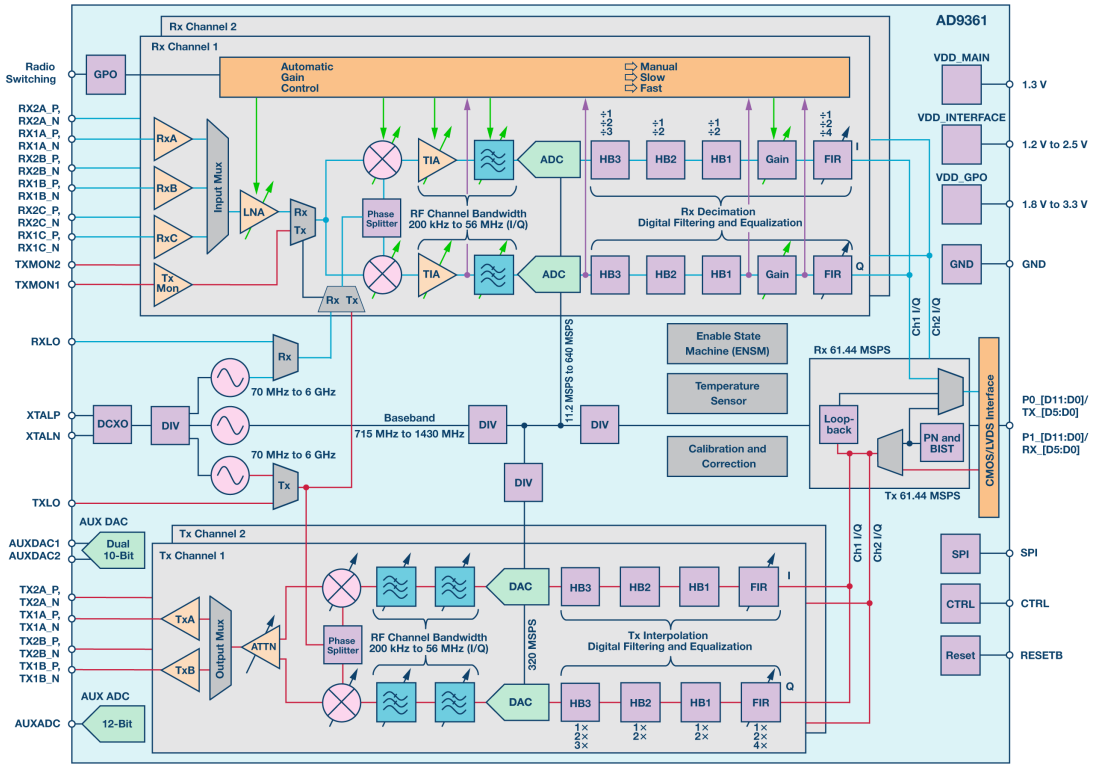

Figure 5.7: AD9361 Block Diagram [33]

The applications for which this evaluation kit is recommended and which are listed by the manufacturer [4] are:

- General design for SDR applications;
- MIMO radio;
- Beamforming and angle of arrival detection for transmission and reception respectively;

By analysing the applications that are listed by the manufacturer as the most suitable implementations for this kit, it is understandable that it fits and fulfils the requirements that were intended to achieve the objectives of this dissertation.

5.5 Antennas

In this section will be presented the design of the antennas for the RADAR system. The motivations of our design options as well as more detailed information is also presented.

[4] Taken from: `http://www.analog.com/en/design-center/evaluation-hardware-and-software/evaluation-boards-kits/eval-ad-fmcomms5-ebz.html#eb-overview`. Accessed on: 18-04-2017

Below is a table with the relevant information about the substrate considered for the simulation and design of the antennas developed for this dissertation. The reason for its choice fall back in their immediate availability in the laboratory of the Instituto de Telecomunicações but also because of the trade off between the characteristics and the cost.

Substrate parameters	
Name	ISOLA IS680
Dimensions	305x460 mm
ε_r	3.38
Thick	1.52 mm
Cooper	35 μm
Loss Tangent	0.0025

Table 5.1: Substrate informations

Knowing that one of the objectives of this dissertation is to be able to detect people or objects through walls or other obstacles, it is necessary to be able to focus radiated energy a narrow beam in order to improve the detection. With this in mind, and after some research, it was decided that the best solution would be the design of an antenna that has a high gain and directivity, so that it can focus the maximum energy in a certain direction.

5.5.1 1^{st} Version

Initially it was considered that it would be necessary to design and implement an antenna with relatively high directivity and gain that will improve the chances of detecting movement.

Taking into account what was described, it was decided that the antenna consisted of 4 rectangular patches fed independently. In this way a relatively good gain was obtained but it was also possible to have a narrower beam reaching what was expected. Table 5.2 contains information about the most important parameters of the designed antenna.

Antenna parameters	
Central Frequency	5.8 GHz
Patch width	12.66 mm
Patch length	18.67 mm
Gain (of each patch)	$\approx$ 7.4 dB
Total gain	$\approx$ 12.5 dB

Table 5.2: 1^{st} version antenna parameters

The figure 5.8 shows the scheme of the antenna simulated with recourse to the CST with information about its dimensions and distance between elements.

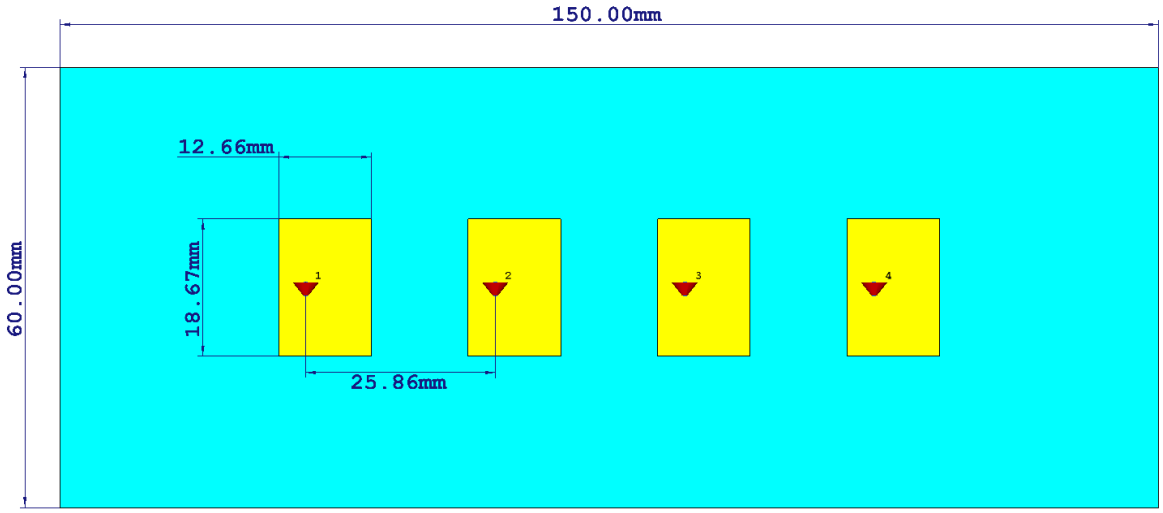

Figure 5.8: Antenna layout at CST

In the figure 5.9 the antenna, which was printed with the CNC available in Instituto de Telecomunicações is presented.

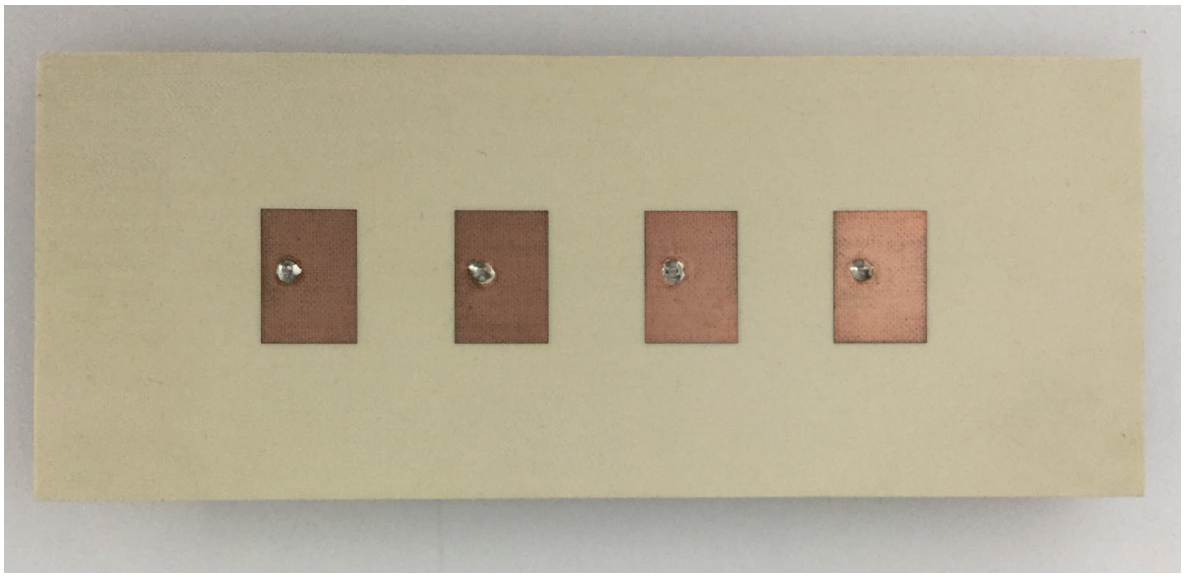

Figure 5.9: 1^{st} version printed antenna

The following graphs presented below correspond to the S_{11} parameter of each patch. The graphs contain 2 curves, one about simulation values provided by the CST simulation and the practical results which were measured using a VNA.

With the analysis of the graphs one can already observe small differences between the results of the simulation in the CST with the practical values measured in the VNA. One

such difference lies in the fact that the printed antenna has a small frequency shift, about 50 MHz to the right side. The other passes through the value of parameter S_{11} since in most patches the simulated value is slightly lower than the one measured.

All these differences between the simulation to the antenna printing can be explained by the fact that the simulation rarely models all the material effects but also can be justified by small errors of the CNC in the impression that can affect both the performance of the antenna but also as was seen in this case can cause a shift in frequency.

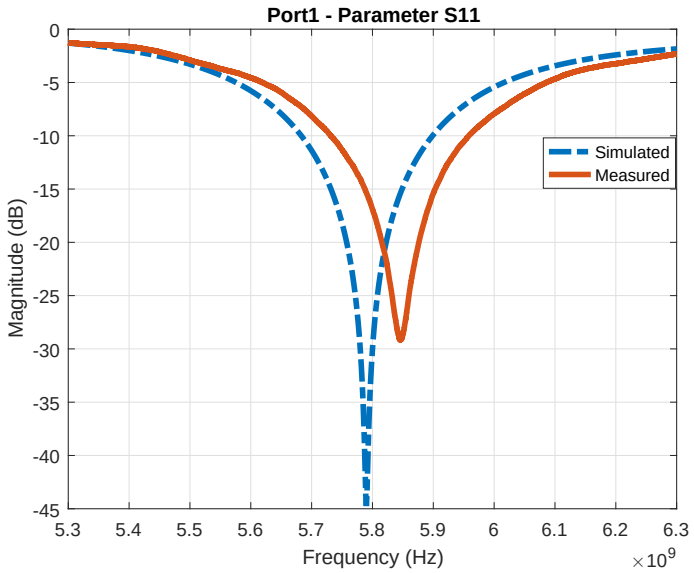

Figure 5.10: Parameter S11 of patch 1

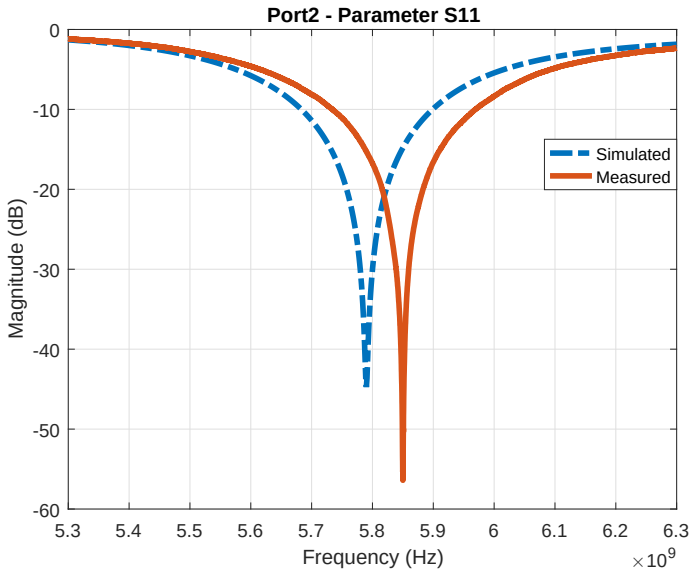

Figure 5.11: Parameter S11 of patch 2

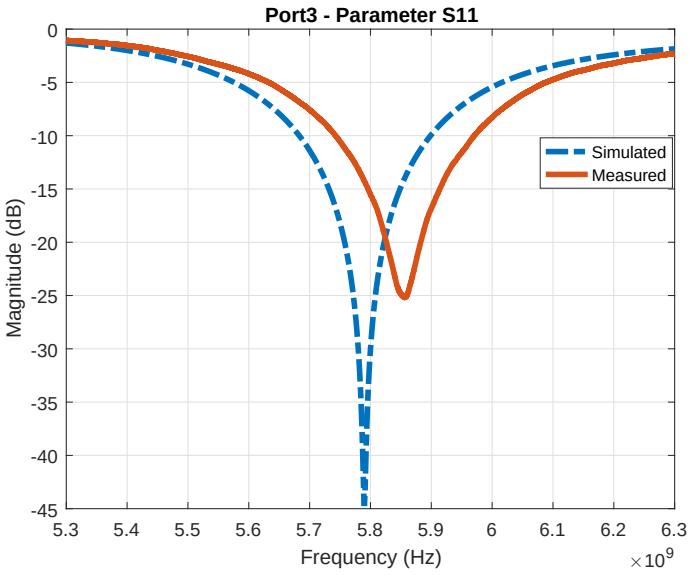

Figure 5.12: Parameter S11 of patch 3

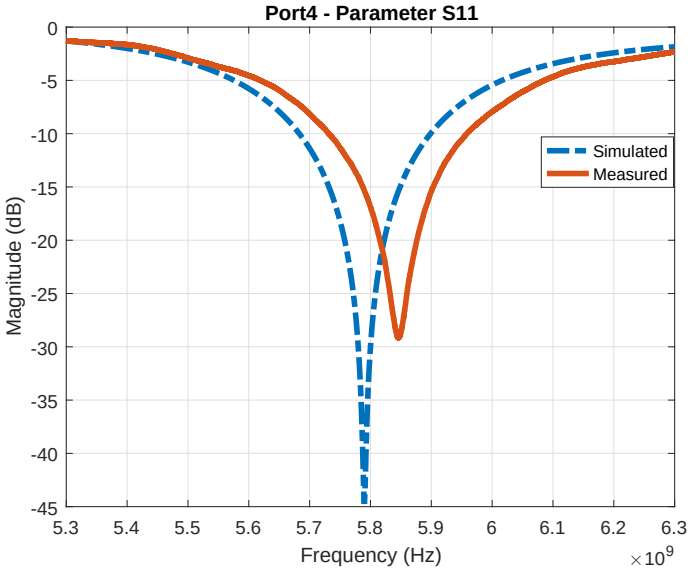

Figure 5.13: Parameter S11 of patch 4

In figure 5.14, the radiation pattern of each one of the elements of the antenna are presented, where it can be seen its gain.

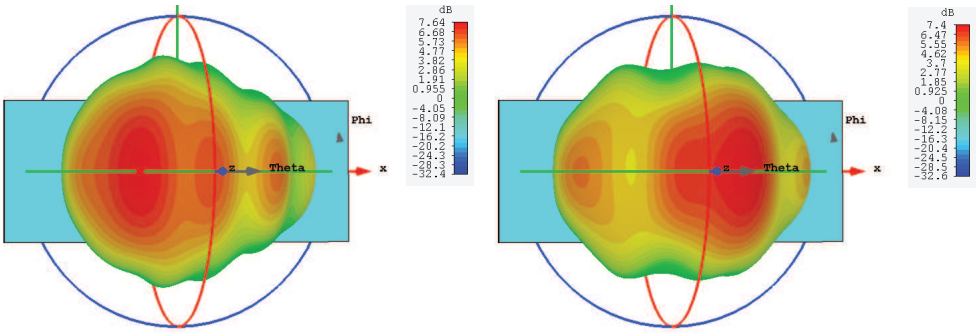

(a) Radiation pattern of patch 1

(b) Radiation pattern of patch 2

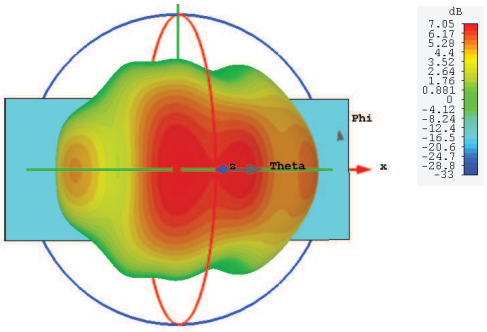

(c) Radiation pattern of patch 3

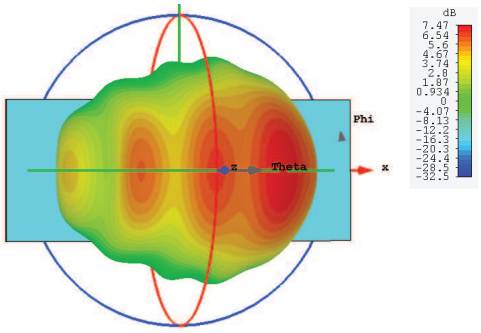

(d) Radiation pattern of patch 4

Figure 5.14: Radiation pattern of each patch

When fed simultaneously, with equal amplitude and in phase, the antenna will present a new radiation diagram when compared to the previous images in which each patch was fed alone. This new radiation diagram can be seen in figure 5.15

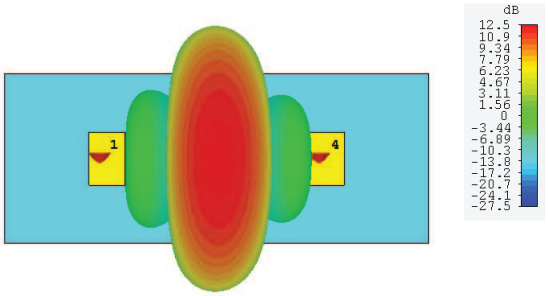

Figure 5.15: Antenna radiation pattern with phase feed of all patch

5.5.2 2^{nd} Version

Although the results of the projected antennas were very positive, it was considered that it could be even more advantageous to have antennas with higher gain, thus focusing the transmitted energy in a single point.

Retaining all the points mentioned above, a study of the linear aggregate that fulfilled the necessary requirements was made, ending with the selection of a 4-element serial fed-array patch antenna. Below is a table containing the most relevant information about the frequency, dimensions and gain of the antenna that was simulated using the CST.

Antenna parameters	
Central Frequency	5.8 GHz
Patch width	7.10 mm
Patch length	13.77 mm
Line width	0.81 mm
Line length	15.28 mm
Gain (of each aggregate)	$\approx$ 13.4 dB
Total gain	$\approx$ 19 dB

Table 5.3: 2^{nd} version antenna parameters

The figure 5.16 represents the scheme of the simulated antenna in the CST with some information about its dimensions.

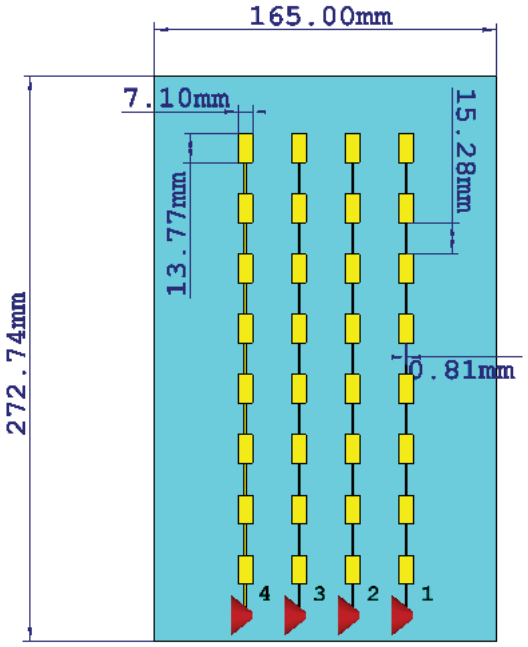

Figure 5.16: Antenna layout at CST

The next figure 5.17 shows the printed antenna, which was printed resorting to the CNC available in Instituto de Telecomunicações.

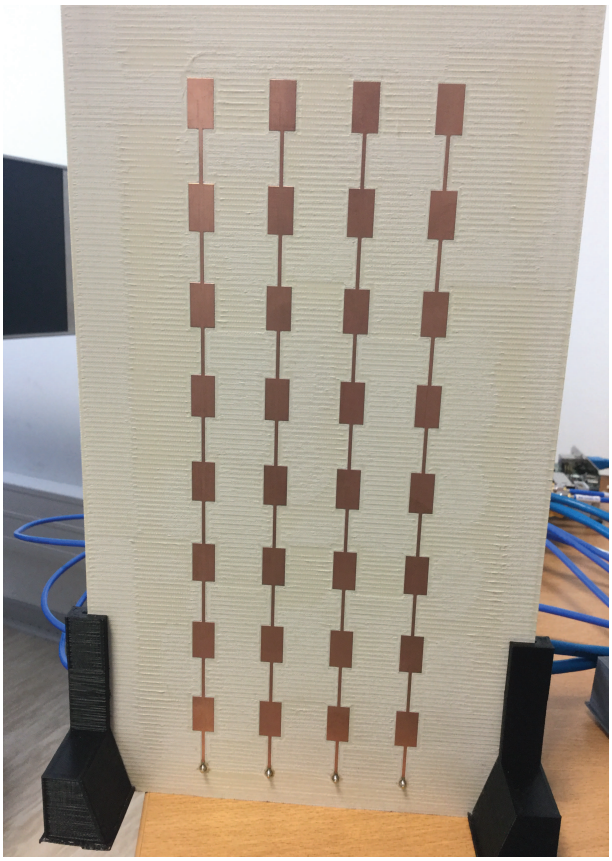

Figure 5.17: 2^{nd} version printed antenna

As can be seen next, the graphs presented below correspond to the S_{11} parameter of each aggregate. The graphs contain information about the simulation values provided by the CST and the practical results which were measured resorting a VNA after its printed.

Observing each one of the figures presented below it is possible to conclude that the practical results differ from the results that were obtained in the simulation performed in the CST. Although the difference of about 16 dB between the practical value measured in the VNA and the value of the CST simulation was achieved that the S_{11} of all antenna elements was less than -10 dB which makes the antenna minimally adapted to the frequency that was designed.

The difference between the practical and simulation values can be justified by the high sensitivity of this type of antennas to small changes in the copper size of the patch or lines [34]. Therefore any small errors occurred while printing the antenna on the CNC may have caused this degradation in the S-parameters, which is perfectly natural since the machines have always some errors and the practical results are never equal to the theoretical or simulated.

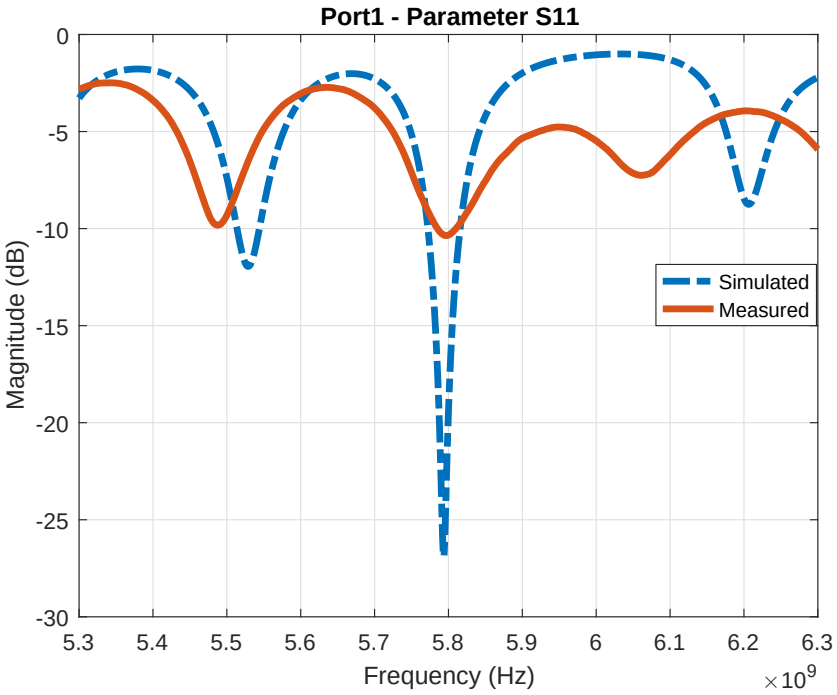

Figure 5.18: Parameter S11 of aggregate 1

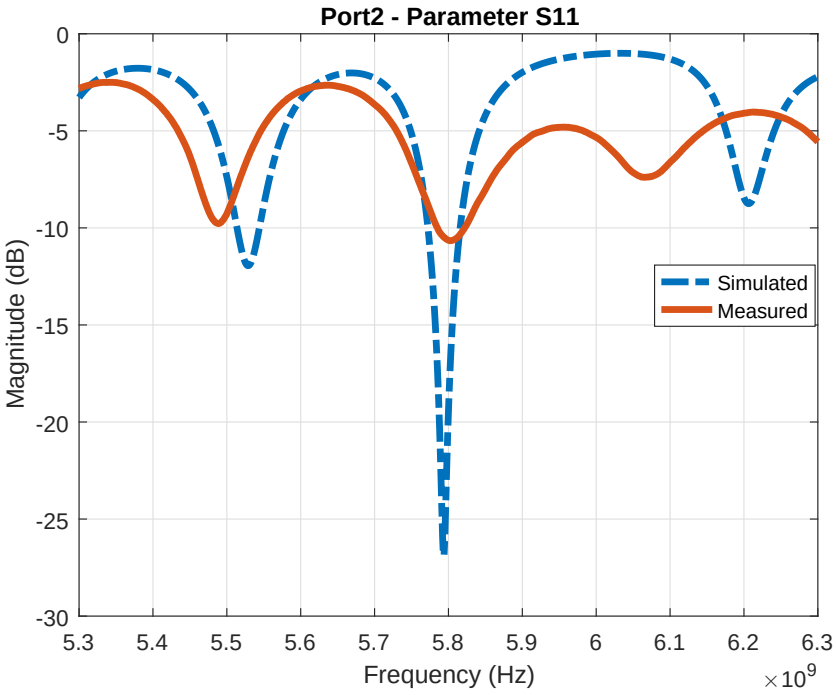

Figure 5.19: Parameter S11 of aggregate 2

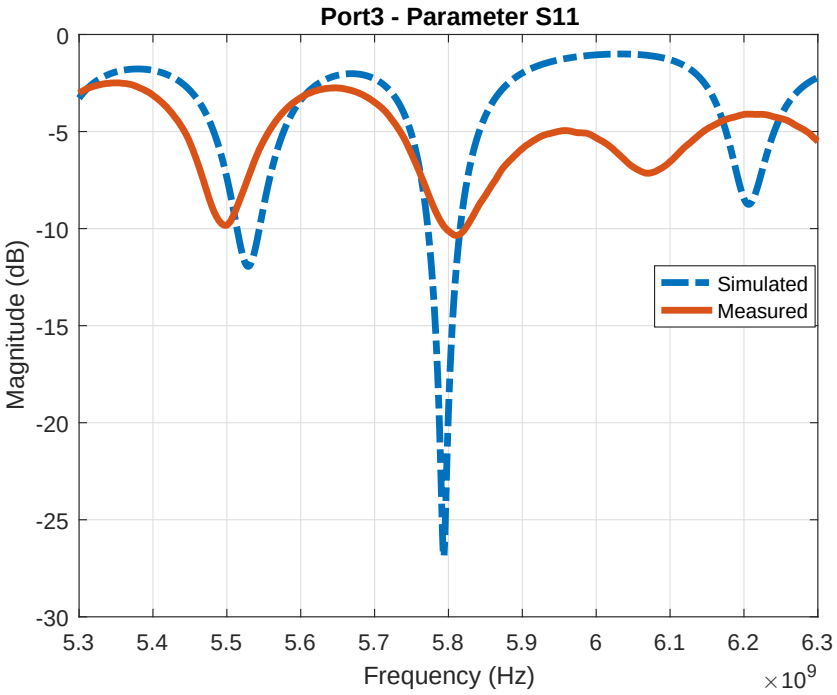

Figure 5.20: Parameter S11 of aggregate 3

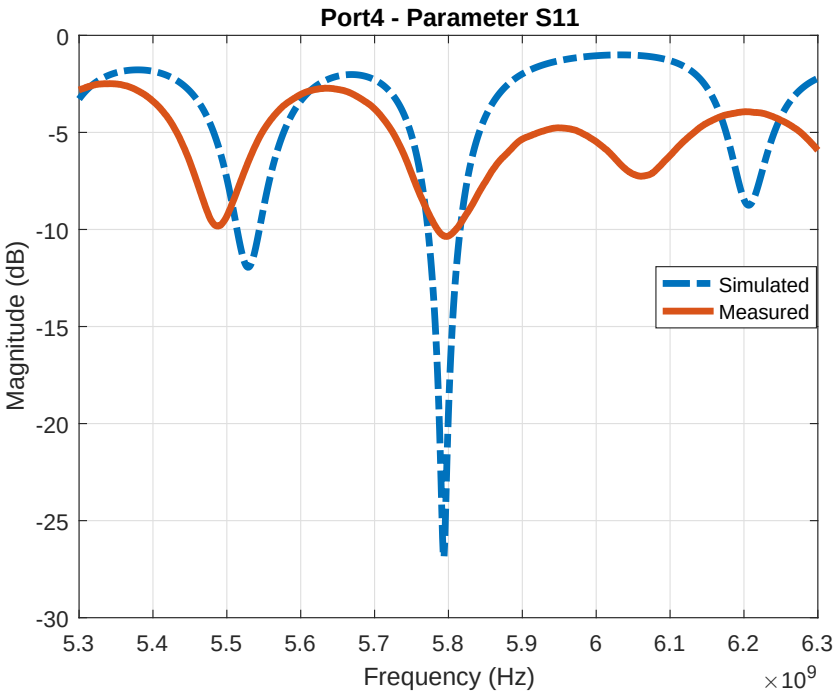

Figure 5.21: Parameter S11 of aggregate 4

In figure 5.22, the farfields of each one of the elements of the antenna are plotted where

it is possible to observe and to confirm its high gain.

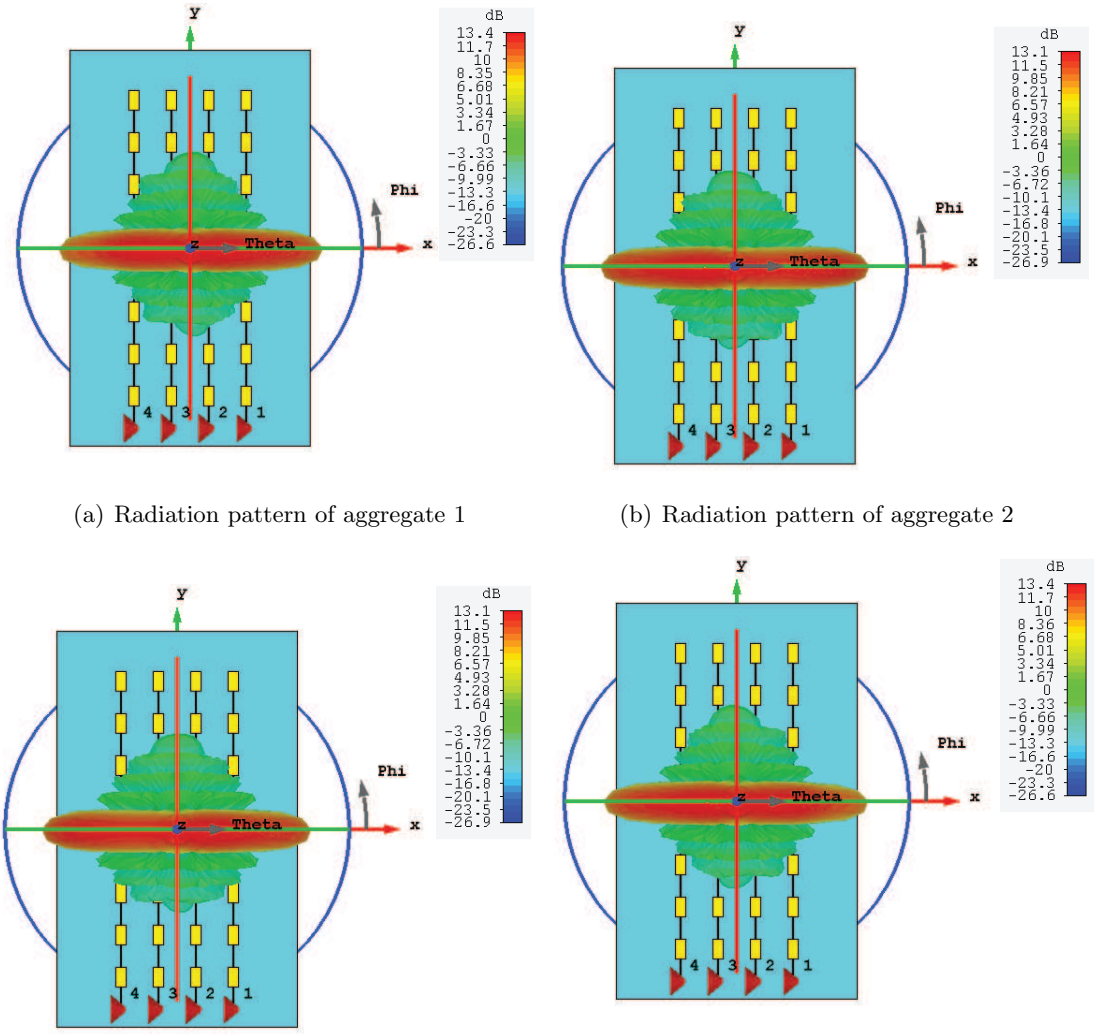

(a) Radiation pattern of aggregate 1

(b) Radiation pattern of aggregate 2

(c) Radiation pattern of aggregate 3

(d) Radiation pattern of aggregate 4

Figure 5.22: Radiation pattern of each aggregate

Considering that all the elements are fed with equal amplitude and in-phase, the antenna will present a new radiation diagram in relation to the previous situation in which each element was fed independently. This radiation diagram can be found in figure 5.23

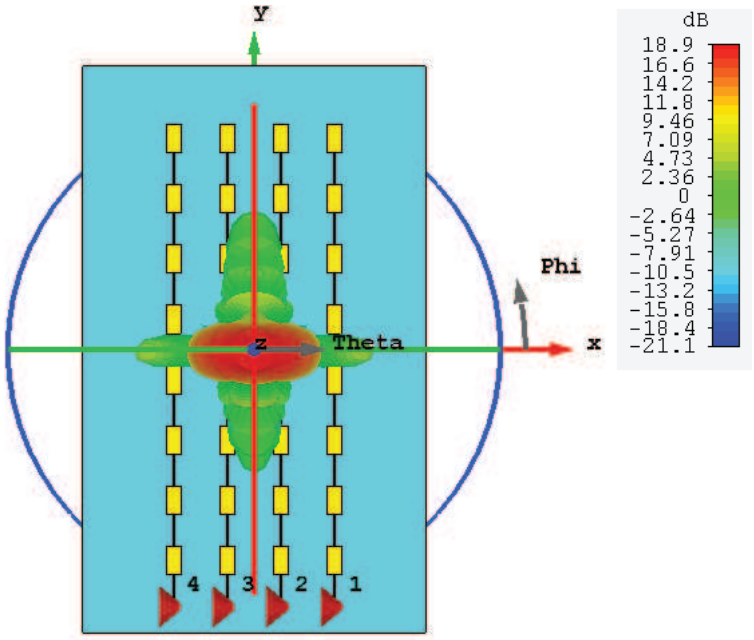

Figure 5.23: Radiation pattern of the full aggregate

5.6 Conclusion

In this chapter a general overview about the system and subsystems was made. A brief description of all of these was also presented in order to explain why this choices will allow to achieve the proposed objectives. In section 5.2 and the following, a general overview of the RADAR system was given with the presentation of block diagrams and their operation, but also was presented all the hardware presented in the system, its main features. The choices made for the system design come from what was presented in the chapters 3. It was also presented the designed antennas, the motivation of its use and later was verified that these fulfilled all of the necessities for this system.

Chapter 6

Results and Analysis

In this section is presented and analysed the results obtained by the algorithm developed for the RADAR system. With the implementation of this algorithm it was intended the detection of movement of the targets but also to be able to discover the direction of the signal that arrives at the RADAR. The experimental setup used for the implementation and validation of the algorithms can be found in figure 6.1.

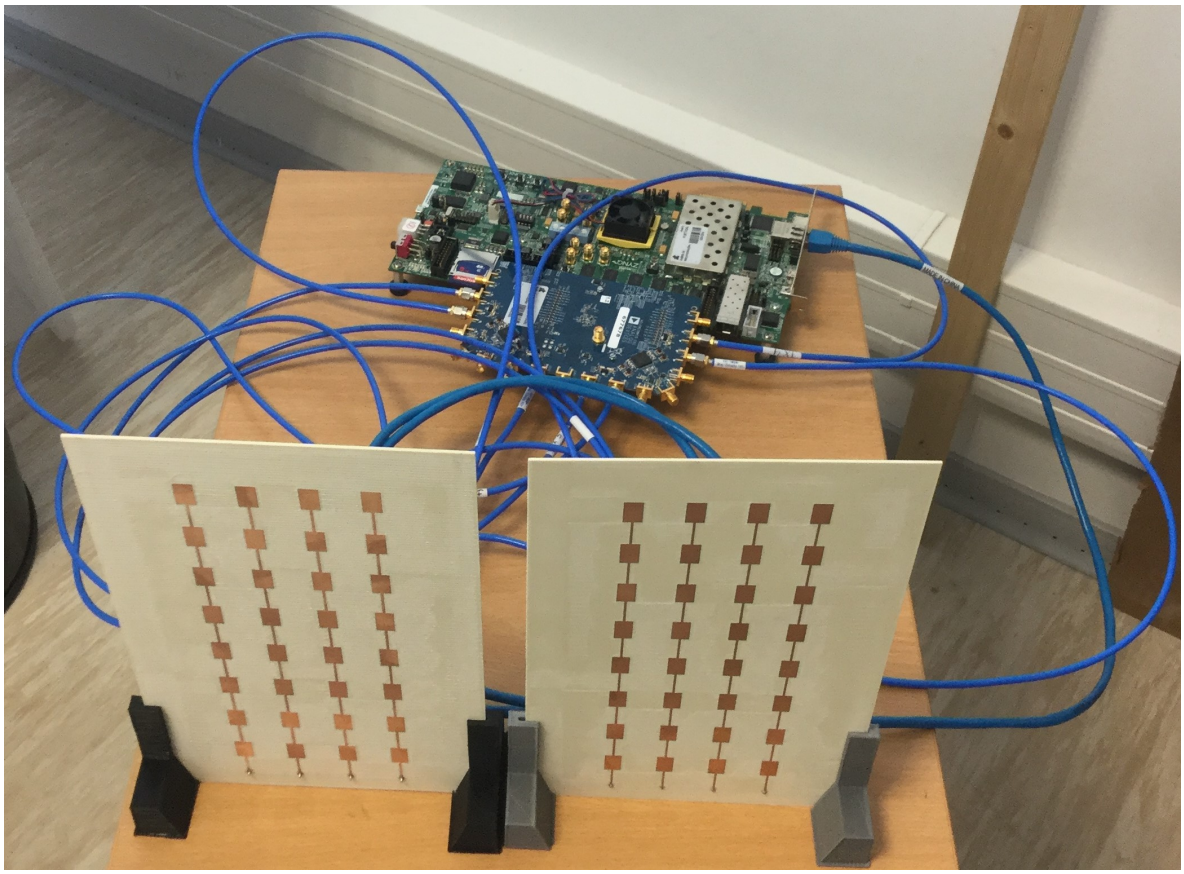

Figure 6.1: Experimental Setup

6.1 Reception Beamforming Algorithm

The algorithm developed consists in the implementation of several techniques in order to detect people, as well as their movements and their origin, that is, the direction from which there is movement.

In this algorithm we opted for the use of a chirp signal, since this provides a better SNR and it is possible to concentrate a greater amount of energy, being also more immune to noise. The table 6.1 contains information about some parameters that were taken into account in the development of the signal that was intended to be generated.

Algorithm parameters	
Central frequency	5.8 GHz
Sampling frequency	30.72 MHz
Gain (Tx & Rx)	50 dB
Waveform	Chirp
Chirp Bandwidth	30.72 MHz

Table 6.1: Algorithm parameters

After generation and modulation of the signal, it is sent through the antennas that were developed. From here the entire process of receiving and processing the received signals starts. In a first instance, the data is received and the signals are reconstructed, passing through a stage of filtering in order to eliminate possible parasitic noise as well as a check for eventual sample losses.

Completed the first step, the four receiver channels of the radar system were then phase calibrated. An external generator is used for this purpose and a USRP B210 with an antenna was used and this was placed completely in line with the center of the receiver antenna array. In this way the phase difference between the 4 channels can be calculated. Calculating this phase difference, take Rx1 as a reference and compensate the others so that all have the same phase, and the system will be calibrated. A representation of the setup used to calibrate the system can be seen in the figure 6.2 and the calculation of the phase differences in the figure 6.3.

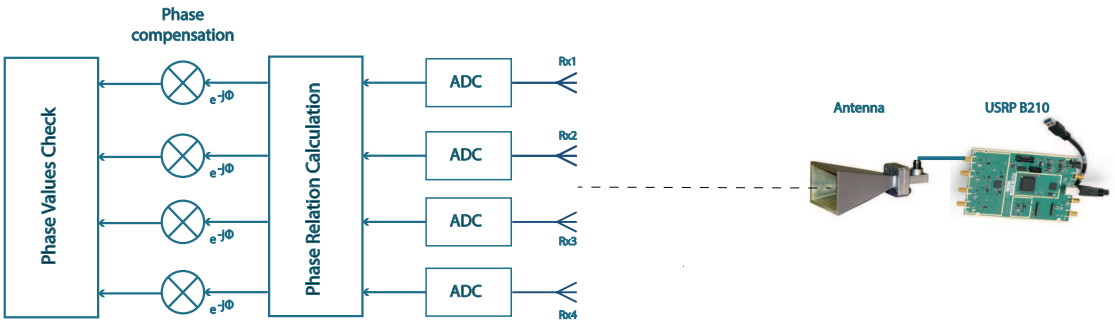

Figure 6.2: Phase calibration setup

After the compensation, a check is made on the phases of each channel to ensure that all are in phase. Again this calculation is performed as before and can be seen in figure6.3.

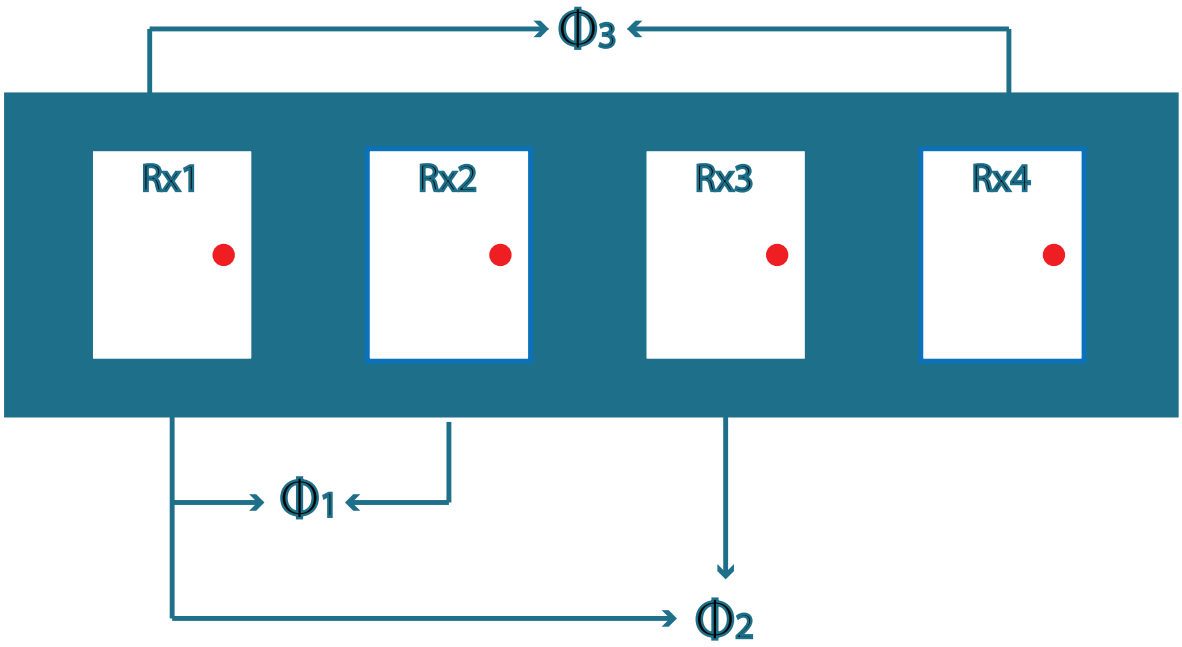

Figure 6.3: Angle of incidence calculation

Where expressions for calculating $\phi_{1...3}$ are:

$$\phi_1 = mean(angle(Rx1. * conj(Rx2))) \tag{6.1}$$
$$\phi_2 = mean(angle(Rx1. * conj(Rx3))) \tag{6.2}$$
$$\phi_3 = mean(angle(Rx1. * conj(Rx4))) \tag{6.3}$$

Achieved the results of the phase relation, it is proceed to a verification of these values in order to confirm if the values presented are in agree with what was expected, that is, these values must be comprehended between -90 and 90 degrees.

After the verification of the values obtained, follows the initiation of the implementation of the beam steering algorithm. The first step is to calculate the value of the phase shift required to point the beam to a certain angle. In this case the value of d and λ is always the same, so the phase shift will depend exclusively on the desired pointing angle. The equation 6.4 is the expression utilized to calculate the value of the phase shift.

$$\Delta\phi = \frac{2\pi\ d\ sin\gamma}{\lambda} \tag{6.4}$$

Where:

$\Delta\phi \longrightarrow$ Phase shift
d $\longrightarrow$ Distance between elements
$\gamma \longrightarrow$ Pointing angle
$\lambda \longrightarrow$ Wavelength

The figure 6.4 has the diagram that presents the general behaviour of the implementation of the beam steering. Calculated the phase shift for the required pointing angle is proceed to the multiplication of the various channels with other signal delayed with the phase calculated before. Usually it takes the first channel as reference, and the following channels are multiplied with an incremental factor of delay, as shown in the figure 6.4. According to the value of the signal of $\Delta\phi$ the beam will be displaced to the left or to the right achieving then the digital beam steering.

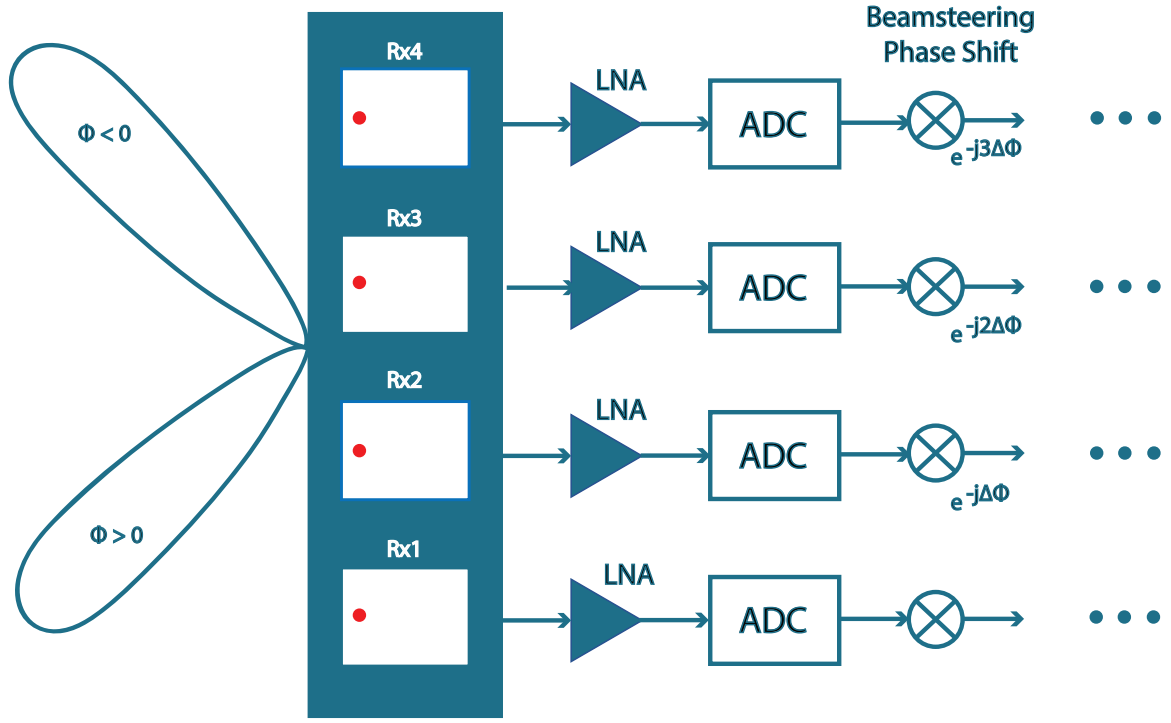

Figure 6.4: Beam steering algorithm diagram

Next are presented a few examples of the operation of beam steering and how was applied in this work. The table 6.2 contains the various different values of $\Delta\phi$ calculated from the equation 6.4 to the desired pointing angle just for demonstration. In the developed practical case a sweep of -60 to 60 degrees is made with 45 defined pointing angles.

$\Delta\phi$	**Patch 1**	**Patch 2**	**Patch 3**	**Patch 4**
-15 °	0 °	-46.6 °	-93.2 °	-139.8 °
0 °	0 °	0 °	0°	0°
30°	0 °	90°	180 °	270°

Table 6.2: Phases of each patch to perform beam steering

Upon completion of this step and the correct application of the beamsteering the energy that is received at each pointed angle is calculated. With this information it is then possible to calculate and know if there are variations in the energy that is being received but also to know the direction in which the energy change occurs, that is, the variance in the signal is calculated. In this way any type of movement will be detected, which in turn is presented to the user in graphic form the direction of this movement.

It is also defined a threshold which is in this case the threshold in which the variations do not correspond to movements, can be for example reflexes in some object, and in this way reduce the possibility of the existence of false positives. The figure 6.5 presents the full algorithm diagram.

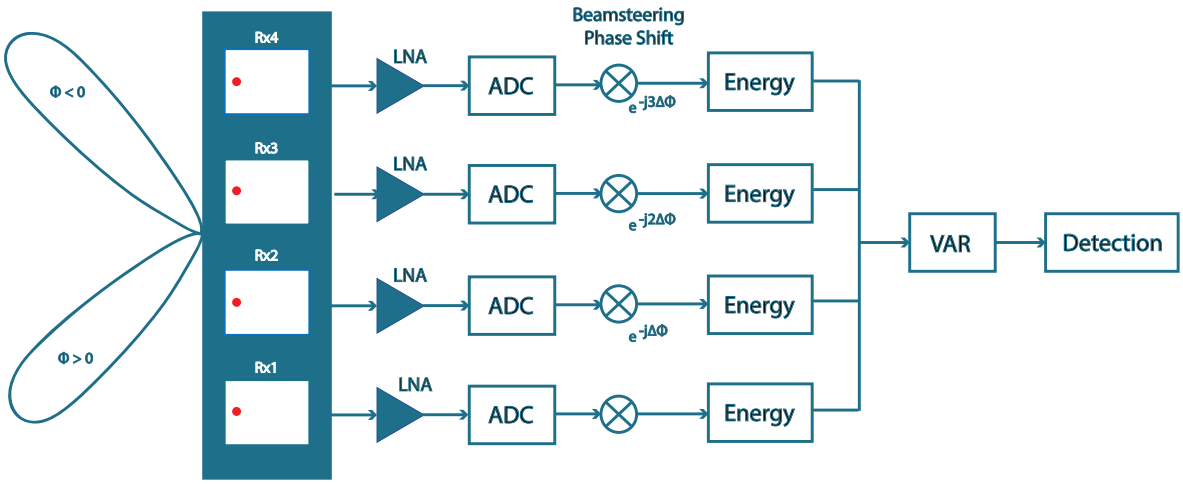

Figure 6.5: Algorithm diagram

In the figure 6.6 it is possible to observe the figures that come following the explanation made about the method used to detect the presence of people and their movements.

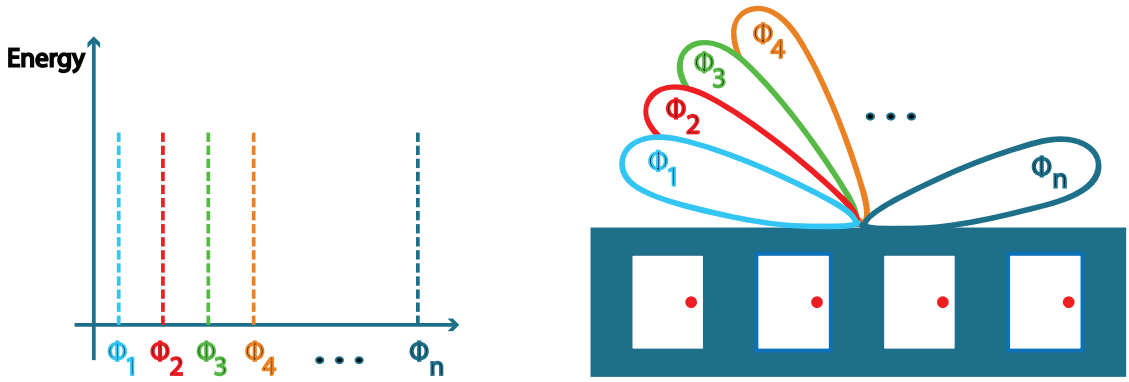

(a) With no movement

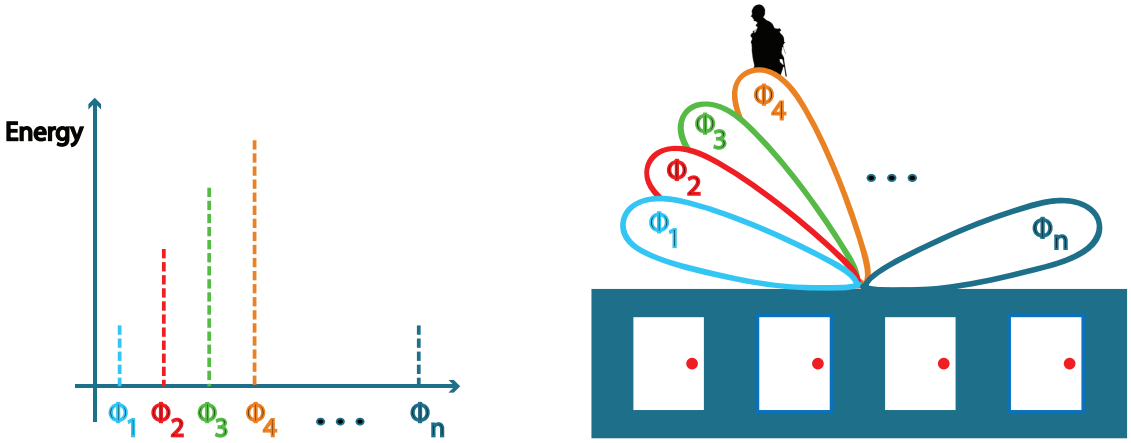

(b) Person and its movement detected

Figure 6.6: Detection method explanation

6.2 Results

In this section we intend to present the results obtained with the implementation of the developed algorithm. In addition to the visual results, photographs of the experience that support the visualization and interpretation of the results are also presented.

The figure 6.7 shows the result presented by the system when the variations in the energy received does not change. In this way the user knows that there has not been any kind of movement of a person. In the event that something has been detected before, when this graphic appears, it shows that although the person is there is not moving, informing that it is in the same place that was detected.

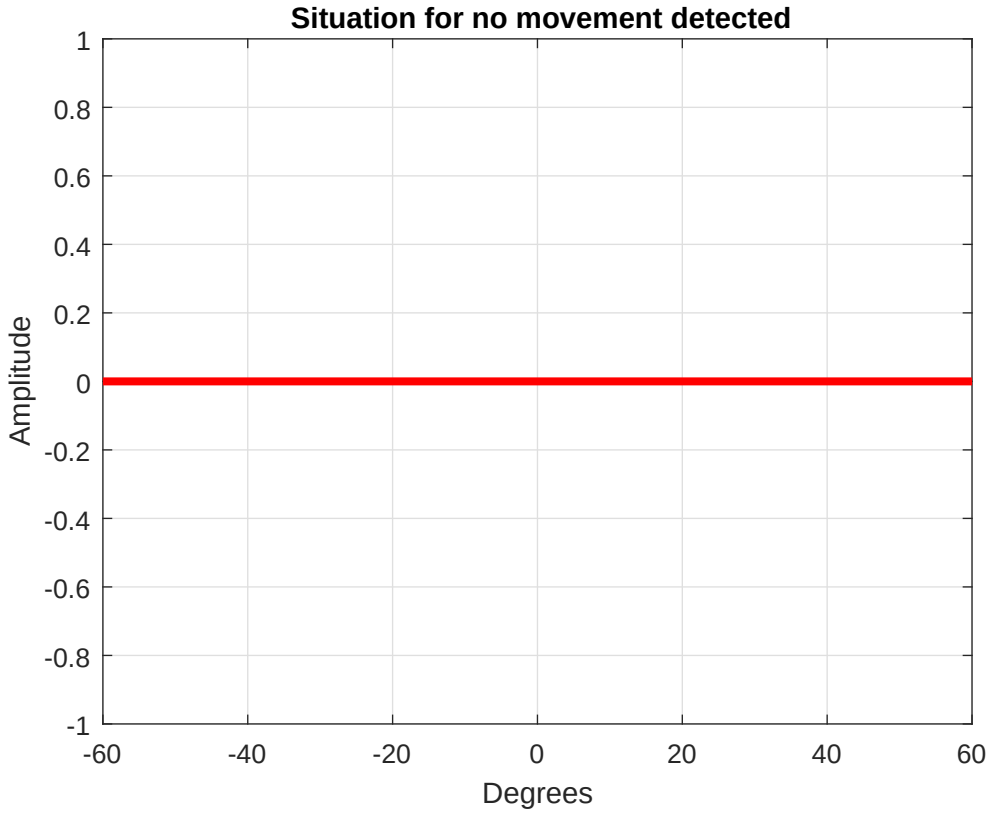

Figure 6.7: Results for situation where there is no movement

Following the presentation of the results, the ones that are presented below consider two scenarios with three different situations for each one for a general demonstration of the system. The two scenarios considered are the detection without any type of object between the antennas and the person and a second scenario in which bricks are placed in front of the antennas. In the three situations presented is considered that the person is detected in front, to the right and to the left of the antennas.

The figure 6.8 refers to the situation in which the person is detected in the center without any kind of objects, where it is possible to observe the conditions of the experience when the data is acquired. The figure 6.9 shows exactly the same situation but in which bricks were placed in front of the antenna. Once again an image is provided with the conditions of the experience.

It can be verified that in both scenarios the detection is carried out correctly, however in the case where the brick is placed in front of the antennas the presence of some secondary lobes is observed. These secondary lobes arise due to the presence of the bricks, that is, as the distance at which the bricks do not correspond minimally to the farfield of the antenna, these will cause changes in the radiation diagram, which justifies the presence of these secondary lobes.

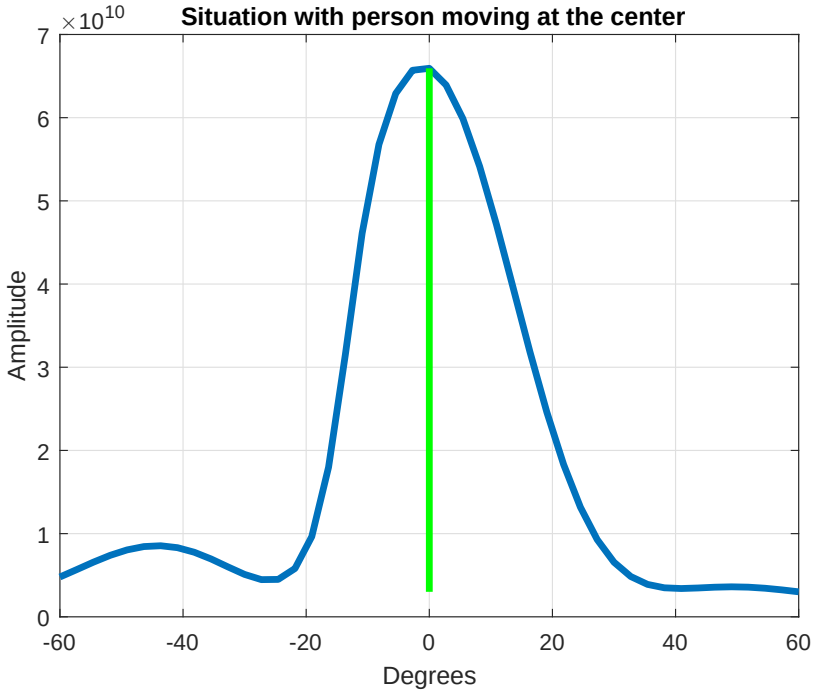

(a) Result obtained

(b) Experimental demonstration

Figure 6.8: Results for situation where the person is detected at the center without brick

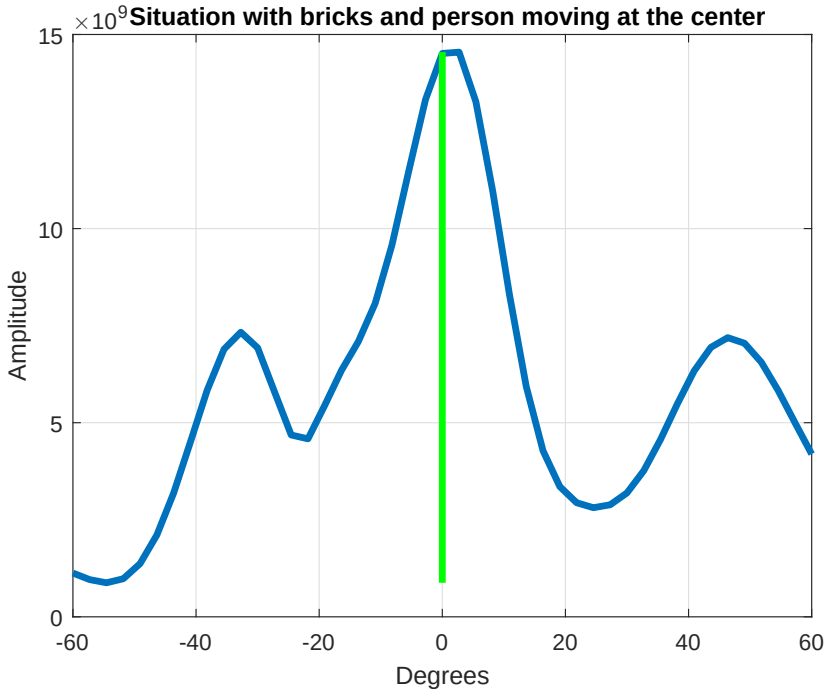

(a) Result obtained

(b) Experimental demonstration

Figure 6.9: Results with bricks where the person is detected at the center

The figures 6.10 and 6.11 show just like the previous results for the two scenarios defined, but in this case with the person placed/detected to the right of the antennas. Once again the coherent results are visible as it is also perceptible that when the bricks are placed in front of the antennas arise some secondary lobes, already justified previously.

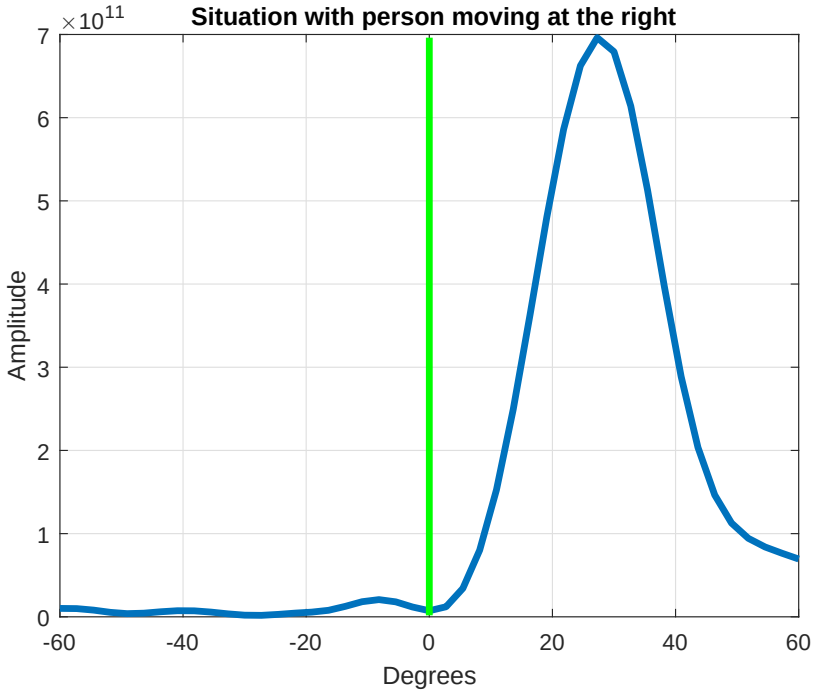

(a) Result obtained

(b) Experimental demonstration

Figure 6.10: Results for situation where the person is detected at the right

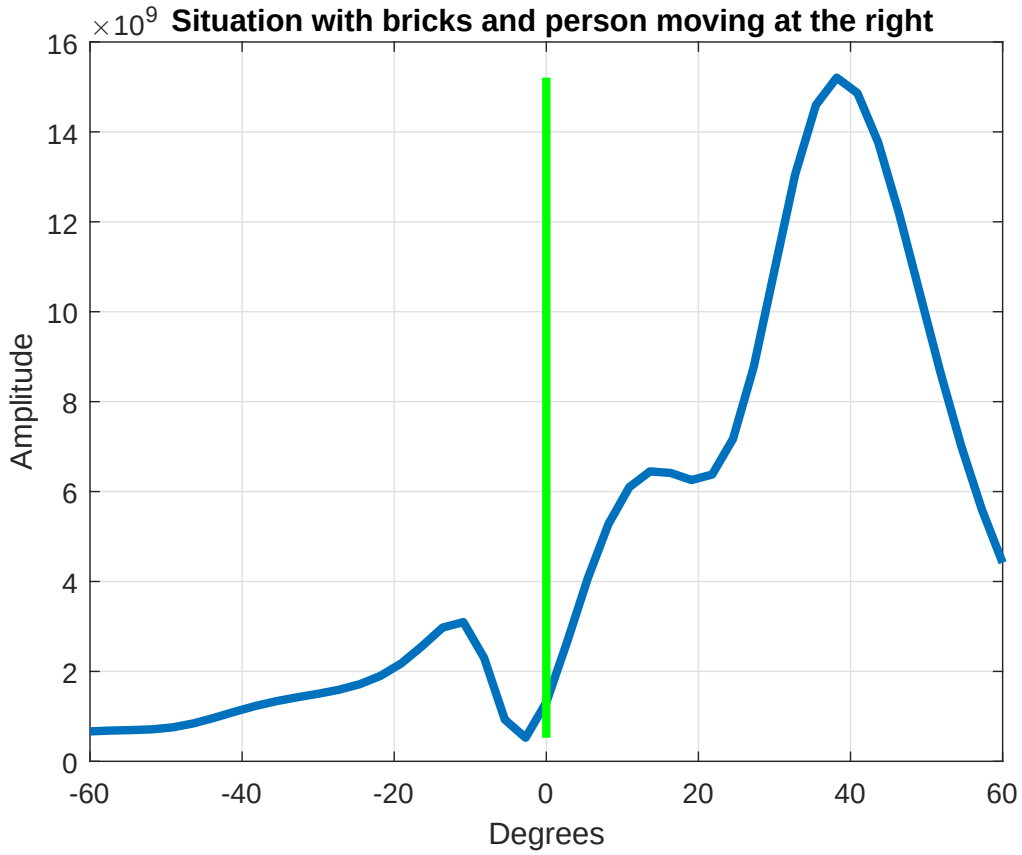

Figure 6.11: Results with bricks where the person is detected at the right

Finally, the results for the person positioned to the left of the antennas in the figures 6.12 and 6.13 are presented, and again, they are against what was expected. Again reinforcing the presence of the secondary lobes with the presence of the bricks, that although in no way affect the performance of the system its presence was justified.

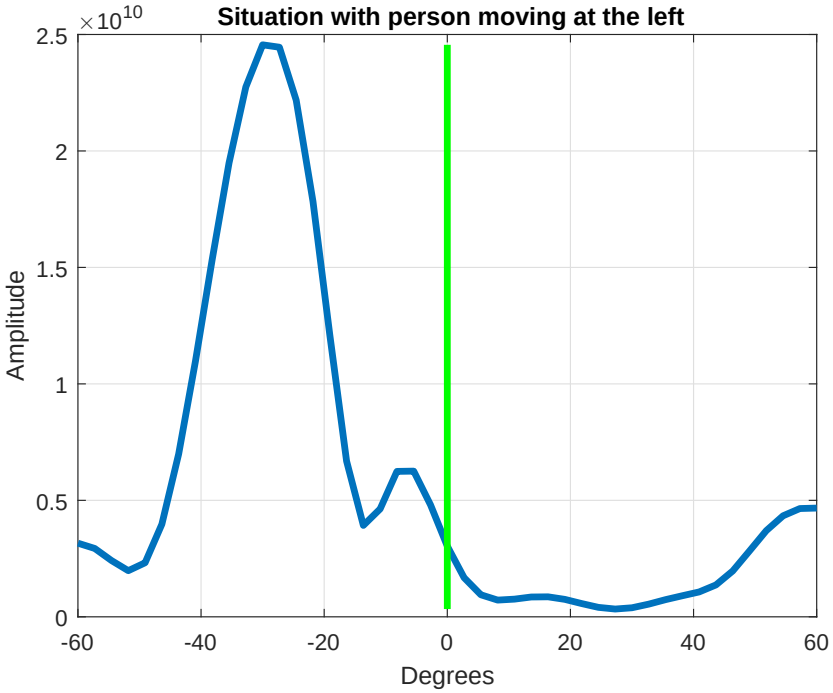

(a) Result obtained

(b) Experimental demonstration

Figure 6.12: Results for situation where the person is detected at the left

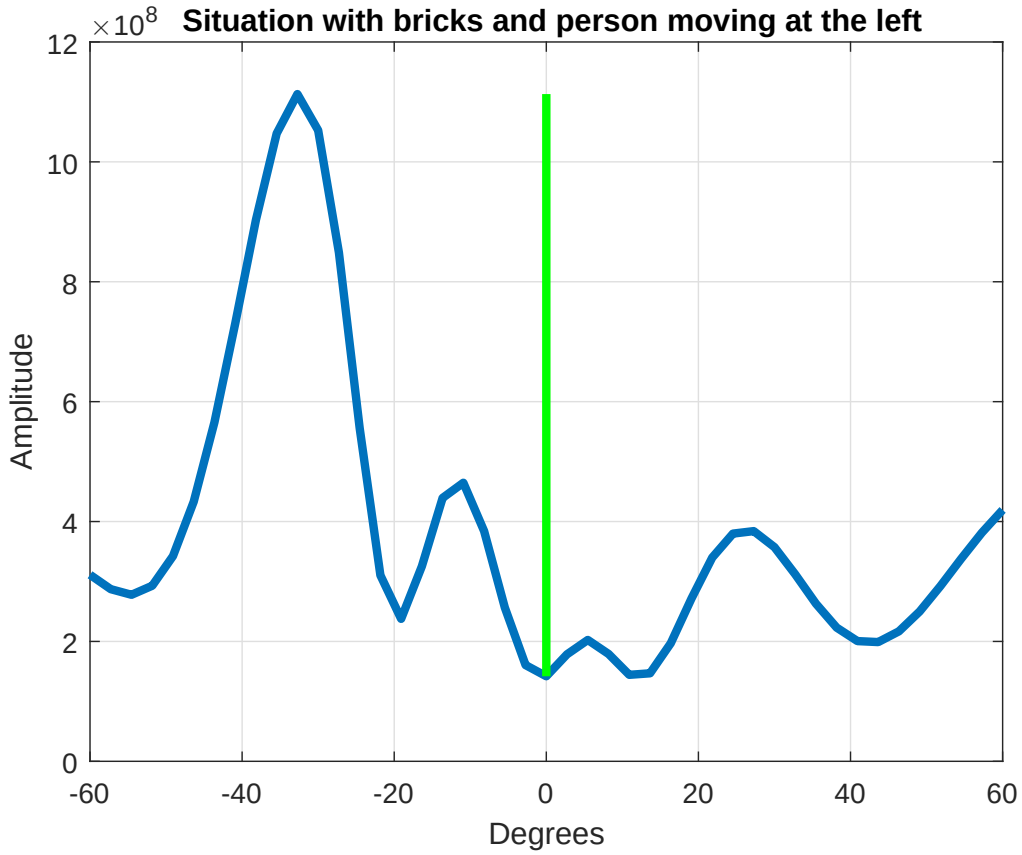

Figure 6.13: Results with bricks where the person is detected at the left

Finally, some results of experiments performed on the interior walls of the Telecommunications Institute are presented. It can be observed in Figures 6.14 and 6.15 that again positive results are obtained, thus being able to detect the position and the movement of a person. Again the presence of the secondary lobes is also visible. This is due to exactly the same phenomenon that was observed in the scenario where the bricks were used, but without any kind of influence on the veracity of the results.

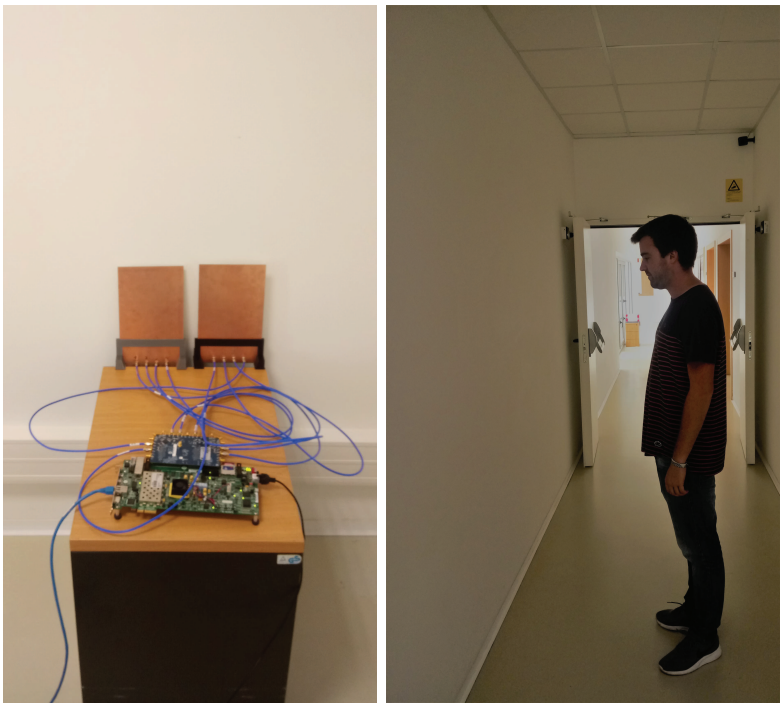

(a) RADAR positioning

(b) Positioning of the person behind the wall

Figure 6.14: Experimental demonstration of detection behind the wall

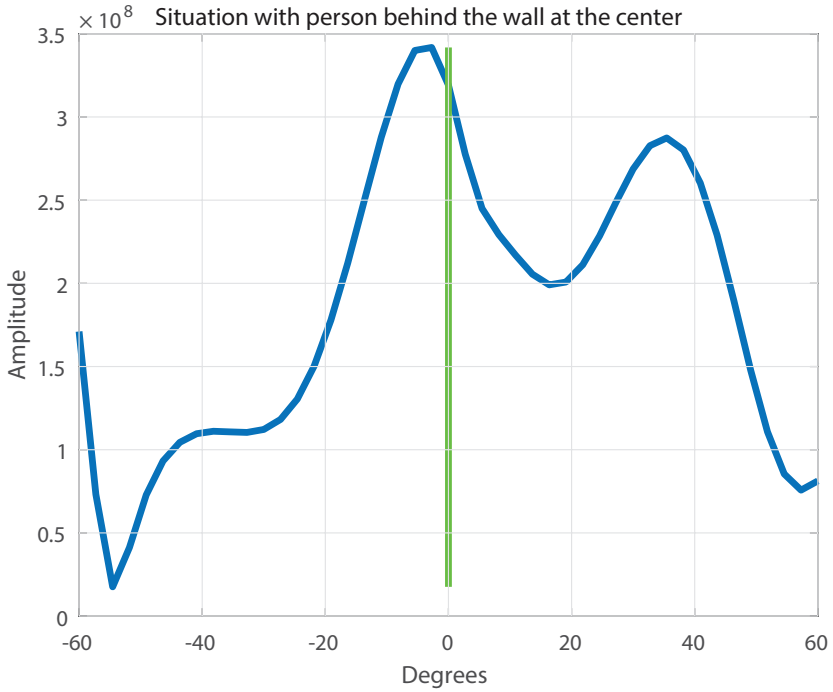

Figure 6.15: Results with person detected behind the wall at center

6.3 Conclusions

With the implementation of this algorithm, it was possible, as it was intended to detect people as well as to know the direction of their movement in free space but also with bricks and through a wall. It can then be concluded that the algorithm developed fulfils all the needs to solve the initial problem. Despite the good performance of the algorithm, this sometimes presents some delay in the presentation of the results, which could be beneficial to the efficiency of the system, making it as real time as possible.

The table 6.3 contains information about some radar characteristics as well as conclusions drawn after the entire process.

Radar features	
Max power emitted	12.24 dBm
Max distance detection in free space	≈ 6 meters
Max distance detection with obstacles	≈ 3 meters

Table 6.3: Radar features

Although the system can distinguish two different people, it shows some shortcomings with regard to the presentation of the results, since there is some delay in the presentation of the same ones.

Chapter 7

Conclusion and Future Work

7.1 Conclusions

In general the main objectives for this dissertation have been reached, and slight improvements are possible. Being that the work to be developed was divided in two great parts also its conclusions will be separated.

Starting with the characterization of materials, it can be concluded that the results were not close to what was expected from the literature. Despite all the effort and attempts of different ways to perform the measures these have never been against what was already known from published works presented in chapter 4. However a critical analysis of what was obtained was done, trying to justify the phenomena present and that may be damaging the results, as well as some suggestions of possible systems to produce the results that are expected.

Regarding to the purposed RADAR system, the implementation of a RADAR based on SDR architecture was clearly achieved, enjoying their advantages for the implementation of MIMO and the performing of beamforming, making possible the exploration of new algorithms. This way, the problem presented at the beginning of this dissertation was solved and a functional prototype that allows to detect people through walls or objects like bricks, but also to know their position and to follow possible movements was developed with success.

In terms of hardware developed, MIMO antennas arrays were developed in which a great directivity and gain is possible. The antennas allow then to improve the penetration in the walls and the power transmitted. Although small problems occurred with the CNC during printing, these were perfectly functional for the purpose they were designed.

7.2 Future Work

For future work it would be interesting and beneficial to invest in an exclusive project for the study of the characterization of materials, being able to characterize a greater diversity of materials. It would also be advantageous to use the most suitable and certified components, that is to say, in the case of antennas, the use of antennas with approximately equal adaptation and gain throughout their cover band would be appropriate. It would also be

interesting to try other ways of measuring those that were used and developed throughout this dissertation, because despite all efforts some results were not the most encouraging.

It is also important to explore new signal processing algorithms to improve the SNR and thereby improve RADAR performance, explore the implementation of a MIMO RADAR 8x8, or more. The use of amplifiers at the input of the antennas would also be a viable solution to explore, as it would allow a greater penetration power for thicker walls and with great attenuation. Finally it would be interesting to analyse other frequency bands and know what is the best frequencies to use in this type of applications. Since the presented system presents some delays in the presentation of the results it would be interesting make the system as real time as possible.

Appendices

Appendix A

Poster for Students@DETI

students @deti

Person Detection System

Diogo Silva Matos

Orientador: Prof. João Nuno Matos

Mestrado Integrado em Engenharia Eletrónica e Telecomunicações

2017

Abstract

This work intends to set up a radar based on a SDR architecture, that is capable of detecting people and/or objects through walls, thus it was necessary in the first instance to study the attenuation in RF signals of the most common materials used in the construction of houses or walls. Therefore, it was necessary to elaborate several setups capable of providing the desired measurements.

Materials Attenuation

In recent years, some researchers have characterized the attenuation of materials that constitute walls usually to study the implementation of radio access network services. To make a good characterization of the materials to be studied, it is necessary to know the losses in the free space first, in order to make a comparison with the different types of materials. In the figure below, it is presented one possible configuration to measure the values, using a VNA.

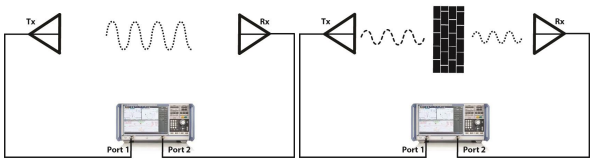

a) Measurement in free space b) Measurement with the material

Fig 1 - Measurement setup.

This measurement is called Shielding Effectiveness and is measured for normal incidence by comparing the module of scattering parameters of transmission in free space to that obtained when the wall is placed between the antennas.

$$SE = S_{21\,(Free\ Space)} - S_{21\,(Wall)}$$

The following table shows some measurements for different materials [1].

Material	Thickness	Attenuation (dB) @ 6 GHz
Plywood (Wet)	2 cm	4
Lumber (Dry)	15 cm	22
Brick	27 cm	40
Concrete	20 cm	50
Reinforced Concrete with iron	20 cm	65
Brick-faced Concrete	20 cm	72

[1] NISTIR 6055 NIST Construction Automation Program Report No . 3 Electromagnetic Signal Attenuation in Construction Materials

Radar System

In order to detect people as well as their movements it was intended to implement a MIMO Radar 4x4 (4 transmitters and 4 receivers). One of the ways to do this is to choose an architecture based in Software Defined Radio (SDR) because of its flexibility.

The implemented system consists of three main blocks, the FPGA Xilinx ZC706, the RF front-end AD-FMCOMMS5 and the developed antennas, as shown in figure 2. The FPGA provides a connection to the RF front-end and it is also responsible for all digital signal processing, as well as data analysis and processing.

The two AD9361 chips present in AD-FMCOMMS5, have as basic function to generate digital signals in baseband, these signals are modulated in RF frequency. Finally, antennas are responsible for transmitting signals generated and modulated by the RF front-end to the air, as well as receiving echoes from the reflections in the most diverse objects and forwarding them back to the RF front-end to proceed to the processing of the received data.

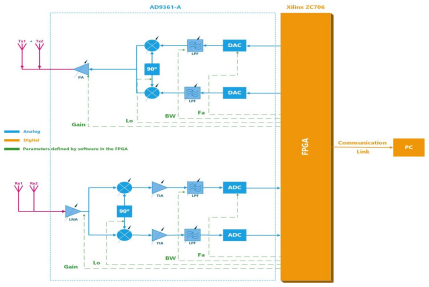

Fig 2 – System block diagram

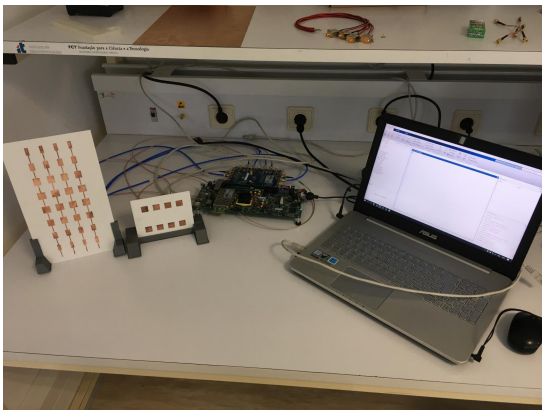

Fig 3 – Experimental Setup

Conclusions

- Materials attenuation measured;
- Radar MIMO 4x4 based in SDR architecture implemented;
- Detection of persons/objects by power variations;
- Detection of movement by measuring the angle of signal arrival.

Bibliography

[1] Yaşar B. Yetkil, Design of an FM-CW Radar Altimeter. Master's thesis, December 2005.

[2] History of radar, https://en.wikipedia.org/wiki/History_of_radar. Accessed on 30-01-2017.

[3] Merrill. I. Skolnik, Radar Handbook, Second edition, 2009.

[4] Merrill. I. Skolnik, Introduction to Radar Systems, Second edition, 1981.

[5] K. Yadav, K. Taneja, M. Chauhan. Radar Frequency Bands. *International Journal of Innovative Research in Technology*, 2349-6002, 2014.

[6] Radar, https://en.wikipedia.org/wiki/Radar. Accessed on 20-11-2016.

[7] Radar Basics, http://www.radartutorial.eu/index.en.html. Accessed on 20-02-2017.

[8] S. Singh, Q. Liang, D. Chen and L. Sheng. Sense through wall human detection using UWB radar. *Journal on Wireless Communications and Networking*, 2011.

[9] Teófilo J. M. Monteiro. *Projecto de um Analisador de Espectros Baseado em SDR*. Master's thesis, University of Aveiro, 2010.

[10] J. Mitola. The Software Radio Architecture. *IEEE Communications Magazine*, 33(5):2638, May 1995.

[11] João C. C. da Silva. *Implementação em hardware de um analisador de espectros baseado em SDR*. Master's thesis, University of Aveiro, 2010.

[12] J. Li, P. Stoica. MIMO Radar Signal Processing. John Wiley & Sons, Inc., 2009.

[13] Constantine. A. Balanis. Antenna Theory Analysis and Design. John Wiley & Sons, Inc, 2005.

[14] Tiago M. V. Varum. *Antena para Comunicações DSRC*. Master's thesis, University of Aveiro, 2010.

[15] W. Lee, B. Min, C. Kim, J.C. Kim and J. Yook. "A compact switched Beamforming Network using silicon IPD technology for low-cost 5G communication" in *Microwave Symposium (IMS), 2016 IEEE MTT-S International*.

[16] Suhil S. M. Omran. *Beamforming Network using Switch Line Phase Shifter*. Master's thesis, University of Malaysia, 2008.

[17] V. Rabinovich and N. Alexandrov, Antenna Arrays and Automotive Applications, Springer, 2013.

[18] R. Ricon, T. Fatoyinbo, B. Osmanoglu, S. Lee and K. Jon Ranson. "Development os NASA's Next Generation L-Band Digital Beamforming Synthetic Aperture RADAR (DBSAR-2)", in *European Synthetic Aperture Radar Conference 2014; 3-5 Jun. 2014*.

[19] John E. Peabody, Jr., Gregory L. Charvat, Justin Goodwin, and Martin Tobias. Through-Wall Imaging Radar. *Lincoln Laboratory Journal* Vol. 19, number 1, 2012.

[20] John E. Peabody, Jr., Gregory L. Charvat, Justin Goodwin, and Martin Tobias. Detection Algorithm Implementation and Measured Results for Real-Time, Through-Wall Radar System using a TDM MIMO Antenna Array, 2012.

[21] D. Micheli, A. Delfini, F. Santoni, F. Volpini, and M. Marchetti. Measurement of Electromagnetic Field Attenuation by Building Walls in the Mobile Phone and Satellite Navigation Frequency Bands. *IEEE Antennas and Wireless Propagation Letters*, Vol. 14, 2015.

[22] D. Micheli, A. Delfini, F. Santoni, F. Volpini, and M. Marchetti. Electromagnetic Shielding of Building Walls. *IEEE Antennas & Propagation Magazine*, 1045-9243, Oct. 2016.

[23] William C. Stone. *NIST Construction Automation Program Report No. 3, Electromagnetic Signal Attenuation in Construction Materials*. Oct. 1997.

[24] David D. Ferris and Nicholas C. Currie. Microwave and millimeter-wave systems for wall penetration. *SPIE Conference on Targets and Backgrounds: Characterization and Representation IV* April 1998.

[25] D. Malafaia, B. Oliveira, P. Ferreira, T. Varum, J. Vieira and A. Tomé. Cognitive bioradar: The natural evolution of bio-signals measurement. *Journal of Medical Systems*, 0148-5598, 2016.

[26] Rohde&Schwarz. Vector Signal Generator SMU200A, Nov. 2006.

[27] Keysight Technologies. FieldFox Handheld Analyzers Data Sheet, 2016.

[28] Keysight Technologies. N1913A and N1914A EPM Series Power Meters E-Series and 8480 Series Power Sensors Data Sheet. March 2016.

[29] Ettus Research. USRP B200 / B210 Bus series, 2015.

[30] Mini-Circuits. Power Splitter/Combiner ZN2PD2-63+.

[31] Xilinx. Zynq-7000 All Programmable SoC Overview, Sep. 2016.

[32] Xilinx. ZYNQ-7000 SoC ZC706 Boards and kits EVALUATION KIT, 2012.

[33] D. Pu, A. Cozma and T. Hill. Four Quick Steps to Production: Using Model-Based Design for Software-Defined Radio. *Analog Dialogue 49-09*, Sep. 2015.

[34] T. Yuan, N. Yuan and L. Li. A Novel Series-Fed Taper Antenna Array Design. *IEEE Antenna and Wireless Propagation Letters*, Vol. 7, 2008.